Proceedings

Seminar on

DESIGN OF EXPOSED BRIDGE PIERS

1. DYNAMIC ICE LOAD

Copenhagen, January 22, 1991

DANSK VANDBYGNINGSTEKNISK SELSKAB

DANISH SOCIETY OF HYDRAULIC ENGINEERING

v/ H. F. Burcharth, AUC, Sohngårdsholmsvej 57, 9000 Aalborg. Tlf. 08 - 142333

Introduction

The present publication contains the contributions of invited speakers to a seminar arranged by the Danish Society of Hydraulic Engineering, january 22, 1991.

Members of the Danish Geotechnical Society, Danish Society of Structural Engineering and Danish Society of Risk Analysis were invited to join the seminar.

The seminar is the first one in a series covering design of exposed bridge piers exemplified through investigations carried out in connection with Storebæltforbindelsen.

In the present proceeding various publications covering the themes of the speakers have been used to avoid double work for the speakers. The geotechnical aspects will be described in further detail in a planned volume of dgf-Bulletin (Danish Geotechnical Society). In the present publication two draft manus for the dgf-Bulletin have been included, as they represent extended versions of Knut Andersen's presentations on the seminar.

A description of the extreme ice property analysis has been included as a separate paper.

We are very grateful to Storebæltsforbindelsen a/s (Great Belt a/s) for the permission to arrange the seminar and to publish the proceedings.

We hope through the seminar and the proceedings to have demonstrated the rather advanced design methods being used, so that the experiences being gained may be used for the coming bridge projects in Danish areas and elsewere in the world.

Danish Society of Hydraulic Engineering

Helge Gravesen

c/o Dansk Geoteknik a/s
Granskoven 6
DK 2600 Glostrup

LIST OF CONTENTS

1. EXTREME ICE PROPERTIES

Ready-to-copyedit Manuscript for ASCE 16 October 1990
Journal of Cold Regions Engineering FTC/AB/HEC/1006.01.div.

EXTREME ICE PROPERTIES

by

Flemming Thunbo Christensen [1] and Jesper Skourup [1]

1) Ph.D. C.Eng., Danish Hydraulic Institute, Agern Allé 5, DK-2970 Hørsholm, Denmark

Keywords: ice strength, ice thickness, extreme value analysis, design ice properties, statistical distribution of ice properties.

ABSTRACT

An extreme value analysis was carried out for ice properties in the Great Belt in Denmark. The design of a bridge and tunnel system across the Belt called for knowledge of extreme ice properties because dynamic ice loading governs part of the design. The methodology used in this project is of general interest because of the extremely low exceedance probability specified and because of the poor amount of data available concerning ice at the location of interest.

INTRODUCTION

The result of a preliminary extreme value analysis of ice properties in the Great Belt in Denmark was briefly described by Christensen et al. (1989) as a basis for selection of parameters for model tests. The present analysis is the final version of that for the Great Belt West Bridge. It constitutes a sub-

stantial expansion of the preliminary analysis, and it leads to higher compressive ice strengths. For the West Bridge, dynamic ice loads govern the design of the bridge piers.

The recurrence time of the load due to ice crushing is determined by the recurrence time of the product $\sigma_u h$, where σ_u is the uniaxial compressive ice strength and h the ice sheet thickness. In order to determine a design value of this product, the statistical distribution of $\sigma_u h$ must be known. No combined values of σ_u and h exist for the Danish waters, however, and so distributions for each parameter must be combined. This leads to the question of statistical correlation between ice strength and ice thickness. The correlation must be known in order to properly combine the distributions. It is clear that they are not fully uncorrelated, since cold weather will increase both strength and thickness of the ice, but it is equally clear that they are not fully correlated either, since a warm spell of say $-2^{o}C$ will leave little ice strength while the thickness remains unchanged. In order to circumvent this problem the product $\sigma_u h$ is split into a temperature dependent and a temperature independent part. Distributions for these parts can be combined safely under an assumption of no correlation.

Compressive ice strength variations have been described (e.g. Weeks and Assur, 1969) in the form

$$\sigma_u = \sigma_o f_\sigma(S_i, T_i) \qquad (1)$$

where σ_o is a constant reference strength and f_σ is a function of the mean ice temperature, T_i, and the ice salinity, S_i. In the present analysis it was decided to describe the reference strength as a stochastic parameter. Exponential, Weibull, Gumbel and Log-Normal distributions were fitted to the reference strength data described later. Goodness of fit was determined for each of these by a χ^2 test, by a Kolmogorov-Smirnov test and by visual observation. The Weibull and Gumbel distributions both describe the data well and are clearly superior to the other distributions. The goodness of fit is equal for the Weibull and Gumbel distributions, and the Weibull distribution was selected:

$$\sigma_o \in We(\beta,k) \tag{2}$$

$$f(\sigma_o) = \frac{k}{\beta}\left(\frac{\sigma_o}{\beta}\right)^{k-1}\exp\left(-\left(\frac{\sigma_o}{\beta}\right)^k\right) \tag{3}$$

$$F(\sigma_o) = 1-\exp\left(-\left(\frac{\sigma_o}{\beta}\right)^k\right) \tag{4}$$

where f is the probability density function, F the distribution function, and ß and k distribution parameters.

The ice thickness was calculated from a simple linear differential equation for heat conduction. The resulting expression is of the general form:

$$h = f_h\left(\int T_a dt\right) \tag{5}$$

i.e. a function of the accumulated freezing degree-day (fdd) index. A commonly used formulation of the fdd index is

$$K = \Sigma\ (-\bar{T}_a) \text{ for } T_a < 0^{\circ}C \tag{6}$$

where the index K equals zero at the onset of winter, T_a is the daily average air temperature, and the summation is carried out daily. This index has many shortcomings, e.g. that the effect of thaw periods are not accounted for, but is nevertheless widely used and reported. Wherever daily temperature records are available, the effects of thaw periods should be investigated. But the advantage of the simple index (6) is the availability of data for a large number of years. An estimate of the thickness of the sea ice is

$$h = 0.032(K-50)^{\frac{1}{2}} \text{ meter} \tag{7}$$

where K must be in Celsius degree-days. This formula is derived theoretically from an assumption of one-dimensional heat conduction, except for the subtraction of 50 degree-days which is of empirical nature. It accounts for the freezing point being lower than zero degree Celsius.

By rewriting the equations (1) and (5) it follows that

$$\frac{\sigma_u h}{\sigma_o} = x = f_\sigma(S_i, T_i) f_h(T_a(t), t) \tag{8}$$

$$\sigma_u h = \sigma_o x \tag{9}$$

By defining the parameter x in Eq. (8) as the temperature dependent part of the product $\sigma_u h$, and by letting σ_o represent the temperature independent part of the product, the previously mentioned split illustrated in eq. (9) is achieved. The methodology then entails determination of distributions for σ_o and for x, which are eventually combined into the probability distribution function for the product $\sigma_u h$ by integration:

$$F(\sigma_u h) = \int_o^\infty F(x) f(\sigma_o) d\sigma_o \qquad (10)$$

$F\left(\frac{\sigma_u h}{\sigma_o}\right)$

The simple integration in eq. (10) implies that σ_o and x are statistically independent, which was precisely the reason for the applied split of the product. In the following statistical distributions are determined for the reference strength σ_o and for annual maximum values of the parameter x.

The compressive ice strength of sea ice is known to be strongly strain rate dependent. It would therefore be desirable to determine this functional relationship and to include ice velocity in the probabilistic formulation of ice loading conditions. Because of time constraints this was not included. Instead, compressive strength in this analysis is meant to be representative of the brittle range, in which the rate effects are moderate.

REFERENCE STRENGTH DISTRIBUTION

The specific expression defining reference strength suggested by Weeks and Assur (1969) read:

$$\sigma_u = \sigma_o\left(1-\left(\frac{\nu}{0.275}\right)^{\frac{1}{2}}\right) \tag{11}$$

where ν is the relative brine volume in the ice. This quantity may according to Frankenstein and Garner (1967) be calculated as:

$$\nu = \left(0.532 - \frac{49.185}{T_i}\right)\frac{S_i}{1000} \tag{12}$$

where T_i is in negative Celsius degrees and S_i in parts per thousand. More accurate descriptions are available, e.g. Cox and Weeks (1982), but equations (11) and (12) give sufficient accuracy when fitted to experimental data.

It appears to be a simple matter to determine a σ_o distribution from a large amount of strength measurements in the area of interest. But in Danish domestic waters only low-quality strength measurements are available. By low-quality we refer to the fact that e.g. strain-rate and crystal structure have never been documented. The Danish data all stem from field programs carried out jointly by the Institute of Hydrodynamics and Hydraulic Engineering (ISVA) at the Technical University of Denmark and by Danish Hydraulic Institute. The results have been reported by

Tryde and Zorn (1979), by Mortensen and Zorn (1982) and by Christensen (1986). Because of the low quality of these measurements it was decided to use also the data presented by Fransson and Elfgren (1987) from the Bay of Bothnia, provided that these data could be considered representative of reference strengths in the Great Belt some 1000 kilometres to the south.

The Swedish data were used as published. In the Danish data, measurements with mean ice temperatures of -0.5^{o} or warmer were discarded, leading to omission of 7 out of 57 measurements. These 7 were all from the same location and showed unrealistic results, probably due to faulty temperature measurements. The Danish tests were made with cubes of ice, and the resulting strength was multiplied by 0.67 to obtain the "cylinder strength". The factor 0.67 was adopted from concrete testing technology where it varies between 0.67 and 0.80. The Swedish tests were made using cylindrical ice samples and a constant strain-rate of 2×10^{-4} sec^{-1}.

The description of crystal structures in the Swedish samples offered by Fransson and Elfgren (1987) correspond well to what is expected in the Great Belt, viz. mostly columnar ice with some granular and mixed ice types as well. In Table 1 the two data sets are compared in terms of both reference strength, temperature and salinity. The reference strengths are very close. It is tempting to raise the cylinder to cube strength ratio to 0.75 and thereby achieve identical mean values in the two data sets. Because the strain-rate is unknown, although brittle, in the Danish tests, it cannot be argued that the two mean values

should be equal. The ratio of 0.67 remains the most commonly used value.

The salinities appear identical except perhaps for the minimum values, which is less significant. This is somewhat surprising since the water bodies have distinctly different salinities, viz.: 16-20 ppt in the Great Belt versus 2-4 ppt in the Bay of Bothnia. Part of the explanation lies in the growth process. While growing, the ice rejects salt from its underside and only traps a limited amount when neighbouring fingers of the skeleton layer join to form a brine pocket. Thus as long as the water salinity exceeds typical ice salinities of say 2 ppt, the ice will filter out the excess salt in the growth process. According to Cox and Weeks (1988) salt entrapment during ice growth is proportional to the growth rate. In the present case this may be balanced by the difference in water salinities. Brine drainage will also cause salinities to be similar.

The temperatures clearly show the difference in latitude with the Bay of Bothnia having the lower temperatures. This difference in ice temperatures need not be a problem if the expressions (11) and (12) are capable of extracting the effects of the temperature correctly. This is investigated in a (σ_o, T_i) bias plot, see Figure 1. A salinity (σ_o, S_i) bias plot is also made, see Figure 2.

There are no visible differences in the distributions of σ_o between the two data sets shown in the bias plots. Although the temperatures of the Swedish test samples are generally lower

than the temperatures of the Danish test samples, cf. Table 1 and Figure 1, there is no indication of differing distributions. The same holds true for the salinity plot. Note furthermore that extreme values of T_i and S_i do not coincide with extreme values of σ_o and vice versa.

The agreement between the data sets is good for mean values. The Swedish standard deviation is slightly larger than the Danish one. This can be related to the strain rate as well as the choice of multiplication by 0.67 to obtain cylinder strengths. Due to the good agreement, it was decided to base the σ_o distribution on the joint data set. It would be desirable to include even more data, but none were accessible within the available time-frame.

The present ensemble of Danish and Swedish tests is a compromise. From a purely scientific point of view, the Danish measurements should be discarded, because the strain rates are unknown. Ideally, all scientific measurements of compressive ice strengths (meaning those with fully documented test conditions) from anywhere in the world should be included as long as they were made with appropriate ice types. The Swedish data give some confidence that the Danish measurements are reasonable. The Danish tests are included because they represent waters relatively close to the Great Belt. Through the comparisons in Table 1, they give some confidence that the Swedish data set is applicable, because of the nearly identical parameters. The agreement between the two sets of data is shown in Figs. 1 and 2.

When two data sets are used to validate each other, the validation is of limited value. It is therefore desirable to compare with a broader spectrum of values obtained in scientific measurements. One of the best references for that purpose is an article by Timco and Frederking (1990), published shortly after the completion of this extreme value analysis. The article analyses 283 small-scale measurements of compressive strength of first-year sea ice to formulate an empirical model which gives good results when compared to large-scale measurements. The above data and the final results of this extreme value analysis are in good agreement with the large ensemble of scientific measurements analysed by Timco and Frederking (1990). By 'agreement' we mean that thicknesses, temperatures, strain rates and strengths relate well to each other. The absolute values of extreme ice strengths in the Great Belt need obviously not equal the average values of the 283 tests above.

A Weibull distribution was fitted to the joint set of data on reference strengths. Through a least-squares fit distribution parameters of $\beta = 2.844$ and $k = 2.749$, cf. eq. (4), were determined. Statistical model uncertainty has not been included in the present investigation. Only central estimates have been calculated. Distributions have been fitted by the least squares method. This is assumed to be permissible. A comparison with maximum likelihood estimation and moment estimation results would be interesting, but the effects are assumed to be moderate, and the comparisons have therefore not been carried out.

ICE THICKNESS AND X-DISTRIBUTION

The specific expression for the x parameter corresponding to the general expression (8) becomes:

$$x = \left(1-\left(\frac{(0.532-(49.185/T_i))S_i}{275}\right)^{\frac{1}{2}}\right)0.032(K-50)^{\frac{1}{2}} \qquad (13)$$

where T_i is in Celsius degrees and negative, S_i is in ppt, K is in accordance with eq. 6, and x comes out in meters. This expression can easily be calculated day by day once $\Sigma(-\bar{T}_a)$ exceeds 50. The latter part representing thickness of the ice obviously has a direct effect on the values of x, and it consequently is important to check whether this theoretical expression describes nature well or not. This is investigated in two ways: By comparing with extreme observations from the past 80 years and by comparing with a larger amount of observations near the site of the future bridge.

Annual maximum observations of ice thickness at various locations have been reported in annual bilingual (Danish and English) publications by Statens Istjeneste in the period 1907-86. Locations of interest are shown in Figure 3 for the entire Great Belt and in Figure 4 for the immediate vicinity of the bridge. Observations from the 5 coldest winters in the 80 winters surveyed are shown in Table 2 together with theoretical thicknesses calculated from eq. (7). A reasonable agreement is found. In the coldest winter, 1941-42, the agreement is excellent. In the other 3 winters, eq. (7) appears to slightly overpredict the thickness, but since there is no guarantee of all ice thicknesses

being smaller than the largest thickness observed, this has not resulted in modifications to the expression for x in eq. (13).

Observations near the site of the future bridge have been plotted against the total amount of freezing degree-days for the relevant winters in Figure 5. As indicated in the figure, equation (7) yields ice thicknesses above the best fit to the data, especially for shorter recurrence times. For longer recurrence times the difference vanishes, and this general trend may also be seen in Table 3. The figure furthermore shows that the best fit curve is non-conservative with respect to the data from the Western Channel. Consequently, equation (7) was maintained as a reasonable estimate of the ice thickness. It is worth noting that the factor 0.032 in equation (7) is larger than corresponding factors used in the Arctic.

The problem is then reduced to determining the x-distribution. The development of x through the winter is of limited interest for design. The maximum value from each winter is used to determine design values. The maximum x typically occurs when K has reached about 90% of its final value for the winter. The end of the winter tends to be warmer and thus the maximum x occurs slightly before the maximum or final K.

One of the most serious shortcomings of the preliminary analysis (Christensen et al. 1989) was that the temperature records only covered 19 winters. It was therefore decided to use as many data as possible from nearby measurement stations in the final analysis. From the nearby Røsnæs lighthouse eight temperature

readings per day are available from 1960 onwards. Additional data from Bogø were used for the period 1875-1960. The Bogø station is located about 60 kilometres EastSouthEast of the future bridge, but it is considered representative of temperature conditions at the bridge. The Bogø data contain three daily readings plus a minimum and a maximum reading. The average of the latter two was used as a daily mean value.

The national mean air temperature for each of the winters 1875-1989, defined as Dec. 1st through March 31st, is shown in Figure 6. The figure reveals a relatively mild winter climate and significant interannual variations. These variations were indeed the reason for the preliminary analysis giving unrealistically low design values. It is assumed that the temperature variations can be considered stochastic realizations of a stationary process. Hence, no trend towards a different climate is taken into account.

A 114 year temperature record may seem excessively long, but with design probabilities of exceedance in the range $2x10^{-5}$-$4x10^{-5}$ per year this is not the case. Furthermore, calculations to obtain design values based on two different 30-year periods resulted in extreme values a factor of two apart. Those calculations are not shown here. In the more severe ice winters with relatively thick ice it normally takes about 3-4 days of low temperatures for the temperature profile in the ice to adjust so that the mean value corresponds to the mean of the surface and bottom temperatures of ice. The x values were therefore computed by using average temperatures of the last 3 days. This

reduces the final result by about 10% compared to an analysis using individual day averages. It was decided to use a constant salinity of 1.5 ppt for the ice in the Great Belt. Timco and Frederking (1990) found decreasing gross salinities with increasing thickness. This is not taken into account in the present analysis.

Accurate temperature simulations could have been carried out, e.g. as suggested by Schwarz and Miloh (1972), but because of lack of time it was decided to use the 3-day average temperatures and add a sensitivity analysis. More complex thermodynamic models of ice growth could have been used, e.g. as suggested by Maykut and Untersteiner (1971), by Miller (1981) or by Cox and Weeks (1988). The lack of the necessary data precluded use of these models, however.

The 114 maximum values of x were divided into groups and averaged within each group such that only about 20 points remain for determination of the distribution as shown in Figure 7. The grouping procedure was introduced in order to give equal weight to the information at either end of the curve. Without the grouping, the lower end would have a dominant effect on the best fit distribution. In addition, Figure 7 shows that the extreme maximum values follow another distribution than the maximum values at the lower end. The dashed line indicates the differing lower end distribution. It was also found that the extreme values of maximum x occur at low temperatures and not for temperatures close to the freezing point. Figure 7 is a Weibull plot,

but the Gumbel distribution may be just as relevant for describing the variations. The distribution functions are:

$$F_W(x) = 1-\exp(-(\frac{x}{\beta})^k) \tag{14}$$

$$F_G(x) = \exp(-\exp(-a(x-b))) \tag{15}$$

where the subscripts refer to the distribution names and (β,k,a,b) are distribution parameters to be determined from e.g. least squares fit to the data. A χ^2-test is performed to determine which of the two distributions best fit the data. This means calculating a verification parameter, P, for each distribution as:

$$P = \frac{1}{n-1} \sum_{i=1}^{n} (P_i-P_d)^2 \tag{16}$$

where P_i is the theoretical value according to the distribution function and P_d is the actual value based on the data. The count parameter i runs over the number of points to be fitted to. Because of the interest in extreme values, the χ^2-test is performed in conjunction with the Peaks-Over-Threshold (POT) analysis instead of over all data points.

POT ANALYSIS

A Peaks-Over-Threshold (POT) analysis is performed for the parameter x, being the standard statistic method for extreme statistics. The idea behind this analysis is that only extreme

events belonging to the same family are considered. All non-extreme data are excluded.

The POT-analysis result is a function of the threshold chosen and it is therefore performed with different thresholds both by use of the Weibull distribution function $F_W(x)$, and by use of the Gumbel distribution function $F_G(x)$. If the variation of the extreme values is small and non-systematic for different thresholds, then the confidence in the results from the POT-analysis will be good.

In the present analysis, the value with an exceedance probability of 2×10^{-5} per year was the one to be determined. (It was later shifted to 4×10^{-5} per year and might even shift again. The reasons behind the use of such extreme exceedance probabilities were explained by Christensen et al. (1989)). The 2×10^{-5} per year corresponds to an <u>average</u> recurrence time of 50,000 years, and a distribution function value $F(\sigma_u h) = 0.99998$. This design value of $\sigma_u h$ was computed using all data points in Figure 7 above a threshold, x_{th}, and the results are shown in Table 3 for different thresholds. Both the Weibull distribution function and the Gumbel distribution function are used, and the χ^2-test (according to (16)) is performed to decide which of the two distribution functions that are modelling the x-variation with highest accuracy.

From Table 3 it is seen that the Gumbel distribution gives results that are 10-20% larger than the results from the Weibull distribution. When the Weibull and Gumbel distribution functions

are compared with the data for large values of x it is found that the Gumbel distribution is below the actual data while the Weibull is above. It was therefore decided to base the design value of $\sigma_u h$ on a weighted average between the two distributions, and to use the values of the verification parameters as weights.

Table 3 is a good example of the importance of the theoretical expression of the distribution function when determining extreme values. At a threshold of x = 0.28 the two distributions give design values that are 16% apart, viz.: 2.65 and 3.08 MN/m, based on the exact same data. Note also that both distributions yield $\sigma_u h$ design values which vary non-systematically with x_{th}. This indicates that both distributions describe the general variation of the data well.

The weighted design value of $\sigma_u h$ was with $x_{th} = 0.28$ determined from

$$\frac{205}{343} F_G(\sigma_u h) + \frac{138}{343} F_W(\sigma_u h) = 2 \times 10^{-5} \qquad (17)$$

where after a few iterations it was established that:

$$\sigma_u h = 2.96 \text{ MN/m} \qquad (18)$$

This is the central result of the extreme value analysis. It is, however, necessary to break the product into a strength and a thickness in order to continue with accurate load calculations. Equation (7) was found to describe maximum ice thicknesses well, cf. Table 2. Christensen (1987) found that the K index for Danish domestic waters may be expressed as:

$$K = 103.8\ (\ln(A)+0.04)\ ^{o}C\text{-days} \tag{19}$$

where A is the average recurrence time in years and K is in Celsius degree-days. For the design situation, the equation (19) gives K = 1127^{o}C-days. As mentioned earlier the maximum x typically occurs when K has reached 90% of its final value for the winter. With K = 0.9x1127 = 1014^{o}C-days the thickness is calculated from eq. (7) and the strength is determined by dividing the product $\sigma_u h$ with the thickness. The results are:

$$h = 0.99 \text{ m} \tag{20}$$

$$\sigma_u = 3.0 \text{ MPa} \tag{21}$$

Other breakdowns of the product in eq. (18) are possible. The selected one agrees well with e.g. Timco and Frederking (1990), see their Figure 10 where a thickness of one meter and a strain rate of $2x10^{-4}sec^{-1}$ gives a compressive ice strength close to 3.0 MPa.

Results for various recurrence times are shown in Table 4. For a 10-year recurrence time, the POT-analysis method gives $\sigma_u h$=0.81 MN/m, h=0.42m, σ_u=1.93 MPa, when the double distribution in Fig. 7 is used. The POT-analysis method, however, is suited for extreme recurrence times, and the 10-year value should thus be regarded with caution. Comparison with the preliminary results described by Christensen et al. (1989) shows that the extension of the temperature records to include 114 years resulted in a substantial increase of the design values.

SENSITIVITY ANALYSES

According to Frankenstein & Garner (1967) a more accurate estimate of the relative brine volume ν of the ice than the one given by eq. (12) can be computed by:

$$\nu = (1.189 - 43.795/T_i)S_i/1000, \quad -22.9^oC \leq T_i \leq -8.2^oC \quad (22a)$$

$$\nu = (0.930 - 45.917/T_i)S_i/1000, \quad -8.2^oC \leq T_i \leq -2.06^oC \quad (22b)$$

$$\nu = (-2.28 - 52.56/T_i)S_i/1000, \quad -2.06^oC \leq T_i \leq -0.5\ ^oC \quad (22c)$$

When (22) is used instead of (12) to evaluate ν when the σ_o values are computed, the relative changes in the mean value and standard deviation of the σ_o distribution are less than 1%. Hence it is concluded that (12) is adequate for computing ν in this analysis.

In order to investigate the relative importance of the largest measured σ_o values, computations were carried out with the upper integration limit in (10) lower than infinity (which of course is necessary when a numerical integration is performed). The upper integration limit is chosen to be so large that the truncation error from the numerical integration is immaterial. A numerical integration of the probability density function $f(\sigma_o)$, which was given as a Weibull distribution, from 0 to 8 gives a difference of $1.5 \cdot 10^{-9}$ from the exact value 1. In the computations performed in this report the upper integration limit is chosen as large as 20, and the numerical quadrature is performed with 10000 points between 0 and 20.

The maximum x-values have been computed using mean air temperatures for 1, 3 and 5 day intervals. This gives a variation of the largest value of x computed in the period 1874/75 - 1988/89 between 0.5149 meter for 1 day intervals, 0.5108 meter for 3 day intervals and 0.4911 meter for a 5 day averaging interval.

If the data in Figure 7 are considered a single population, then a POT analysis is sufficient to predict the extreme values. If, on the other hand, they are considered two populations, then the extreme occurrence in both populations must be calculated. If the division point is located at the 75% fractile, then the relevant extreme value of the lower distribution is the $0.75 \cdot 50000 = 37500$ years event in that distribution after integration as specified in eq. (10). This value has been computed as:

$$(\sigma_u h)^* = 1.96 \text{ MN/m} \tag{23}$$

and is thus smaller than that resulting from the POT-analysis. Hence it is concluded that the results from the POT-analysis are conservative with regard to the distribution of the parameter x.

SNOW COVER

The effect of a snow cover on the ice has not been included in the analysis until this point. Because of the good agreement between observed and calculated thicknesses demonstrated in Table 2, it was decided not to include the snow cover in the

theoretical model for ice growth. An additional reason for this is the total lack of sufficient statistics for snow layer thickness, h_s, over sea ice in Danish waters. Instead only the warming effect is included.

The presence of a snow layer will raise the mean ice temperature somewhat. Denoting the thermal conductivities of ice and snow by λ_i and λ_s, respectively, enables expression of the heat flux as a function of the thickness and temperatures, and after some simple calculations the temperature T_I at the ice--snow interface can be expressed by:

$$T_I = \frac{\lambda_s h\, T_a + \lambda_i h_s T_w}{\lambda_s h + \lambda_i h_s} \qquad (24)$$

where T_w is the temperature of the ice-water interface. The thermal conductivities of ice and snow were taken as:

$$\lambda_i = 2.24 \text{ W/(m}^\circ\text{C)} \qquad (25)$$

$$\lambda_s = 2.84 \cdot 10^{-6} \rho_s^{\,2} \text{ W/(m}^\circ\text{C)}, \quad 140 < \rho_s < 340 \text{ kg/m}^3 \qquad (26)$$

where ρ_s is the density of snow, cf. Bergdahl (1977). The density ρ_s and thickness h_s of the snow cover must be estimated. The density of snow varies over a broad range (from 50 kg/m^3 (new snow in still air) to more than 400 kg/m^3 (consolidated snow). In this analysis a value of 280 kg/m^3 is used. This is an average value for windtoughened snow (Gray & Male, 1981). Sensitivity calculations are carried out with a lower value (ρ_s = 200 kg/m^3) and a higher value (ρ_s = 340 kg/m^3) in order to investigate the effect of snow density. The thickness of the snow layer

is estimated based on a mean value of the snow thicknesses from the 10 coldest winters in the period 1938-1988. Daily measurements of snow thicknesses (measured at 8:00 a.m.) are available from 1938 onwards in "Meteorologisk Årbog" published by the Danish Meteorological Institute. Data from three different locations were used and a weighted mean value of the snow thicknesses was 9.7 cm.

This snow thickness was computed on the basis of measurements on open land. The retention coefficient relative to open land is for sea ice 0.4-0.5 (Gray & Male, 1981), thus providing an estimate of the mean snow thickness on the ice sheet as:

$$h_s = 4 \text{ cm} \tag{27}$$

This value was used in the computations. For sensitivity analyses snow thicknesses of 3 cm and 5 cm were also used as input for the computations.

The design value of $\sigma_u h$ is as in the preceeding analysis found as the weighted mean of the design values coming from POT-analyses made with use of the Gumbel- and the Weibull distributions, respectively. The results are shown in Table 5 with the central calculation giving a product of 2.82 MN/m.

A similar calculation for the 25,000 year situation using h_s = 4 cm and ρ_s = 280 kg/m^3 resulted in a product $\sigma_u h$ of 2.67 MN/m. With an ice thickness of 0.96 m, cf. Table 4, the compressive ice strength becomes 2.78 $\approx$ 2.8 MPa. The above analysis

of the effect of a snow cover on sea ice strengths is fairly simple, and a number of questions have been left open. Because of the complexity of the problem it is necessary, however, to use professional judgement to some extent. Reductions in the area of 5% as indicated by Table 5 (relative to the $\sigma_u h = 2.96$ MN/m found without snow) is seen as reasonable.

Equation (7) gave a good estimate of ice thicknesses, cf. Table 2, even though it was based on a fairly simple model, i.e. one-dimensional heat conduction. The addition of a snow layer reduces ice growth significantly. The agreement therefore means either that there is very little snow or that other effects balance the insulating effect of the snow. Both are plausible explanations. A short warming can melt the snow or winds can deposit it in snow drifts leaving large areas without snow. These snow-free areas would grow the largest ice thicknesses, and it is precisely those which are reported in Table 2. The bottom line, however, is that equation (7) gives good agreement with observations. Because of that, it was decided to only include the warming effect on the strength and not on the growth.

An important question is the appropriateness of the mean snow thickness. Many arguments have been weighed: a) extreme winters have northeasterly dry winds with little precipitation, b) extreme winters have few or no thaw periods and thus allow a long continuous snow accumulation without intermittent melting, c) local spatial variations of snow thickness will leave some areas without the insulating snow cover or at least with a reduced snow depth, and d) can snow data from the selected loca-

tions be used as representative? All of these have been weighed, and in the light of lack of sufficient data for a scientific approach, professional judgement was used. This led to the use of h_s = 4 cm with only the warming effect included.

CONCLUSION

An extreme value analysis of ice properties in the Great Belt in Denmark has been carried out. For an annual exceedance probability of 2×10^{-5} an ice thickness of 0.99 meter and a uniaxial compressive ice strength of 2.8 MPa was found, when a snow cover was included in the analysis. Results for larger exceedance probabilities were also given.

Certain conservative assumptions mean that the above values should be considered a "best conservative" estimate rather than a central estimate. Some of these conservative assumptions are the ignoring of thaw periods when accumulating K in eq.(6) and the assumption of a stationary stochastic process, i.e. that climatic trends are disregarded.

A method of circumventing the problem of correlation between ice thickness and ice strength was introduced by splitting their product in temperature dependent and independent parts. The distribution of reference strength proved similar for the Great Belt and the Bay of Bothnia which are 1000 km apart. The analysis relies heavily on air temperature records and is thus well suited for areas with scarce ice information.

The effects of the testing machines on the standard deviations in the reference strength distributions have not been analysed.

ACKNOWLEDGEMENT

The presented analysis was carried out on behalf of the Great Belt Link Ltd. Their permission to publish the result is gratefully acknowledged.

APPENDIX I. REFERENCES

Bergdahl, L. (1977),"Physics of Ice and Snow as Affects Thermal Pressure", Report Series A:1, Dept. of Hydraulics, Chalmars University of Technology, Sweden.

Christensen, F.T. (1986), "Sea ice strength measurements from the inner Danish Waters in early 1985". Proc. first international Ice Technology Conference (ITC-86), pp. 247-253, MIT, Cambridge, Massachussetts, USA.

Christensen, F.T. (1987), "Temporal variations of freezing degree-days in Danish domestic waters", Proc. 9th int. conf. on Port and Ocean engineering under Arctic Conditions (POAC-87), Vol. 3, pp. 201-206, Fairbanks, Alaska, USA.

Christensen, F.T., N.E. Ottesen Hansen, K.-U. Evers, S. Spangenberg and L.J. Vincentsen (1989), "Design of the Great Belt Western Bridge for Ice Forces", 8th int. conf. on Offshore Mechanics and Arctic Engineering (OMAE-89), Vol.4, pp.365-376, the Hague, the Netherlands.

Cox, G.F.N. and W.F. Weeks (1982), "Equations for determining the gas and brine volumes in sea ice samples", Report 82-30, Cold Regions Research and Engineering Laboratory, Hanover, New Hampshire, USA.

Cox, G.F.N. and W.F. Weeks (1988), "Numerical simulations of the profile properties of undeformed first-year sea ice during the growth season", J. Geophysical Research 93(c10):12449-12460.

Frankenstein, G.E. & R. Garner (1967), "Equations for determining the brine volume of sea ice from -0.5°C to -22.9°C", Journal of Glaciology, Vol. 6, No. 48, pp. 943-944.

Fransson, L. & L. Elfgren (1987), "Horizontal uniaxial compressive strength of low-salinity sea ice in the Gulf of Bothnia", Proc. 9th Int. Conf. on Port and Ocean Engineering under Arctic Conditions (POAC-87), vol. 3, pp. 21-29, Fairbanks, Alaska, USA.

Gray, D.M. & D.H. Male (eds.) (1981), "Handbook of Snow", Pergamon Press.

Maykut, G.A. and N. Untersteiner (1971), "Some results of time-dependent thermodynamic model of sea ice". J. of Geophysical Research, 76(6): 1550-1575.

Miller, J.D. (1981), "A simple model of seasonal sea ice growth". Transactions of the ASME, Vol. 103, pp. 212-218.

Mortensen, P. & R. Zorn (1982), "Isundersøgelse Farøbroerne 1982"(in Danish), Report from Danish Hydraulic Institute to Christiani & Nielsen, Consulting Engineers, Copenhagen.

Schwarz, J. and T. Miloh (1972), "On the time dependent temperature variations within ice sheets", Proc. Int. Assoc. of Hydr. Res. (IAHR) Ice Symposium, pp. 262-269, Leningrad, USSR.

Statens Istjeneste (1986),"Ice and Navigational Conditions in the Danish Waters during the Winter 1985-86", published by Statens Istjeneste in Denmark, ISSN 0106-5076.

Timco, G.W. & R.M.W. Frederking (1990),"Compressive strength of sea ice sheets", Cold Regions Science and Technology, vol. 17, No. 3, pp. 227-240.

Tryde, P. & R. Zorn (1979), "Isstyrkemåling i indre danske farvande i vinteren 1978-79" (in Danish), Report from Institute of Hydrodynamics and Hydraulic Engineering at Technical University of Denmark and Danish Hydraulic Institute to the Danish Technical Research Council.

Weeks, W.F. & A. Assur (1969), "The mechanical properties of sea ice", Cold Regions Science and Engineering, Part II, Section C (Old CRREL Monograph Series), Cold Regions Research and Engineering Laboratory, Hanover, New Hampshire, USA.

APPENDIX II. NOTATION

The following symbols are used in this paper

a	parameter in Gumbel distribution
b	parameter in Gumbel distribution
f	probability density function
f_h	function expressing h by k
f_σ	function of T_i and S_i
F	probability distribution function
F_G	Gumbel distribution function
F_W	Weibull distribution function
h	ice sheet thickness
h_s	snow layer thickness
k	parameter in Weibull distribution
K	freezing degree-days index
P	verification parameter
P_d	distribution function based on data
P_i	distribution function based on theory
P_G	verification parameter for Gumbel distribution
P_W	verification parameter for Weibull distribution
S_i	gross ice salinity
t	time
T_a	air temperature
T_i	mean ice temperature
T_I	temperature at ice-snow interface
T_w	temperature at ice-water interface
x	temperature dependent part of $\sigma_u h$
x_{th}	threshold value in POT-analysis
ß	parameter in Weibull distribution
λ_i	thermal conductivity of ice

λ_s thermal conductivity of snow

ν relative brine volume in the ice

ρ_s density of snow

σ_u uniaxial compressive ice strength

σ_o reference compressive ice strength

FIGURE CAPTIONS

Fig. 1 Temperature T_i vs. reference strength σ_o for the Danish and the Swedish tests.

Fig. 2 Ice salinity, S_i vs. reference strength σ_o for the Danish and the Swedish tests.

Fig. 3 Locations for ice thickness observations in the entire Great Belt; 1: Røsnæs Lighthouse, 2: Kerteminde Bay, 3: Lohals, 4: Keldsnor, 5: West of Albuen, 6: Nakskov outer Fiord, B: Bridge

Fig. 4 Locations for ice thickness observations near the site of the future bridge; 7: Nyborg Harbour, 8: Nyborg Fiord, 9: Western Channel, 10: Eastern Channel, 11: Access to Korsør Harbour, 12: Korsør Harbour.

Fig. 5 Maximum observed ice thicknesses (annually) versus number of freezing degree days according to Statens Istjeneste.

Fig. 6 Mean air temperature in each winter during the period 1874/75-1988/89. The solid curve shows a centered 30 years average winter temperature. (Figure courtesy of the Danish Meteorological Institute).

Fig. 7 Annual exceedance probability for x based on temperature data from 1875-1988. The data points correspond to the upper limits of the division intervals.

TABLES

	Mean value	Standard dev.	min	max
Reference strength:				
Swedish σ_o (MPa)	2.76	1.07	1.49	6.51
Danish σ_o (MPa)	2.44	0.86	1.31	5.27
Joint σ_o (MPa)	2.61	0.99	1.31	6.51
Salinity:				
Swedish S_i (o/oo)	1.85	1.00	0.00	3.78
Danish S_i (o/oo)	1.69	0.95	0.8	3.5
Temperature:				
Swedish T_i (^oC)	-4.01	1.87	-10.0	-1.0
Danish T_i (^oC)	-1.88	0.82	- 4.1	-0.9

Table 1 Comparison of the Danish and Swedish measurements regarding reference strength, salinity and temperature.

Location		Kerte-minde Bay	Nyborg Harbour	Nyborg Fiord	Lo-hals	Keld-snor	West of Albuen	Nak-skov outer Fiord	Eq.7
Year	K_{max}								
1941-42	497.5	65	60	-	-	-	65	67	64
1946-47	378.0	45	50	50	40	44	-	48	55
1939-40	368.5	-	35	50	-	-	-	30	54
1962-63	300.3	-	-	-	-	-	-	-	47
1940-41	290.7	40	35	45	-	-	25	37	47

Table 2 Measured ice thicknesses (in cm) at locations in the vicinity of the future bridge during the 5 coldest winters in the period 1907-86 compared with the results from eq. (7).

x_{th} (m)	0.22	0.23	0.24	0.25	0.26	0.27	0.28
No.data	29	26	23	17	14	12	11
$\sigma_u h$(We)	2.60	2.66	2.80	2.71	2.65	2.60	2.65
$\sigma_u h$(Gu)	3.32	3.35	3.42	3.33	3.21	3.04	3.08
P_W	0.0095	0.0075	0.0031	0.0051	0.0095	0.0208	0.0205
P_G	0.0063	0.0058	0.0035	0.0051	0.0071	0.0111	0.0138

Table 3 Design values of $\sigma_u h$ from a POT-analysis with Weibull and Gumbel distributions. The product $\sigma_u h$ is in MN/m.

RETURN PERIOD (Years)	50	100	1000	10000	25000	50000
$\sigma_u h$ (MN/m)	1.26	1.48	2.05	2.58	2.82	2.96
K^u (^oC-days)	410	482	721	960	1055	1127
h (m)	0.57	0.63	0.78	0.91	0.96	0.99
σ_u (MPa)	2.21	2.35	2.63	2.84	2.94	2.99

Table 4 Results for various recurrence times excluding the effect of a snow cover on the ice.

ρ_s	h_s 3.0 cm	4.0 cm	5.0 cm
200 kg/m^3	2.76	2.71	2.66
280 kg/m^3	2.85	2.82	2.78
340 kg/m^3	2.89	2.86	2.84

Table 5 Design values of $\sigma_u h$ in MN/m for various values of the snow density ρ_s and snow thickness h_s.

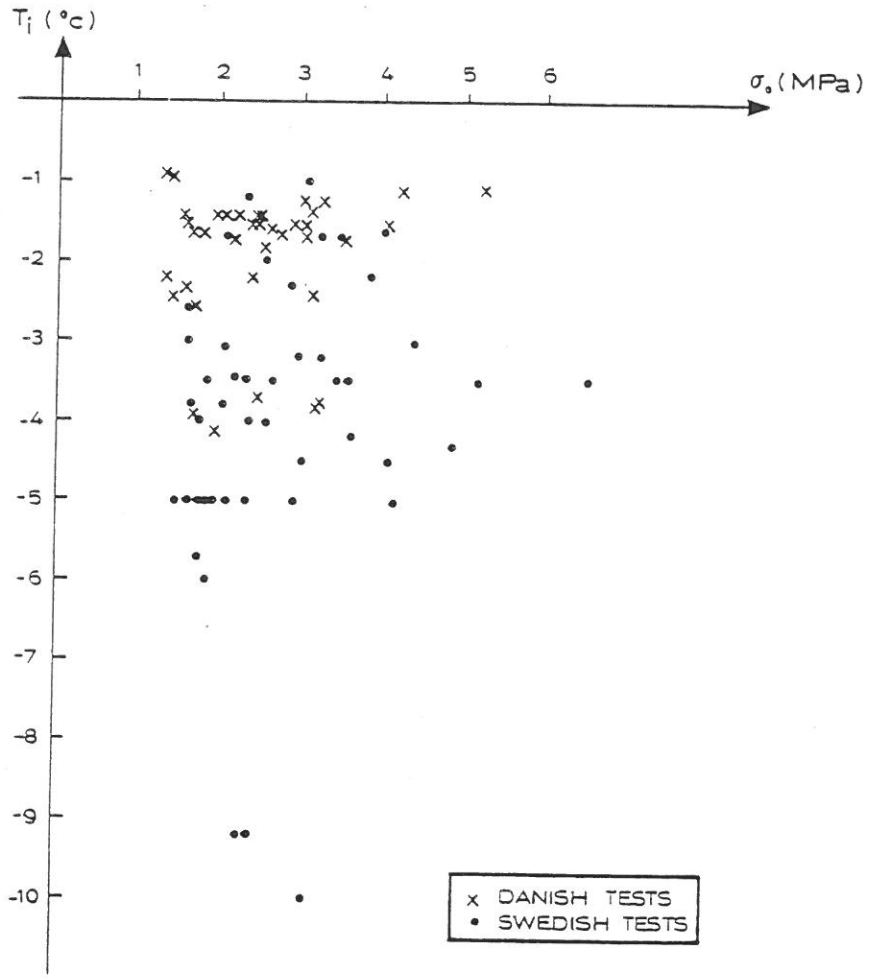

Christensen and Skourup
Extreme Ice Properties
Figure 1

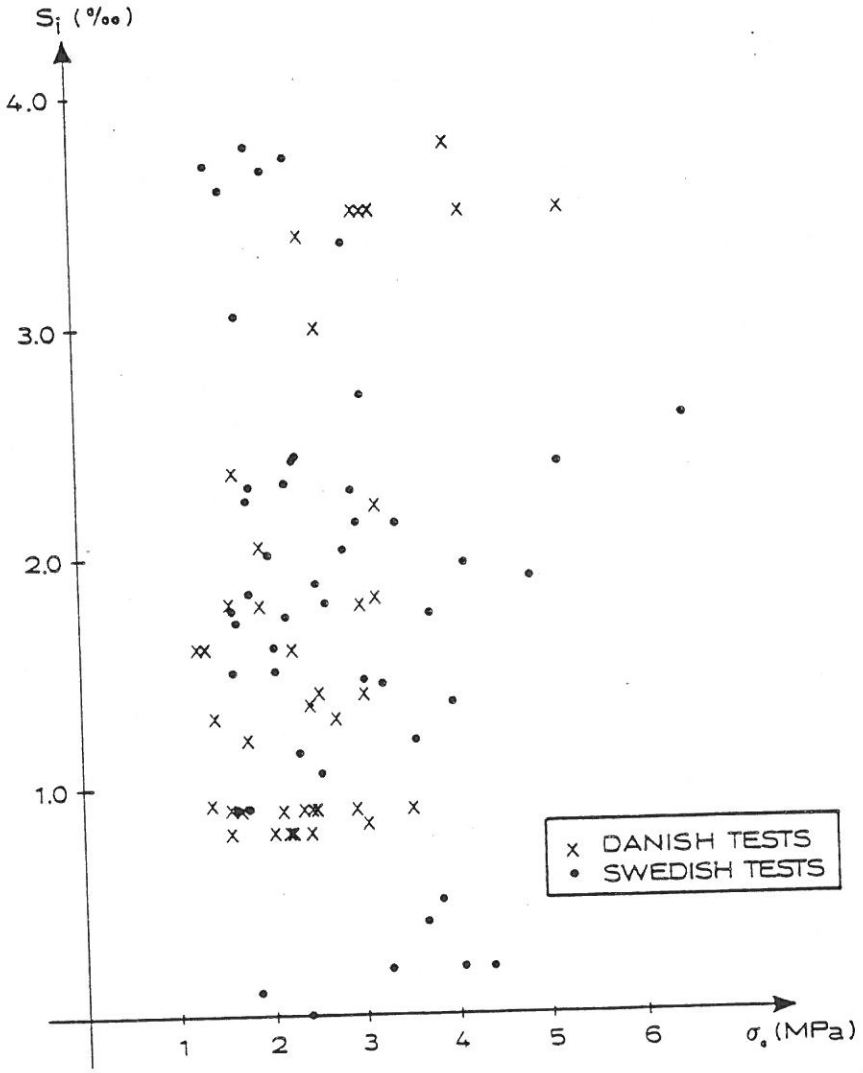

Christensen and Skourup
Extreme Ice Properties
Figure 2

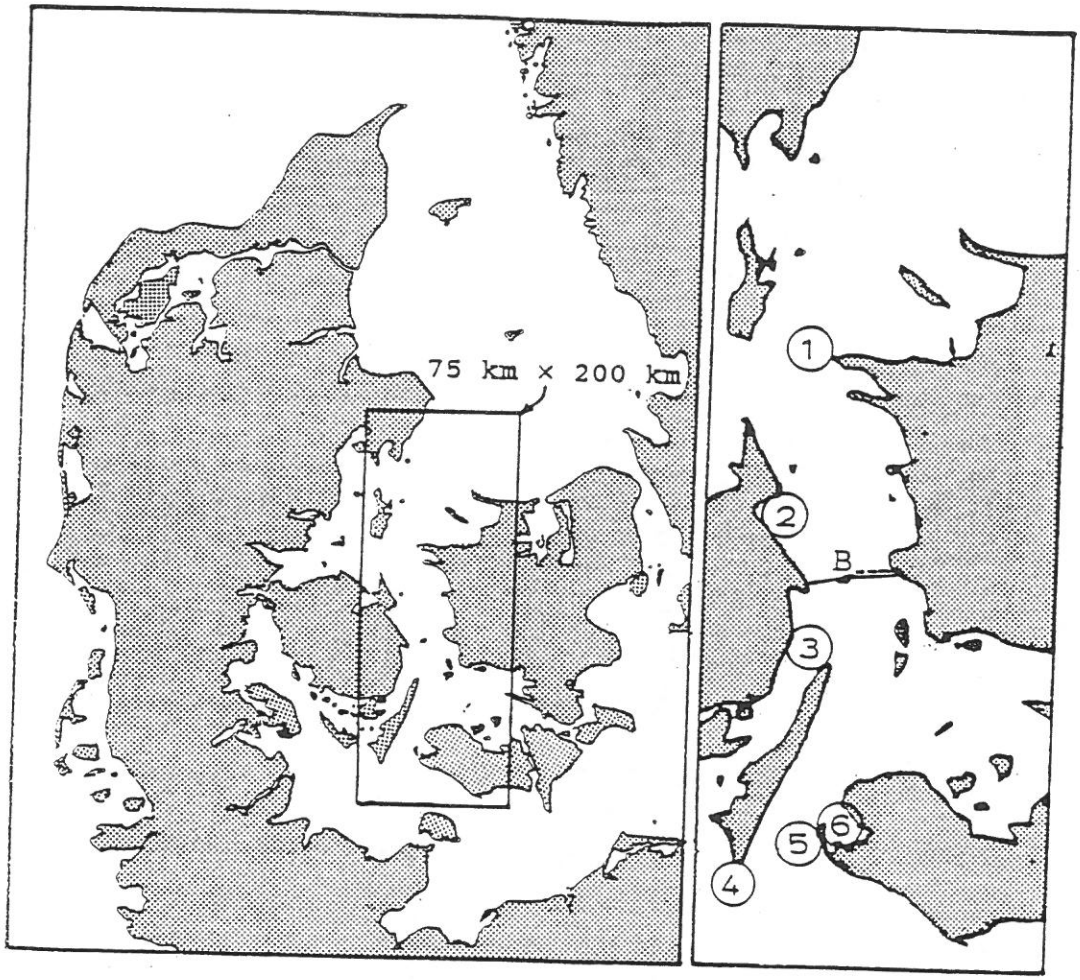

Christensen and Skourup
Extreme Ice Properties
Figure 3

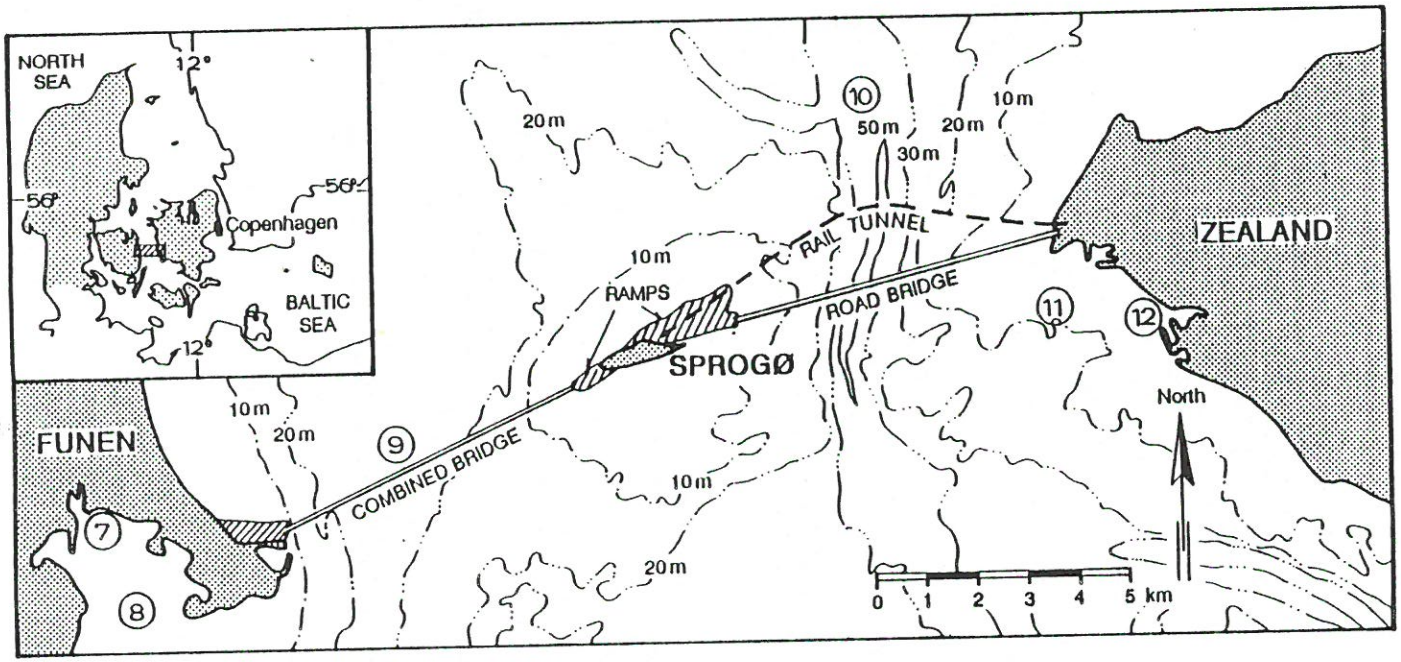

Christensen and Skourup

Extreme Ice Properties

Figure 4

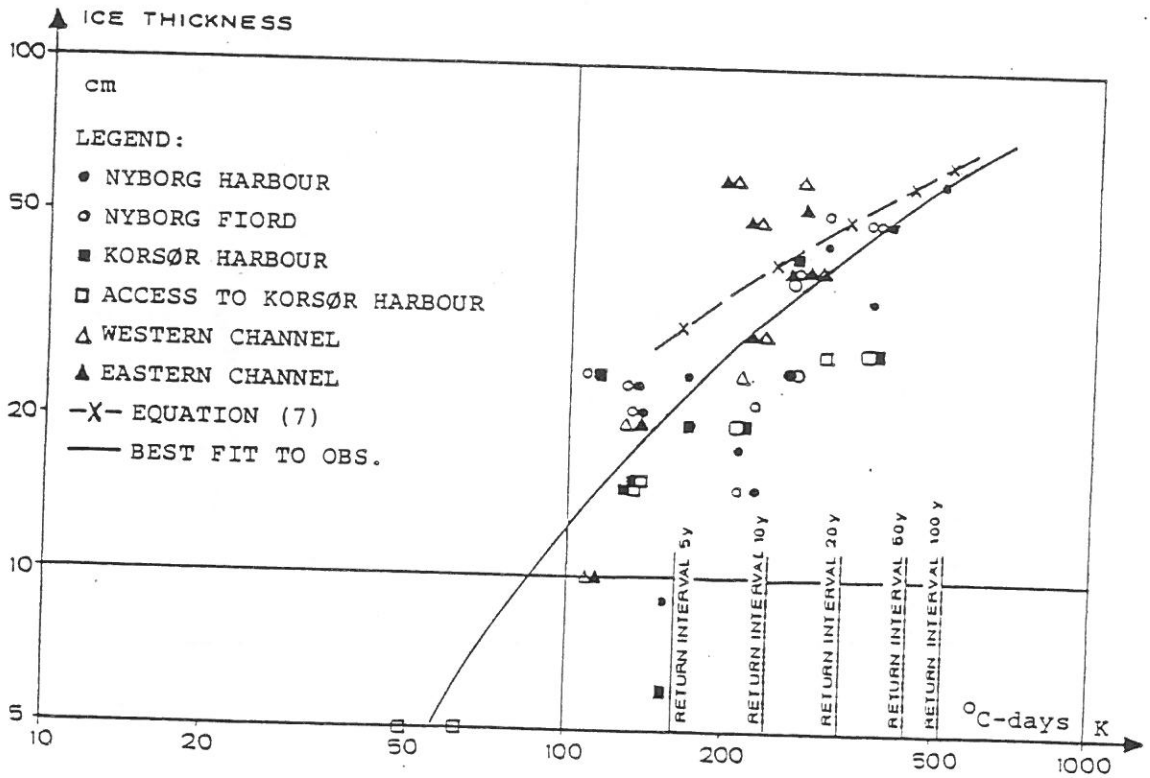

Christensen and Skourup
Extreme Ice Properties
Figure 5

Christensen & Skourup
Extreme Ice Properties
Figure 6

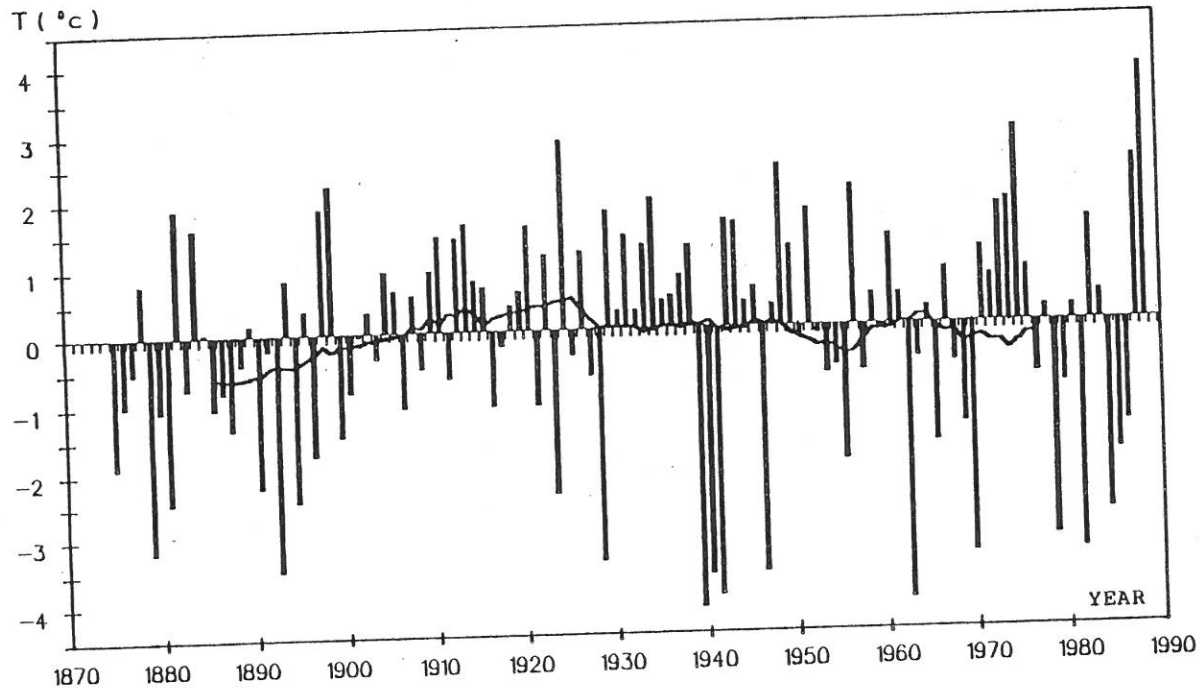

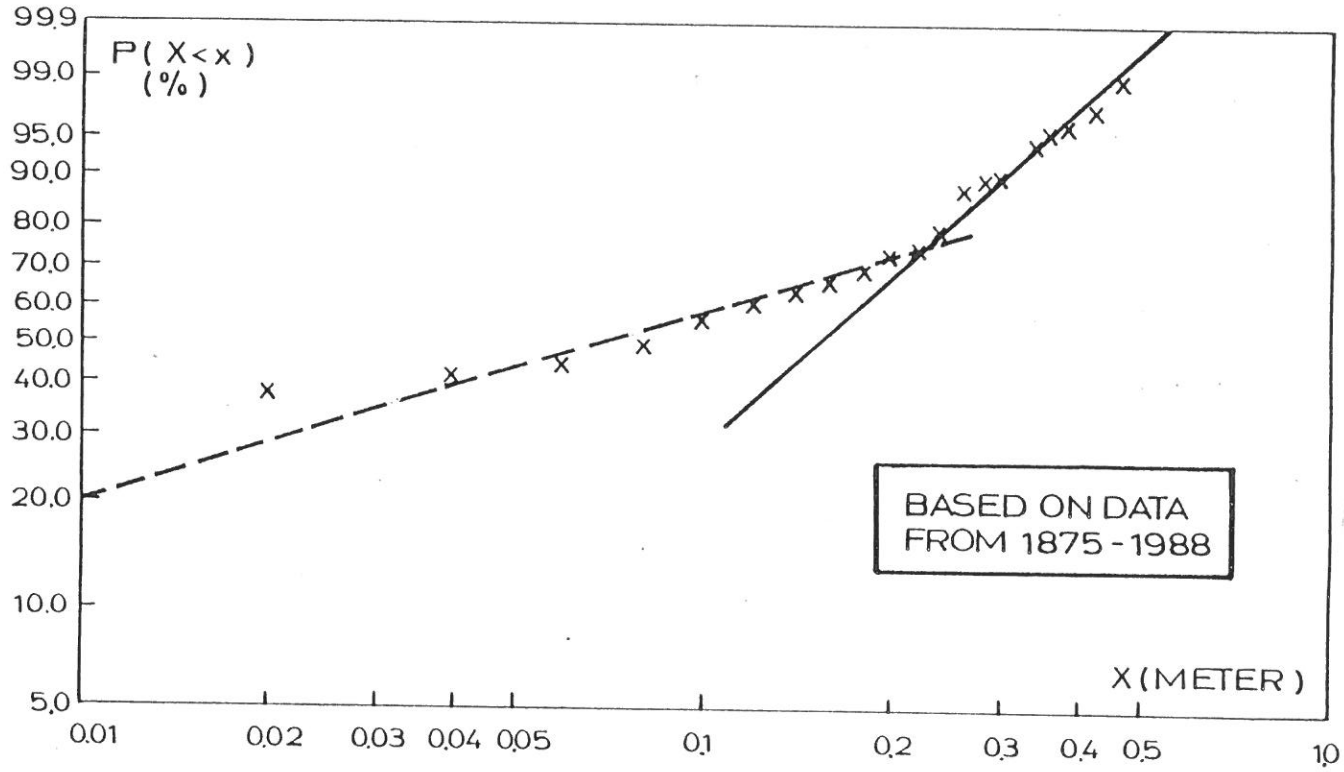

Christensen and Skourup
Extreme Ice Properties
Figure 7

2. GREAT BELT, FOUNDATION OF THE WEST BRIDGE

Great Belt - Foundation of the West Bridge

by

Per S. Kristensen, Lars Erichsen and Carsten S. Sørensen,
COWIconsult, Denmark

Synopsis: This paper describes aspects of the soil investigations and geotechnical evaluations for the foundation design of the 6.6 km long Great Belt West Bridge. The gravity foundations rest predominantly on glacial tills and prequaternary limestone. Special investigations for assessment of the soil properties for ship impact and ice loading are described briefly, and first experiences from settlement monitoring of the structure during erection are presented.

INTRODUCTION

The Great Belt is part of the inland sea area and approximately 18 km wide. It divides Denmark's population in two halves. In 1986 the Government established a political agreement for construction of a fixed link for both rail and road traffic across the Belt.

As the Belt is separated into two channels by the tiny island of Sprogø, it was decided to establish the link in three major structures: a bored railway tunnel and a high level road bridge across the eastern channel, and a low level bridge for combined traffic across the western channel, see Fig. 1.

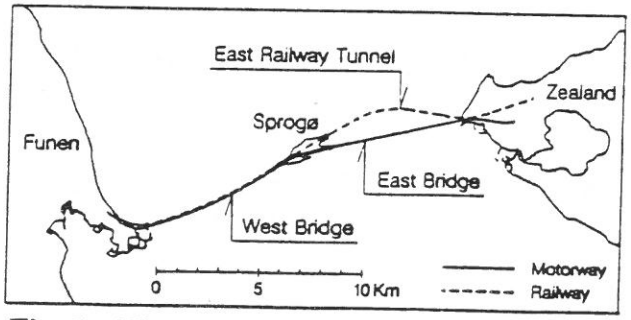

Fig. 1. The Great Belt Link

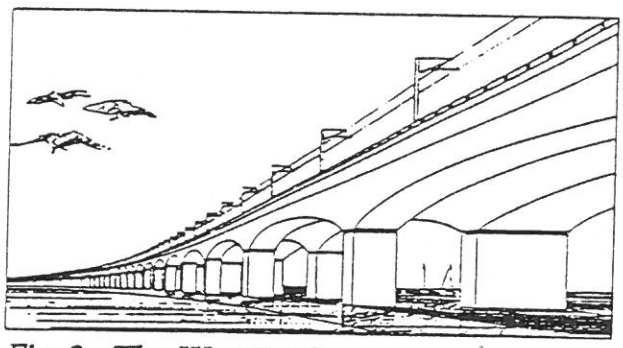

Fig. 2. The West Bridge

A limited company, Great Belt A.S., was founded by the Danish state with the objective of building and operating the link.

THE WEST BRIDGE

The overall concept for the 6.6 km long twin girder concrete bridge, see Fig. 2, is based on prefabrication of all main

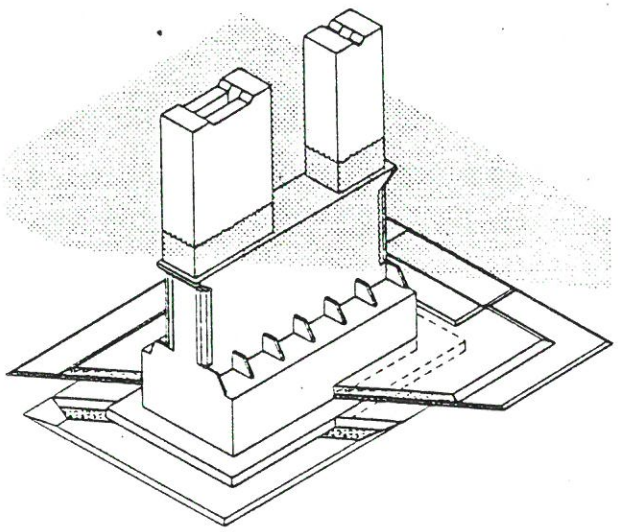

Fig. 3. Substructure

elements. The bridge consists of two parallel box girders supported on separate pier shafts which share a common substructure designed as a gravity founded caisson.

The bridge elements are cast in a reclaimed harbour area. Transportation and installation of the elements are performed by a large catamaran crane vessel.

The girders weighing up to 5700 tons are placed on temporary bearings. After the mid span joints are cast and continuity is established, the girders are adjusted and the permanent bearings connected. Regular spans are 110 m, and 12 expansion joint spans are 82 m.

The substructure includes 2 abutments and 62 offshore piers with a foundation level between -11 m and -29 m. With regard to the design and construction, differences between the shallow and deep water piers are of a dimensional nature only. The caisson consists of a base plate, from min. 17.5 m x 29.5 m to max. 22.5 m x 34.0 m in size, with the bottom part of the caisson being 6-9 m high and the shaft to level -3.5 m. The up to 7300 tons heavy caissons are placed on compacted, levelled stone beds of 1.5 m - 4 m thickness. After the caissons are sand filled, the pier shafts are placed on top. A typical substructure, including scour protection, is shown in Fig. 3.

Organization

The tender design and documents were formulated for The Great Belt A.S. from December 1987 to April 1988 by a joint venture, CCL, between COWIconsult, Carl Bro Group and Leonhardt, Andrä und Partner. Based on tenders received, an alternative solution, submitted by the European Storebælt Group, ESG, was chosen. ESG is a consortium comprising Højgaard & Schultz A/S, Ballast Nedam Civil Engineering, Taylor Woodrow Construction Ltd., Losinger Ltd., C.G. Jensen A/S and Per Aarsleff A/S. The contract was awarded in June 1989.

The detailed design of the West Bridge structures is performed by the contractor, ESG, parallel to the design activities entrusted to CCL and other consultants. As project manager, CCL coordinates all design activities. The Design Basis is prepared by CCL, including the assessment of soil design parameters and environmental loading.

Great Belt A.S. takes care of the site supervision with assistance from the CCL joint venture regarding the technical aspects.

GEOLOGY

Several site investigations have been carried out since the early 1960s for various Great Belt crossing solutions, including a large number of boreholes and vibrocores, supplemented with extensive seismic surveys. Optimization of the entire link in the late eighties resulted in

a relocated alignment of the West Bridge, and thus early investigations were largely located to the north of the present alignment. After the overall geometry of the bridge was known, detailed site investigations were carried out.

The occurrence of the principal subsoil units is shown in Fig. 4.

Danien limestone constitutes the base to any depth important for the foundation. Selandien (Upper Palaeocene) deposits in the form of calcarenite, calcisiltite and marl are encountered at several locations on top of the Danien deposits. Biostratigraphic investigation and other observations suggest that tectonic block-faulted movements took place in a period after the formation of the marl. Most of the upthrow blocks have been removed by erosion, but some can be recognized in the profile where the Selandien sediments are missing, see Fig. 4.

The glacial deposits have been subdivided into three units: Knudshoved Till, Lower TIll and Upper Till. The Knudshoved Till is found exclusively at the western part of the bridge. It is an extremely hard clay and sand till unit. It is characterized by its content of marl and a relatively high plasticity. The plasticity index is 10-20%, and the natural water content is generally high, 12-30%. The $CaCO_3$ content is typically greater than 30%. The Lower Till consists of alternating layers of clay till, sand till and melt water sand. The Upper Till is predominantly a clay till. The Upper and Lower clay tills are essentially low plasticity clays with plasticity indices in the order of 4-8% and liquid limits around 16%. The $CaCO_3$ content in the Upper Till is generally less than 25%, and in the Lower Till generally above 30%. Natural water contents vary generally between 9% and 15%.

With depth, the undrained shear strength of the Upper Till unit has a decreasing tendency in the profile. The strength can vary considerably vertically, typically from 200-250 kN/m^2 at the

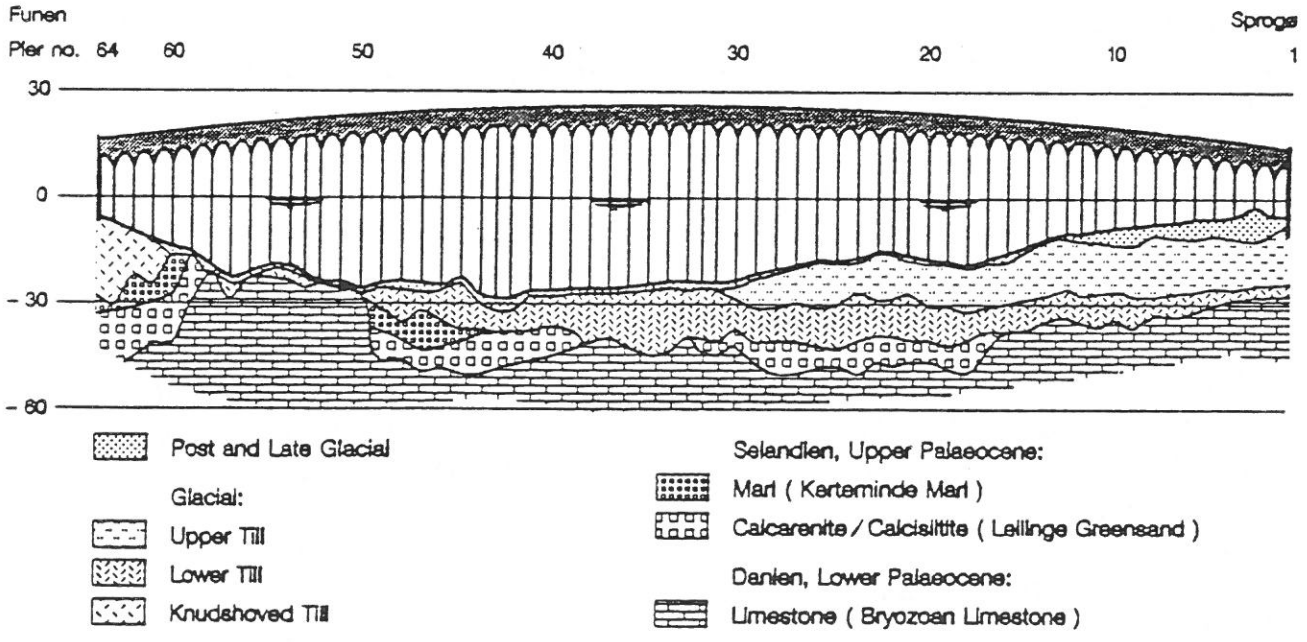

Fig. 4. Longitudinal profile.

upper part and down to values as low as 100-150 kN/m^2 at the lower part. Large local horizontal variations are also seen.

The Lower Till unit is generally very dense/hard with an undrained shear strength of the clay till typically better than 200-300 kN/m^2. In some areas the base of the unit is of a lower strength, normally associated with a high content of $CaCO_3$.

According to thermoluminescence dating of sand layers, the Lower Till descends from the next youngest ice age, Saale, or older glaciations. The Upper Till is evaluated to be part of a young terminal moraine complex, of the last ice cover of the area, Weichsel.

The glacial deposits are covered with Late and Post Glacial sediments which are less than 2 m thick and dominated by sandy marine sediments in the main part of the alignment. Thicker deposits including freshwater gyttja are found in the eastern area. The Late and Post Glacial deposits are of little significance for the project. Sediments above level -10 m have been excavated to provide access for marine equipment.

All geotechnical and topographical data are filed in a 3-D computerized information system developed for the Great Belt Project (Porsvig et al., 1989).

DETAILED SITE INVESTIGATIONS

Generally the detailed site investigations comprise 2 geotechnical boreholes and 8 CPTs at each pier. The investigations were performed by Geodan A/S and Fugro-McClelland. A typical site plan is shown in Fig. 5.

For some piers at the eastern part of the bridge an increased number of CPTs, and extra boreholes at a few piers, were deemed appropriate due to large variation locally in Upper and Lower Till. The additional investigations were made by Fugro-McClelland and Danish Geotechnical Institute.

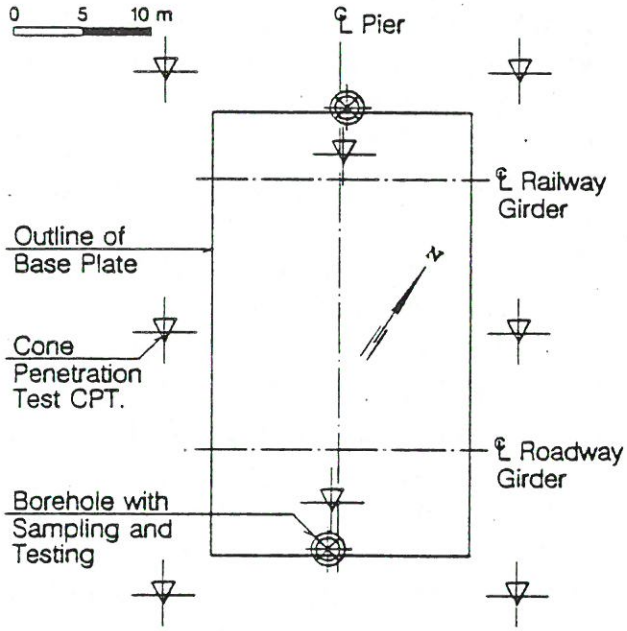

Fig. 5. Locaton of boreholes and CPTs

The boreholes were sunk to 20-40 metres below the seabed. Vane Tests were performed in cohesive material, and Standard Penetration Tests were performed in sand/gravel. Disturbed and intact samples (thin walled tubes) were taken, where advancing was performed by bailing. Cores were taken where coring was possible/necessary. A few Menard Pressuremeter Tests were performed, especially to assess the property of dubious limestone at the limestone ridge, piers 50-58.

Generally CPTs reached refusal at limited (few metres) depth at the western and central part of the bridge. At the eastern part a depth of 20 metres or more was often reached, corresponding to full penetration through the Upper Till.

A ratio has been established between the vane shear strength, c_v, and the CPT

cone resistance, q_c, for clay till of the Upper Till unit (Mortensen et al. 1991). For in-situ data (uncorrected), the relation used was:

$$c_v = 0.10\, q_c \qquad (1)$$

LABORATORY INVESTIGATIONS

The laboratory investigations were performed by Danish Geotechnical Institute, Geodan A/S, Norwegian Geotechnical Institute and Aalborg University.

The main aim of the laboratory investigations was to assess the strength and deformation properties of the weak parts of limestone and clay till of the Upper Till unit.

Assessment of the preconsolidation stress σ'_{pc} based on traditional oedometer tests proved to be hardly possible due to the low plasticity and heterogeneous nature of the soils.

Therefore, a large part of the oedometer tests were verified by assessment of preconsolidation stress from triaxial tests.

In the triaxial cell the specimen was preconsolidated to the σ'_{pc} evaluated from oedometer tests. Unloading to in-situ stress was then performed and the triaxial compression test was run. Based on the critical state method, the preconsolidation stress was reassessed. If the latter was higher than the one given to the sample in the laboratory it was assumed that the strength obtained reflected a lower bound value of the in-situ strength. (Jacobsen, 1992).

It has been confirmed that the relation between the vane shear strength, c_v, and the undrained shear strength, c_u, for the clay till is:

$$c_u = c_v \qquad (2)$$

Multistage tests in the laboratory further confirmed the SHANSEP function (Mayne, 1988) between the undrained shear strength, c_u, the in-situ vertical stress, σ'_o, and the preconsolidation stress, σ'_{pc}:

$$c_u = 0.4\, \sigma_o'(\sigma'_{pc}/\sigma'_o)^{0.85} \qquad (3)$$

Based on equations 1, 2 and 3 the undrained shear strength and the preconsolidation stress in the field can be assessed. (Foged and Steenfelt, 1992; Steenfelt and Foged, 1992).

For the Danien lime (stone) it has been demonstrated that soil with a cone resistance, q_c, not less than 1 MPa, increasing with depth, would behave satisfactorily.

The oedometer tests showed that for preconsolidated soils the initial tangential modulus of compressibility, K_t, can be written as:

$$K_t = K_{t,o} + \Delta K_t\, \sigma'_{red} \qquad (4)$$

where $K_{t,o}$ and ΔK_t are constants and σ'_{red} is the minimum vertical stress corresponding to unloading.

SHIP IMPACT AND ICE LOADS

A small amount of triaxial tests were performed with a very high strain rate to failure. The strain rate was also increased for a short while in some of the normal triaxial tests in order to assess the effect of strain rate increase similar to the rate expected at a ship impact.

The results confirm a significant increase in the undrained shear strength as a result of increased rate of strain, see Fig. 6.

Large scale sliding tests have been performed (Bjerregaard Hansen et al. 1991). The sliding resistance in the transition

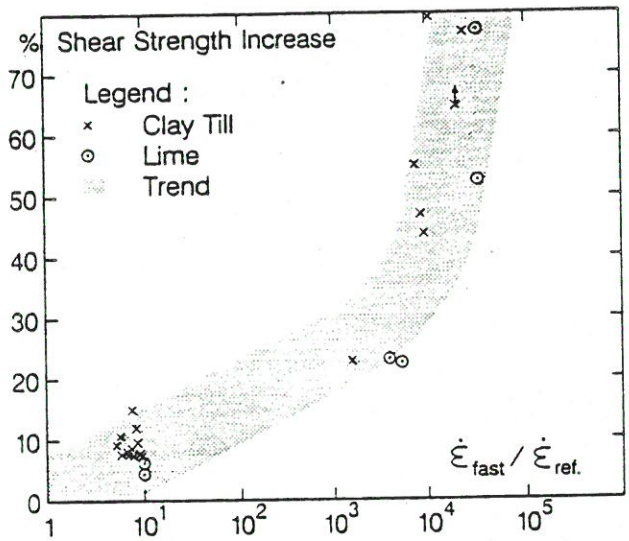

Fig. 6. Shear strength increase as a function of relative strain rate increase.

zone between the stone bed and subsoil of clay till was determined for different degrees of disturbance of the clay till. The tests showed that the ratio between the horizontal sliding resistance, τ_u, and the effective vertical consolidation stress, σ'_c, can be assessed to be (rate 25 mm/sec):

Intact clay till	$\tau_u/\sigma'_c \sim 0.53$
Disturbed clay till	$\tau_u/\sigma'_c \sim 0.46$
Remoulded clay till	$\tau_u/\sigma'_c \sim 0.42$

A comprehensive test programme was formulated in order to assess the soil parameters to be used in combination with ice loads, as the nature of ice loading is cyclic and to some extent dynamic.

Due to the dynamic interaction between ice force, structure and soil it was necessary in the first place to assume soil properties which could be used to assess the forces on the structure and the response of the structure before a test programme could be determined. (Christensen et al., 1991; Kristensen et al., 1992).

FOUNDATION DESIGN

The footings of the bridge are designed in limit states with reference to high foundation and safety classes according to "DIF's Code of Practice for Foundation Engineering, DS 415". For layered soil, sliding and torsional moment, additional design rules were developed and used. The following loadings were considered:

- Dead loads
- Train, traffic and other live loads
- Wind loads (10^{-2} event)
- Wave and current action (10^{-2} event)
- Ship impact loads from a 2000 DWT ship
- Ice loads (10^{-4} event)

The ground conditions facilitate direct foundation on the strata below Late and Post Glacial deposits. Hence, substructures are generally designed for foundation on stonebed layers at or slightly below the seabed level. For some piers, however, it was necessary to excavate soft till of the weak Upper Till unit, and to place the foundations on competent Lower Till.

SETTLEMENT MODELS

Two settlement models have been used.

At the western part, where the overconsolidation ratio is high, a linear elastic soil model has been assumed to be sufficient. The Skempton-Bjerrum method (Skempton and Bjerrum, 1957), where the A-factor has been taken as 0,25, has been used for the overall settlement model. Thus, the relation between initial settlements and consolidation settlements can be assessed.

At the eastern part, where the overconsolidation ratio is low, Bjerrum's theory of Delayed Compression (Bjerrum, 1973) has been used for the settlement model. As the theory itself is cumbersome, the initial and consolidation settlements have been assessed using a modulus of compressibility - or compression index - only, and the development of secondary settlements depends on the apparent age of the soil in question.

The settlement model established for weak soil has been substantiated by field model tests. The tests were carried out on Upper Till of low preconsolidation at the island of Sprogø. The main tests were performed on dia. 1.0 m and 2.0 m foundations. The tests did show creep behaviour, basically in accordance with the theory of Bjerrum on Delayed Compression. A time curve is shown in Fig. 7.

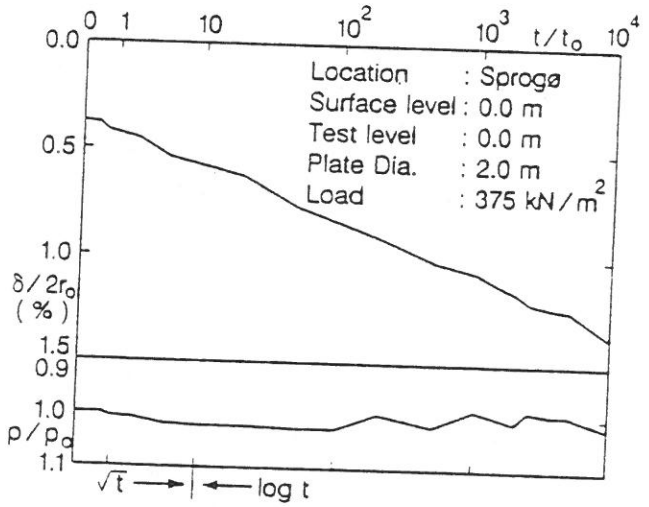

Fig. 7. Time - settlement curve.

SETTLEMENTS OBSERVED

The bridge is constructed from the west. At the time of writing this paper both girders have been placed at Piers Nos. 63-54, and placing of stonebeds and caissons is in progress at Piers Nos. 53 through 45.

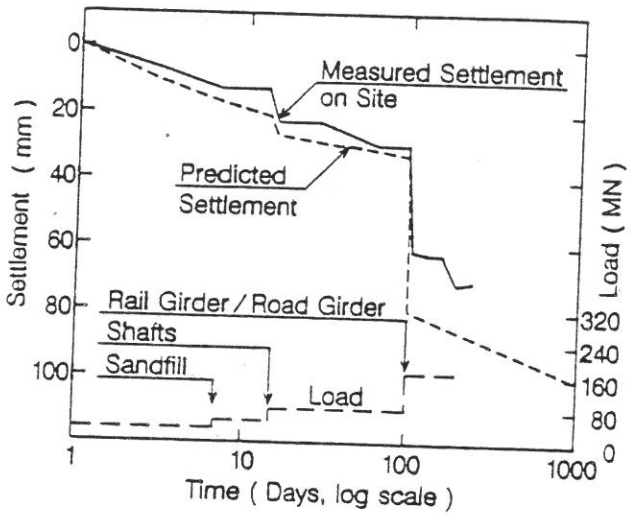

Fig. 8. Predicted and observed settlements of pier No. 60

The erection method with the full dead load instantly applied when the main elements are placed, offers a unique possibility to monitor settlements, especially the relation between initial and consolidation settlements, which is not possible to detect for prolonged construction on glacial tills.

The results of settlement monitoring at Piers 63-54 show a good correspondence between predicted and actual settlements, both being in the order of 4-8 cm from when the caisson is placed until both girders are resting on the pier, see Fig. 8 as an example.

The tilt transverse to the bridge axis is experienced to be 0.5 to 1.5 per mille due to the eccentric load of the road girder. After placing the rail girder the tilt is reduced to less than 0.5 per mille. The tilt parallel to the bridge axis is generally experienced to be less than 0.5 per mille.

ACKNOWLEDGEMENTS

The authors are grateful to the Client, Great Belt A.S., for permission to publish this paper. Especially, the comments from Mr. Aage Hansen are appreciated.

Furthermore, we wish to thank the following companies who have been involved in the assessment of geotechnical properties of the soil below the West Bridge: Danish Geotechnical Institute, Aalborg University, Norwegian Geotechnical Institute, Geodan A/S, Fugro-McClelland, Rambøll & Hannemann A/S, and B. Højlund Rasmussen A/S.

REFERENCES

Bjerregaard Hansen, P., Denver, H., Mollerup, E. (1991), Lateral sliding resistance - Large scale sliding tests, *Proc. of the Tenth European Conf. on Soil Mechanics and Found. Eng.*, Florence, May.

Bjerrum, L. (1973), Problems of Soil Mechanics and Construction on Soft Clays. *Norwegian Geothecnical Institute. Publication No. 100.*

Christensen, F.T., Gravesen, H., Thomsen, J.R., Ennemark F., and Spangenberg, S. (1991), Accidental Limit State Ice Loads on Bridge Piers. *PIANC Bulletin* No. 72.

Foged, N., Jørgensen, M., (1988), Triaxial Tests on Soft Carbonate Rocks. *10. Nordiske Geoteknikermøte*, NGM-88, Oslo, May.

Foged, N., Steenfelt, J.S. (1992), An Engineering Geological Approach to Preloaded Clay Till Strength. *11. Nordiske Geoteknikermøde*, NGM 92, Aalborg, May.

Fries, C., Hommel, D.L. (1990), Great Belt Link: Tender Design and Contract Design for the West Bridge. *Second Symposium on Strait Crossings*, Trondheim, June.

Jacobsen, H.M. (1992), Bestemmelse af forbelastningstryk. *11. Nordiske Geoteknikermøde*, NGM 92, Aalborg, May.

Jacobsen, H.M. (1992), Karakteristiske belastningstilstande for moræneler. *11. Nordiske Geoteknikermøde*, NGM 92, Aalborg, May.

Kristensen, P.S., Gravesen, H., Andersen, K.H., Hansen, Aa., Spangenberg, S. (1992), Dynamic Properties of soil for Ice Load: A case story of bridge pier design for the Great Belt - West Bridge. *Danish Geotechnical Society, dgf-Bulletin 8*, (to be published).

Mayne, P.W. (1988), Determining OCR in Clays from Laboratory Strength, *ASCE*, Vol. 114, No. 1, January.

Mortensen, J.K, Hansen, G., Sørensen, B. (1991) Correlation of CPT and Field Vane Tests for Clay Tills. *Danish Geotechnical Society, dgf - Bulletin 7*, June.

Porsvig, M., Christensen, F.M., Hansen, Aa. (1989), Great Belt Information System with a 3-D Model. *Proc. of the Twelfth Int. Conf. on Soil Mechanics and Found. Eng.*, Rio de Janeiro, August.

Project Reports (unpublished).

Skempton, A.W., and Bjerrum, L. (1957). A Contribution to the Settlement Analysis of Foundations on Clay. *Geotechnique, Vol. 7*, December.

Steenfelt, J.S., Foged, N. (1992), Clay Till Strength - SHANSEP and CSSM. *11. Nordiske Geoteknikermøde*, NGM 92, Aalborg, May.

Steensen-Bach, J.O., Foged, N., Larsen, G. and Baumann, J., (1988), Geological and Geotechnical Properties of Kerteminde Marl., *10. Nordiske Geoteknikermøte*, NGM-88, Oslo, May.

3. CYCLIC LABORATORY TESTS ON STOREBÆLT CLAY TILL

Cyclic Laboratory Tests on Storebælt Clay Till

by

Arne Kleven, Norwegian Geotechnical Institute
Knut H. Andersen, Norwegian Geotechnical Institute

ABSTRACT

The laboratory soil testing performed on Storebælt clay till to establish the soil parameters required to analyse the bridge piers under ice loading is presented. The parameters needed to calculate bearing capacity, displacements, stiffness and hysteretic damping are given. The soil parameters presented are also valid for other cyclic loading conditions, like sea waves.

INTRODUCTION

The piers of the Western Storebælt bridge need to be designed for cyclic loading from sea ice (Gravesen, 1991). Foundation design aspects where cyclic effects are important, include:

- bearing capacity of the piers
- cyclic and permanent displacements of the soil foundation
- non-linear soil spring characteristics to represent the soil foundation in the dynamic analyses

The following soil parameters are needed to analyse these foundation design aspects:

- static shear strength
- cyclic shear strength
- deformation properties under cyclic loading
- post-cyclic recompression modulus

These soil parameters have been determined from laboratory tests on samples of the Storebælt clay till. The testing programme and the results of the tests are presented in this paper.

Even though this paper focuses on cyclic loading from sea ice, the test results are equally valid for foundation design under cyclic loading from sea waves.

ICE LOADING AND STRESSES IN THE SOIL

The ice load history assumed in the foundation design analyses of the Western Storebælt bridge is illustrated in Fig. 1 (Gravesen, 1991). The ice causes cyclic loading with two frequencies. The low frequency load may consist of 200-1500 cycles. The low frequency load causes a "one-way" loading, which may be divided into an average and a cyclic component. The low frequency load on each pier has an equal probability of occurrence between 20 and 50 MN. The high frequency load is assumed to be symmetrical (i.e. "two-way loading"), and thus has an average component equal to zero. The double amplitude high frequency load varies between 18 and 30 MN.

The ice loads are transmitted to the soil foundation. The soil is subjected to static loads from the weight of the pier and the bridge in addition to the ice loads. These loads cause rather complicated stress conditions in the soil beneath the piers. The soil elements are subjected to both average shear stresses, τ_a, and cyclic shear stresses, τ_{cy}. Examples of simplified stress conditions for a few typical elements along a potential failure surface are shown in Fig. 2. In this paper τ denotes the shear stress on the horizontal plane in the direct simple shear (DSS) test and on the 45° plane in the triaxial test.

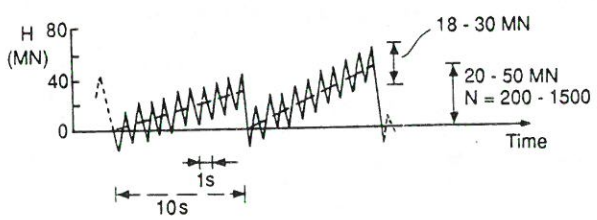

Fig. 1. Ice loading history.

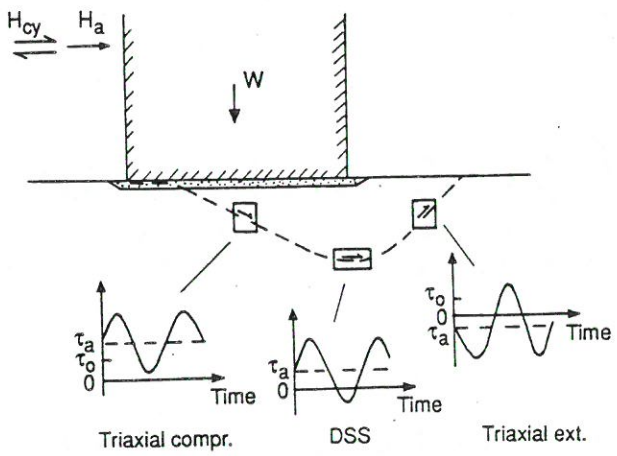

Fig. 2. Simplified shear stress conditions beneath a pier.

The average shear stress, τ_a, is composed of: (1) The initial shear stress in the soil prior to the installation of the structure, $\tau_o = 0.5 \cdot (1-K_o)p'_o$, where p'_o = the effective overburden stress; and K_o = the coefficient of earth pressure at rest; and (2) an additional shear stress, $\Delta\tau_a$, which is induced by the weight of the pier and the bridge and by the average ice load component.

The initial shear stress, τ_o, has been acting under drained conditions, and the soil is consolidated under this stress. The average shear stress due to the weight will first act under undrained conditions, but as the soil consolidates under the weight, this shear stress will also act under drained conditions. The average shear stress due to the average ice load component will act under undrained

conditions.

The cyclic shear stress, τ_{cy}, is caused by the cyclic ice load components.

The cyclic shear stress will vary continuously from one cycle to the next, and it will contain both a high and a low frequency component. The average shear stress may also vary with time, due to redistribution of stresses caused by the cyclic loading.

The illustration in Fig. 2 indicates that the various soil elements will be subjected to different stress paths. With the existing types of laboratory equipment, it is not possible to accurately reproduce all relevant in-situ stress conditions in laboratory tests. However, triaxial and direct simple shear (DSS) conditions are representative for some important elements. The results from triaxial and DSS tests also provide information that can be used to evaluate the soil properties for other stress conditions. Previous experience from cyclic testing of soils (e.g. Andersen et al., 1988), is that cyclic soil behaviour depends on both the average and the cyclic shear stresses. Since the soil elements beneath the bridge piers are subjected to various combinations of average and cyclic shear stresses, the cyclic laboratory tests on the Storebælt soil were also run with various combinations of average and cyclic shear stresses.

LABORATORY TEST PROGRAMME

Soil Types

The soil conditions vary substantially along the length of the bridge (Kristensen, 1991).

The laboratory tests were performed on four different types of clay till samples:

- Glacial clay till with an undrained shear strength of about 225 kPa was selected to represent relatively competent glacial till. This material was in the laboratory consolidated to an overconsolidation ratio, OCR, of 3. The plasticity index of this clay till was about 7 to 12%. The water content was between 9 and 10% after consolidation. A typical grain-size distribution curve is shown in Fig. 3.
- Glacial clay till with an undrained shear strength of 225 kPa was also used for a few static tests on specimens consolidated to OCR=40.
- Glacial clay till with an undrained static shear strength of about 150 kPa was selected to represent less competent soil. This clay till was in the laboratory consolidated close to or slightly above the in-situ preconsolidation stress, i.e. OCR=1. The plasticity index of this clay till was about 7 to 12%. The water content was between 10 and 11% after consolidation.

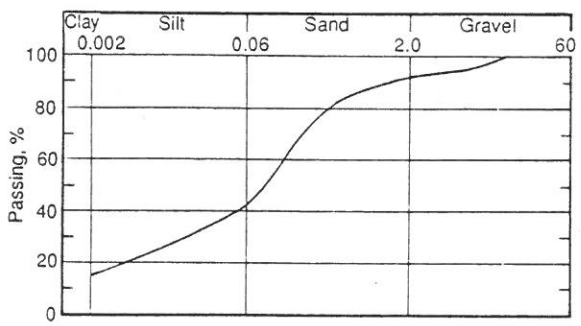

Fig. 3. Typical grain size distribution curve for Storebælt glacial till.

A typical grain-size distribution curve is shown in Fig. 3.

- Glacial clay till with an undrained shear strength of about 150 kPa was also used to produce disturbed samples. These samples were used to study the behaviour of a potentially weakened upper zone at the bottom of the excavation which is made to prepare the clay bed. The batch of disturbed clay till was produced by removing all gravel grains >5 mm and kneading the clay samples by hand inside a plastic bag. The average water content of the remoulded samples was 9.4% after consolidation.

Upon arrival at NGI the clay till samples were X-rayed to ensure that the testing was performed on the most intact soil material and to avoid the numerous large gravels inside the test specimens.

Consolidation

The specimens were consolidated as shown in Table 1. The specimens were first consolidated to maximum effective normal stresses slightly above the estimated in-situ preconsolidation stresses. The normally consolidated specimens remained at these stresses. The overconsolidated specimens were unloaded to small effective stresses and allowed to swell, to reproduce the overburden stress conditions in-situ just prior to placing the piers. Then the effective stresses were increased to simulate the stress increase due to the weight of the pier and the bridge deck.

Table 1. Consolidation stresses applied in laboratory

OCR	Maximum		Minimum		Final	
	σ_{vpc}'	σ_{hpc}'	σ_{vo}'	σ_{ho}'	σ_{vc}'	σ_{hc}'
1	-	-	-	-	600	240
3	1200	480	30	84	400	200
40**	1200	480	30	84	30	84
Disturbed*	-	-	-	-	400	-

** *DSS tests only*

* *Static DSS tests only*

Maximum: *Preconsolidation*

Minimum: *Overburden*

Final: *Overburden + submerged weight of pier*

The tests are referenced to by the overconsolidation ratio corresponding to their laboratory stress history. Since the maximum effective stresses are only slightly above the in-situ preconsolidation stress, one should be aware that the samples probably have not been in a truly normally consolidated state. The overconsolidation ratio based on the laboratory consolidation stress history may therefore not be fully representative of the actual state of the soil.

The tests were consolidated under conditions corresponding to no lateral strain. This condition was automatically achieved in the DSS tests. In the triaxial tests, the condition of no lateral strain was approximated by using a ratio between horizontal and vertical effective stresses, K_o, determined from Brooker and Ireland (1965) for unloading. For reloading the K_o value was estimated from the expression given by Mayne and

Kulhawy (1982). The actual consolidation stresses are given in Table 1.

Type and Number of Tests

The laboratory testing programme is summarized in Table 2.

The triaxial tests were run on specimens with full cross section (72 mm diameter) and a height to diameter ratio of 1.0. Smooth end caps were used.

The DSS tests were run in the NGI DSS device on specimens with 35 cm^2 area and about 16 mm initial height. Two of the specimens on disturbed clay till were run on specimens with 50 cm^2 area.

The static tests were sheared with a constant rate of shear strain of 3.9%/hr in the triaxial tests and 4.7%/hr in the DSS tests.

The cyclic tests were run stress-controlled with various combinations of average and cyclic shear stresses. The load period was 10 s, apart from 3 DSS tests which were run with a load period of 1 s.

The average shear stress at the end of consolidation was $\tau_o=0$ in the DSS tests and $\tau_o=0.5\cdot(\sigma'_{vc}-\sigma'_{hc})$ in the triaxial tests. In some tests the average shear stress was increased or decreased by $\Delta\tau_a$ from τ_o to τ_a. The $\Delta\tau_a$ was applied undrained and kept for 1 to 1.8 hours before undrained cyclic loading was started. The cyclic loading was sinusoidal with an amplitude which was kept constant for each test. The values of τ_a and τ_{cy} used for the various tests can be seen from the points in the diagrams in Figs 7 and 8.

Table 2. Summary of laboratory test programme

OCR	Static			Cyclic		*	K_o-oedo-meter
	Triax compr.	Triax ext.	DSS	Triax	DSS	G_{max}	
1	4	-	4	5	7(1)	20	2
3	3	1	6	5	10(2)	24	2
40	3	-	-	-			
Disturbed	-	-	5	-		12	

* *Includes 4 res. col. tests*

( ) *Cyclic tests with 1 s period*

Other cyclic tests have 10 s period

All cyclic tests are stress controlled

STATIC SHEAR STRENGTH

The static shear strength values obtained are summarized in Table 3. Typical stress-strain curves for the various test types and consolidation histories are presented in Fig. 4. The variation in the test results is seen to be significant. The two main causes of the scatter in the results are believed to be sample disturbance and variation in the in-situ stress history of the samples.

Figure 5 presents the average static shear strengths as functions of the OCR. The undrained static shear strength is clearly anisotropic, with triaxial compression strength the highest, triaxial extension strength the lowest, and DSS strength in the middle.

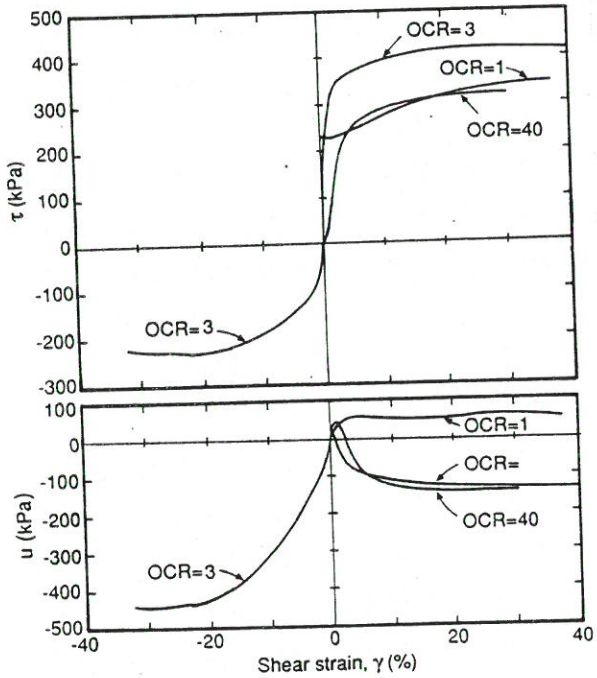

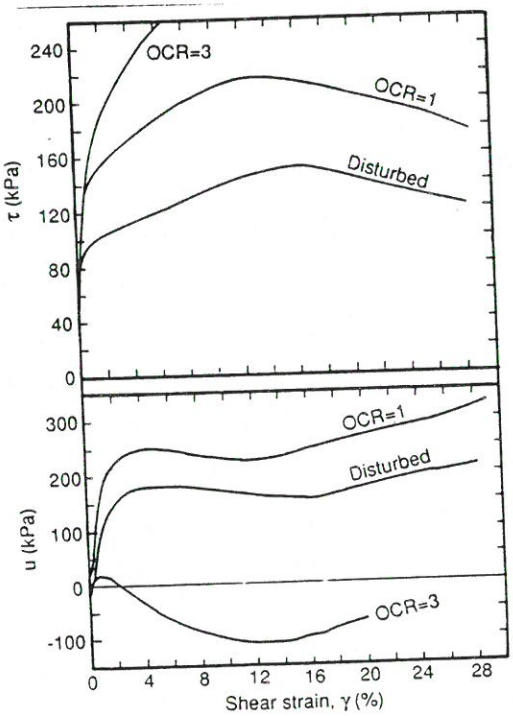

Fig. 4. (a) Undrained static compression and extension triaxial test results for Storebælt clay till.

(b) Undrained static DSS test results for Storebælt clay till.

Table 3. Summary of undrained static shear strengths

Type of test		Undrained shear strength (kPa)		
		Compression triaxial	Direct simple shear	Extension triaxial
Disturbed	Average	-	145**	-
OCR=1	Average	287 (4)	205 (5)*	-
	Maximum	366	233	-
	Minimum	225	173	-
OCR=3	Average	423 (4)*	284 (6)	216
	Maximum	455	316	-
	Minimum	400	231	-
OCR=40	Average	298		
	Maximum	306		
	Minimum	286		

* *Includes one test which first experienced 1500 cycles with small strains.*

** *Best estimate at γ = 15% from 4 tests*

( ) *Number of tests*

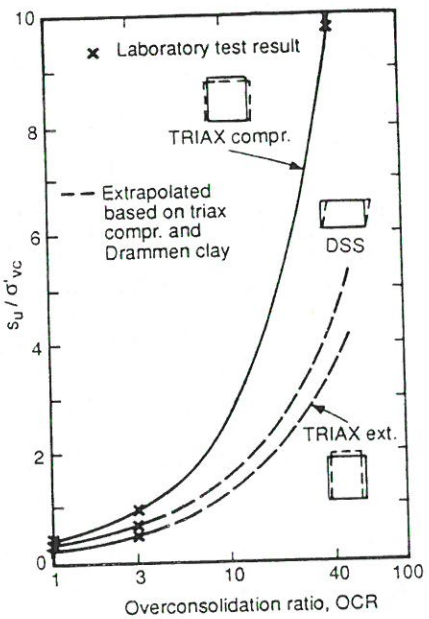

Fig. 5. Static shear strengths of Storebælt clay till.

CYCLIC SHEAR STRENGTH

The cyclic shear strength, $\tau_{f,cy}$, is defined as the sum of average and cyclic shear stresses that cause failure after a given number of cycles (Andersen et al., 1988b); i.e.:

$$\tau_{f,cy} = (\tau_a + \tau_{cy})_f$$

The cyclic shear strength is stress path dependent and also depends upon OCR, τ_a, τ_{cy} and the number of load cycles.

The test program included triaxial and direct simple shear tests on clay till with OCR=1 and 3, and direct simple shear tests on disturbed clay till.

The combinations of τ_a and τ_{cy} that cause failure after 1, 10, 50, 100 and 1000 cycles are plotted in Figs 7 and 8. Each point in the diagrams represents one test and defines the number of tests and the combinations of τ_{cy} and τ_a that were used in the tests. The τ_{cy} and τ_a were normalized with respect to the static shear strength. To attempt to minimize the effect of soil variation, the static strengths used for normalization were taken from static tests on specimens as close as possible to the specimens used for cyclic testing. Different static shear strengths were therefore used for normalization for the various cyclic test.

The number of cycles to failure, N_F, for each test is specified at the respective points in Figs 7 and 8.

Failure was defined as either large cyclic shear strains (γ_{cy}=15%) or large average shear strains (γ_a=15%) in compression or extension. The cyclic and average shear strains are defined as $\gamma_{cy}=0.5\cdot(\gamma_{max}-\gamma_{min})$ and $\gamma_a=0.5\cdot(\gamma_{max}+\gamma_{min})$ where, γ_{max} and γ_{min} are the maximum and minimum shear strains within a load cycle. The average and cyclic components of shear stresses, shear strains and pore pressures are illustrated in Fig. 6. In tests with low shear stresses, failure was not reached within the specified maximum number of cycles applied (1500 cycles).

Based on the results for the individual tests, the curves shown in Figs 7 and 8 were constructed. Each curve shows the combinations of τ_a and τ_{cy} that will cause failure after the number of cycles indicated on the curve.

The failure mode (i.e. the combination of average and cyclic shear strains at failure) is specified along the failure curves in Figs 7 and 8. The failure mode was also determined by interpolation and extrapolation of the failure mode measured in the individual tests.

In the triaxial tests the failure mode is large compression average shear strains for τ_a approaching the static compression shear strength and large extension average shear strains for τ_a approaching the static extension shear strength. For a limited range of τ_a be-

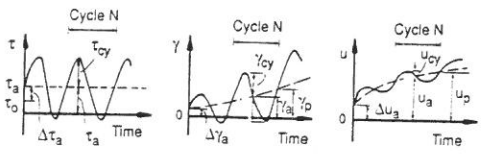

Fig. 6. Components of shear stress, shear strain and pore pressure under cyclic loading.

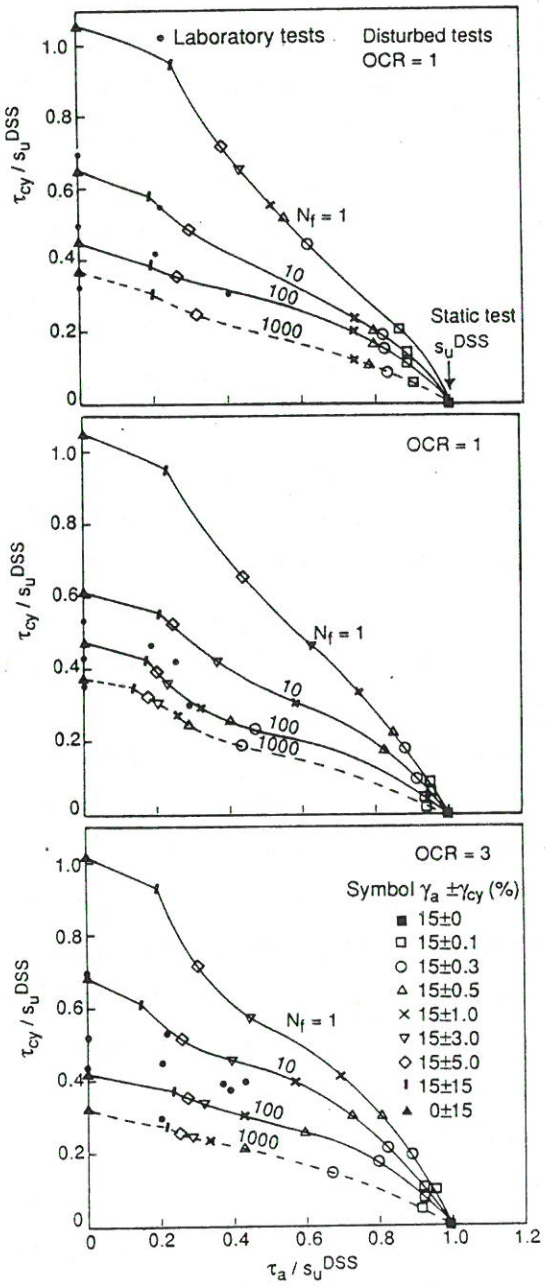

Fig. 7. Number of cycles to failure, N_F, for various combinations of τ_a and τ_{cy} in DSS tests on Storebælt clay till:

(a) Disturbed clay till

(b) OCR=1

(c) OCR=3

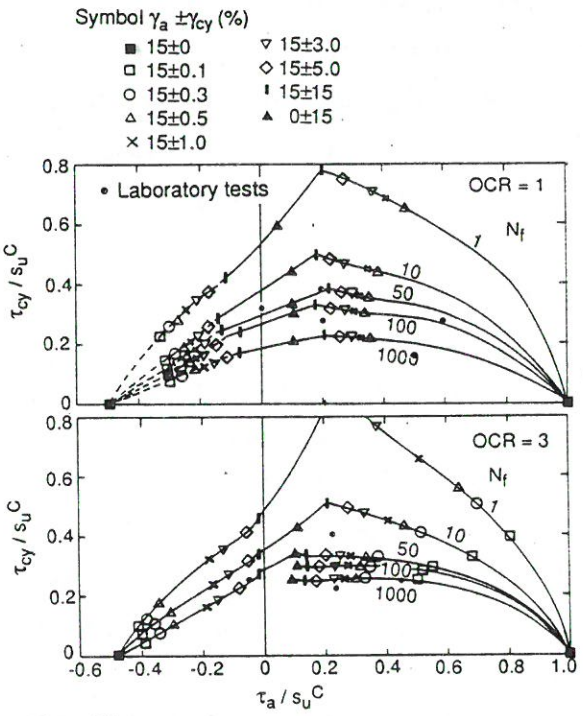

Fig. 8. Number of cycles to failure, N_F, for various combinations of τ_a and τ_{cy} in triaxial tests on Storebælt clay till:

(a) OCR=1

(b) OCR=3

tween the above failure modes, the failure mode is large cyclic shear strains.

In the DSS tests the failure mode is large cyclic shear strains for small values of τ_a and large average shear strains for larger τ_a values.

The curves have been drawn to intersect the horizontal axis at $\tau_a/s_u=1.0$, i.e. at an average shear stress equal to the static shear strength. The actual intersection with the horizontal axis and the location of the failure curves for high values of τ_a, depend on the duration of τ_a due to undrained creep. This should be taken into account when analysing

field situations with high τ_a values.

By inspection of the curves in Figs 10 and 11, one will find that cyclic failure will occur when the sum of average and cyclic shear stresses is lower than the static shear strength for all number of cycles except N=1. The information in Figs 10 and 11 are used to construct diagrams of cyclic shear strengths in Andersen et al. 1991.

Three of the cyclic DSS tests were run with a load period of 1 s and with OCR=1 and 3. The shorter load period lead to an increase in number of cycles to failure.

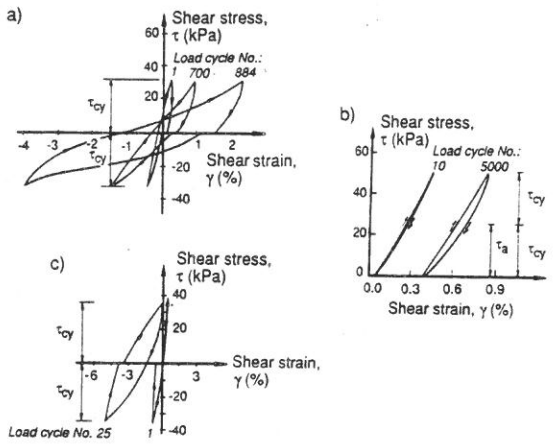

Fig. 9. Examples of stress-strain behaviour of clays under various cyclic loading conditions:
(a) Symmetrical DSS loading
(b) Non-symmetrical triaxial loading
(c) Symmetrical triaxial loading
(After Andersen et al. 1988)

DEFORMATION PROPERTIES

General

The stress-strain behaviour under cyclic loading is a function of the average and cyclic shear stresses and the stress direction. This is examplified in Fig. 9. If the cyclic loading in the DSS test is symmetrical, the resulting cyclic shear strain will be relatively symmetrical (Fig. 9a). The loading and unloading curves are different showing that there is hysteretic damping in the soil. The cyclic shear strain amplitude increases and the secant shear modulus decreases with number of cycles.

If the shear stress is not symmetrical, the increase in average shear strain with number of cycles may become predominant compared to the cyclic shear strains (Fig. 9b).

In the triaxial test there will in most cases be average shear strains even if the shear stress is symmetrical around zero (Fig. 9c). The reason is that the static extension shear strength is lower than the static compression shear strength, and symmetrical cyclic shear stresses will lead to higher degree of mobilized strength on the extension side than on the compression side.

Average and Cyclic Shear Strains

To get a complete picture of the development of shear strains during cyclic loading, where the factors discussed above are taken into account, the test results were used to construct diagrams of the type shown in Figs 10 and 11. The figures show the average and cyclic shear strains as functions of normalized cyclic shear stress, τ_{cy}/s_u, and normalized average stress, τ_a/s_u, after 1, 10, 50 and 100 cycles.

The diagrams in Figs 10a to c are for DSS tests on disturbed clay till and on undisturbed clay till with OCR=1 and OCR=3, respectively. The corresponding diagrams for triaxial tests on undisturbed clay till with OCR=1 and 3 are presented in Figs 11a and b. The diagrams show that in the DSS tests, γ_{cy} is mainly a function of τ_{cy} with relatively small influence of τ_a. Similar observations may be made from the triaxial test diagrams,

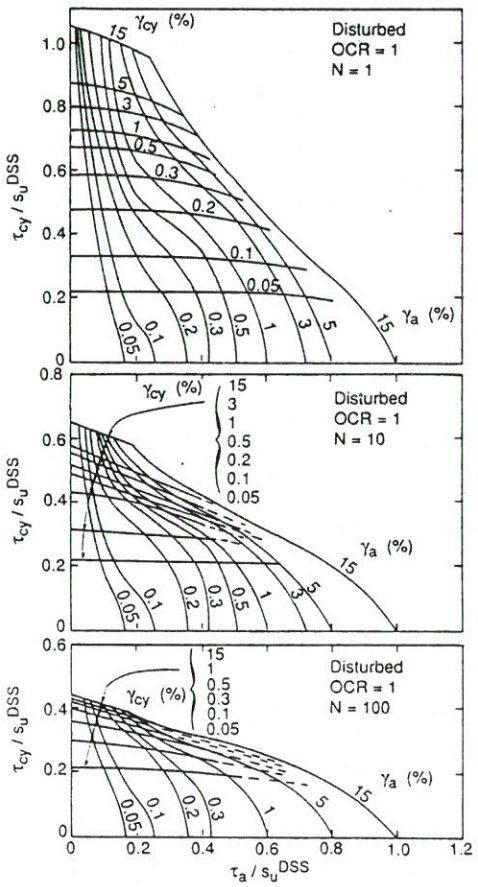

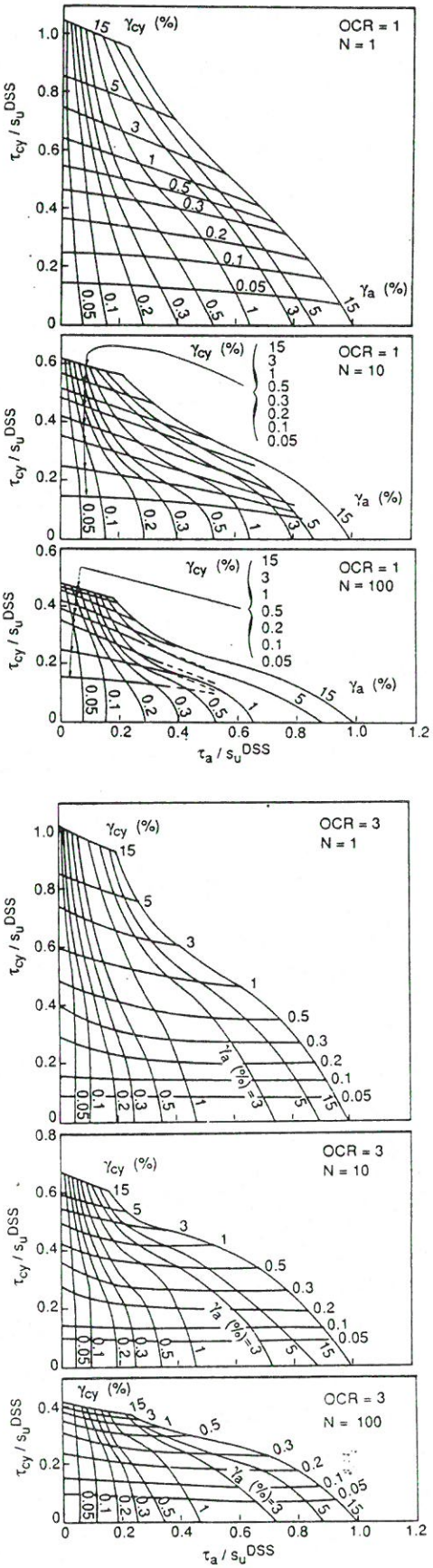

Fig. 10. Average and cyclic shear strains in DSS tests on Storebælt clay till:

(a) Disturbed clay till

(b) OCR=1

(c) OCR=3

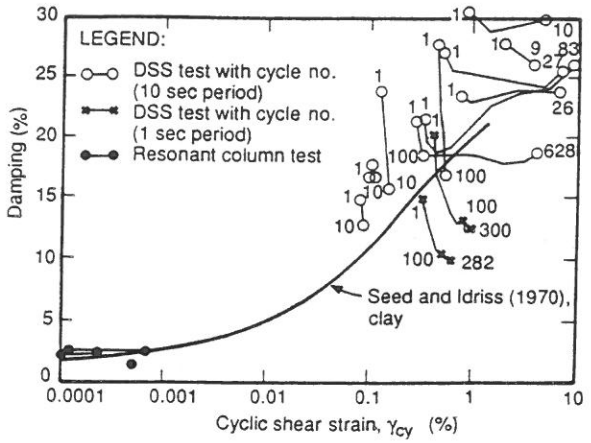

Fig. 13. Damping values measured on Storebælt clay till. Hysteretic damping in cyclic DSS tests, OCR=3 and viscous damping from resonant column tests.

tests with 10 s load period, the damping ratio approaches the Seed-Idriss 1970 curve after 100 cycles.

Further, it can be seen that the damping ratio increased with increase in the shear strain.

For clay till with OCR=3, two DSS tests with 1 s period gave damping ratios 45 to 60% lower than the corresponding 10 s tests. This effect was not seen in the one DSS test with 1 s period on clay till with OCR=1. The results are too few to make firm conclusions about the effect of load period on damping.

Resonant column tests gave damping ratios between 1.6 and 2.6% These results were in agreement with a previous literature study at NGI, Selnes (1986), which concluded that a typical range for the minimum damping value (in the 10^{-4}-10^{-3}% strain range) is 1.5 to 4% for clay.

Based on the test results, the Seed-Idriss (1970) damping curve was used for the Storebælt clay till with 10 s load period after 100 cycles in the foundation analyses, Andersen et al., 1991.

PORE PRESSURE GENERATED BY CYCLIC LOADING

As for the shear strains, the average pore pressure, u_a, generated by undrained cyclic loading, is a function of the average and the cyclic shear stresses, the number of cycles, the OCR and the type of test. The pore pressure was therefore plotted in the same type of diagram as the shear strains (Figs 14 and 15). The average pore pressure is normalized with respect to the effective vertical consolidation stress. The value of u_a in the diagrams includes the pore pressure occurring when the shear stress was increased from τ_0 to τ_a. The pore pressure increase due to the change in normal stresses is not included in the triaxial test results.

The diagrams can be used to calculate settlements due to cyclically induced pore pressures as described in Andersen et al., 1991. The finite element calculations used to determine cyclic and permanent displacements also yield values of the average and cyclic shear stresses and the stress path for the soil elements underneath the foundation. Using this information together with Figs. 14 and 15, the average pore pressures induced in the foundation soil may be determined. The

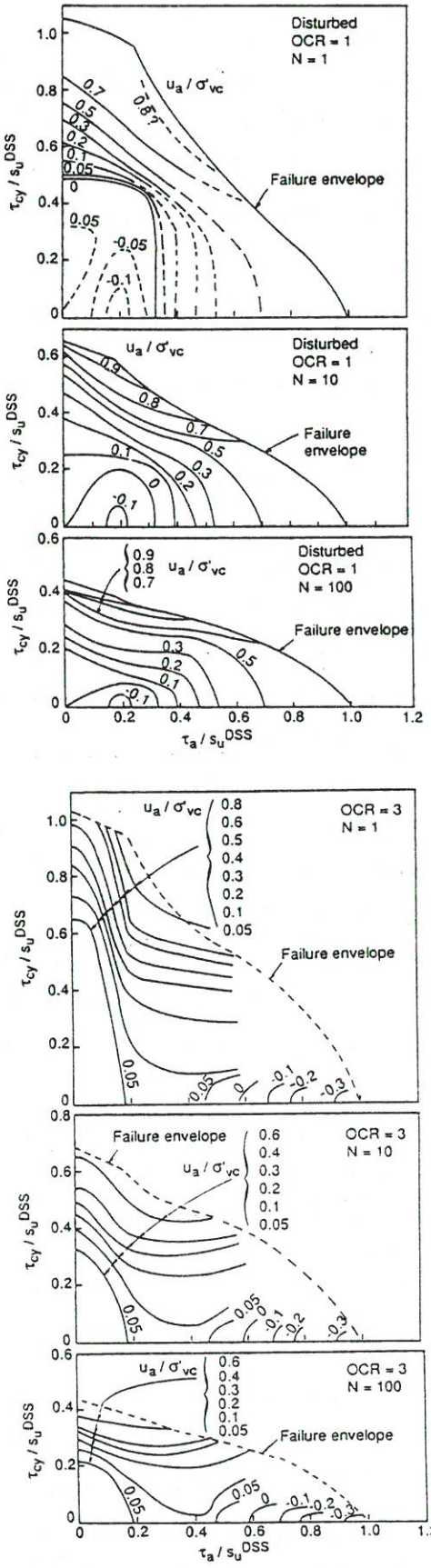

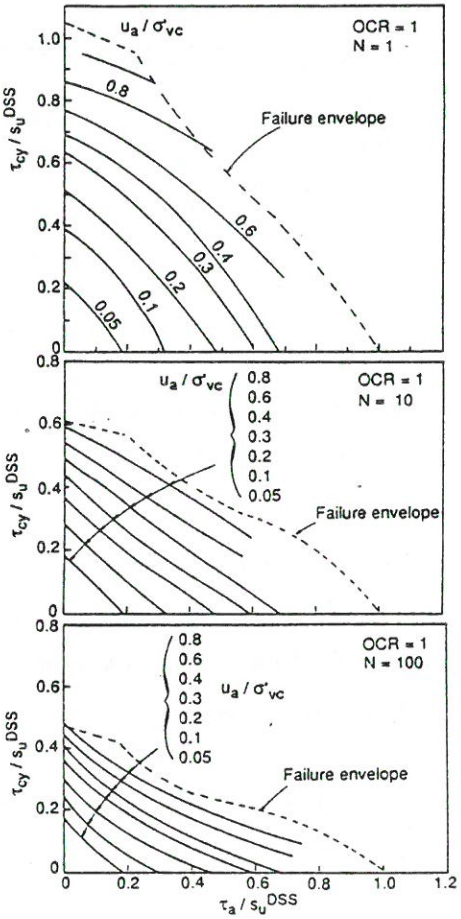

Fig. 14. Average pore pressure generated in DSS tests on Storebælt clay till:

(a) Disturbed clay till

(b) OCR=1

(c) OCR=3

vertical displacement may then be calculated assuming an effective stress reloading equal to the average pore pressure. The calculation requires the use of a reloading modulus of the clay till and this was obtained from the reloading branch of the K_0-oedometer tests as described below.

The three cyclic DSS tests run with a load period of 1 s showed that a 1 s load period

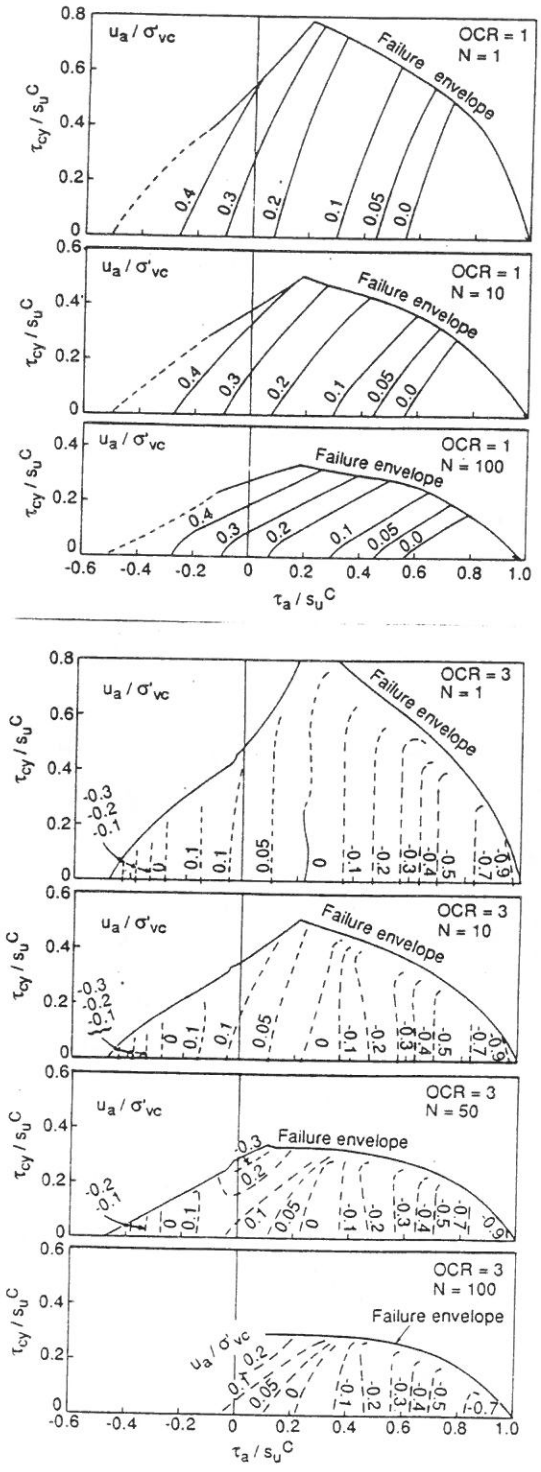

Fig. 15. Average pore pressure generated in triaxial tests on Storebælt clay till:
(a) OCR=1
(b) OCR=3

gives a smaller rate of pore pressure generation with number of cycles than a 10 s period.

POST-CYCLIC RECOMPRESSION BEHAVIOUR

The post-cyclic recompression modulus can be determined from unloading/reloading sequences in oedometer tests. In the present case, the recompression modulus was determined in two special oedometer tests which were primarily run to determine the horizontal stresses during the consolidation stress history. The special equipment used for these tests is described in Dyvik et al. (1985). The tests were loaded to 1200 kPa, unloaded to 30 kPa and reloaded to 400 kPa. The reloading modulus of the clay till can be determined from the test results as shown in Fig. 16. The numerical value of the reloading modulus will depend on the effective stress and on the size of the effective stress increment. The reloading modulus was used

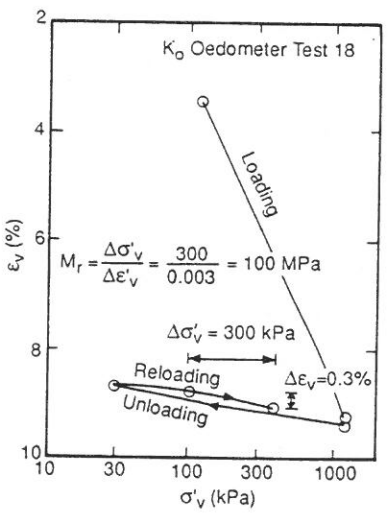

Fig. 16. Estimate of reloading modulus of Storebælt clay till.

in the calculation of settlements due to dissipation of cyclically induced pore pressures as described in Andersen et al. 1991.

REFERENCES

Andersen, K.H., A. Kleven and D. Heien (1988a). Cyclic soil data for design of gravity structures. *ASCE Journal of Geotechnical Engineering*, Vol. 114, No. 5, May, 1988, pp. 517-539. Also publ. in: *Norwegian Geotechnical Institute*. Publication, 175.

Andersen, K.H, O.E. Hansteen and M. Gutierrez (1991). Bearing capacity, displacements, stiffness and hysteretic damping of Storebælt bridge piers under ice loading. A case history of bridge pier design for Western Bridge, Storebælt. *DGF Bulletin* No. 8.

Andersen, K.H., R. Lauritzsen, R. Dyvik and P.M. Aas (1988b). Cyclic bearing capacity analysis of gravity platforms; calculation procedure; verification by model tests, and application for the Gullfaks C platform. Proc. International Conf. the Behaviour of Offshore Structures, *BOSS'88*, Vol. 1, pp. 311-324.

Brooker, E.W. and H.O. Ireland (1965). Earth pressures at rest related to stress history. *Canadian Geotechnical Journal*, Vol. 2, No. 1, pp. 1-15.

Dyvik et al. (1985). Coefficient of lateral stress from oedometer cell. 11th ICSMFE, San Francisco, 1985. Also publ. in: *Norwegian Geotechnical Institute*. Publication, 163.

Dyvik, R. and C. Madshus (1985). Lab measurements of G_{max} using bender elements. Advances in the art of testing soils under cyclic conditions, *ASCE*, New York, N.Y., 120-147.

Gravesen, H. (1991). Brief description of ice load - structure - soil system. Dynamic properties of soils for ice load. A case history of bridge pier design for Western Bridge, Storebælt. *DGF Bulletin* No. 8.

Kristensen, P.S. (1991). Geology for Western Bridge. Dynamic properties of soils for ice loads. A case history of bridge pier design for Western Bridge, Storebælt. *DGF Bulletin* No. 8.

Mayne, P.W. and F.K. Kulhawy (1982). K_0-OCR relationships in rock. *JGED, ASCE*, Vol. 108, No. GT6, pp. 851-872.

Richart, F.E., Jr., J.R. Hall, Jr. and R.D. Woods (1970). Vibrations of soils and foundations. Prentice-Hall, Inc., Englewood Cliffs, N.J.

Seed, H.B. and I.M. Idriss (1970). Soil moduli and damping factors for dynamic response analysis. *University of California*, Berkeley, College of Engineering. Earthquake Engineering Research Center. Report, EERC 70-10, 18p.

Selnes, P.B. (1986). Damping in Soils. A literature study. NGI report 40013-28, 8 May 1985, rev. 9 April 1986.

4. BEARING CAPACITY, DISPLACEMENTS, STIFFNESS AND HYSTERIC DAMPING OF STOREBÆLT BRIDGE PIERS UNDER ICE LOADING

Bearing Capacity, Displacements, Stiffness and Hysteretic Damping of Storebælt Bridge Piers under Ice Loading

by

Knut H. Andersen, Norwegian Geotechnical Institute
Ole E. Hansteen, Norwegian Geotechnical Institute
Marte Gutierrez, Norwegian Geotechnical Institute

ABSTRACT

Foundation analyses are presented for two idealized piers of the Western Storebælt Bridge under ice loading. The geometries and the soil conditions for the two piers are representative for piers on "stiff" and "soft" clay tills, respectively. The analyses include bearing capacity, displacements, and "backbone curves" for use in dynamic analyses. Calculation procedures and numerical results are presented. The soil parameters are determined from laboratory tests on the clay till. The results of the analyses are used to calibrate simpler, more conventional procedures used in the detailed design.

INTRODUCTION

This paper describes analyses of the foundation behaviour of two idealized models of the Western Storebælt bridge piers. These analyses were performed with procedures similar to those used by NGI in the foundation design of offshore gravity structures. The analyses assumed that the ice loads act along the bridge axis without any torsional component. The results of the analyses described herein were used to calibrate more conventional design calculations which are used in the detailed design of the individual piers (Kristensen, 1991b).

GEOMETRIES AND SOIL PROFILES

The soil conditions vary substantially along the length of the bridge (Kristensen, 1991a). The ice load is most critical for the bridge in deep waters, and two idealized models representative of piers in deep water were selected for the comprehensive analyses described in this paper (Fig. 1).

Site A consists of relatively stiff clay till layers in the upper 13 m. The preconsolidation stress is 1095 kPa, corresponding to an overconsolidation ratio, OCR, of 3 under the weight of the pier.

Site B consists of an 11.5 m softer clay till overlying an 11 m stiffer clay till. The preconsolidation stresses are 570 and 1095 kPa, respectively, corresponding to OCR-values of 2 and 3 under the weight of the pier.

It was assumed that the clay till is consolidated under the weight of the pier prior to ice loading.

The clay till layers are underlain by hard calcarenite or calcilisite.

A 1.5 m gravel blanket with a relative density of at least 70% is placed on top of the prepared clay till beds.

Weights and geometries of the bridge piers are given in Fig. 1.

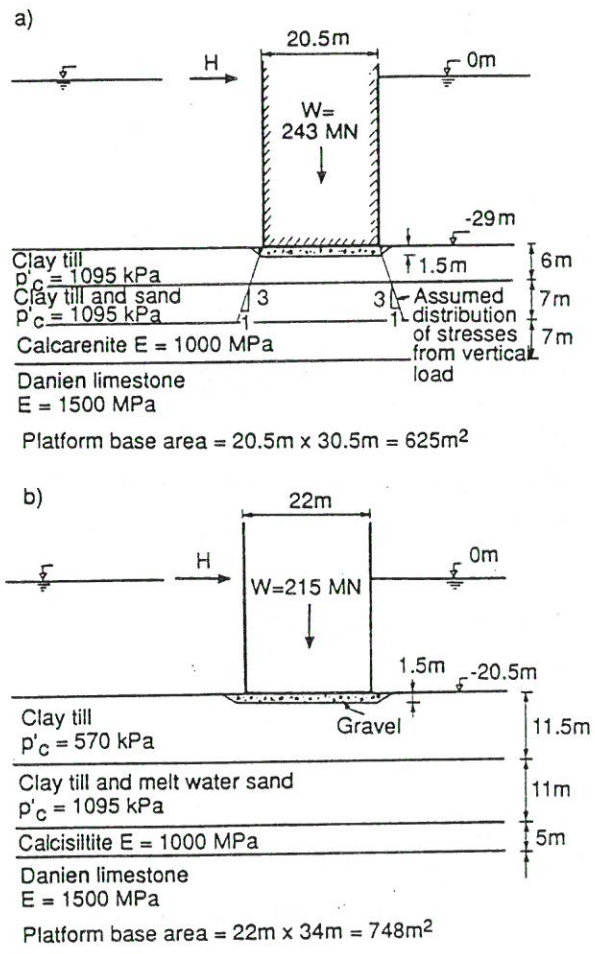

Fig. 1. Geometry and soil profiles

a) Site A: "Stiff" clay till

b) Site B: "Soft" clay till

ICE LOAD

The ice load history used in the calculations is given in Fig. 2. The ice load history contains two frequencies. It represents a simplification of the actual ice load history (Gravesen, 1991).

The low frequency component has a period of 10 s, and contains between 200 and 1500 cycles. The double load amplitude varies

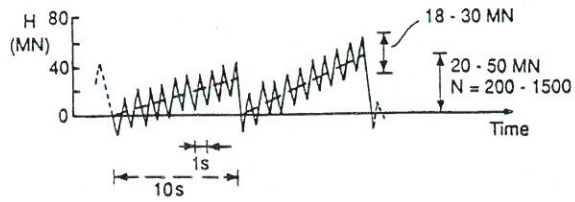

Fig. 2. Ice loading history

from 20 to 50 MN, with a constant probability density between 20 and 50 MN.

The high frequency component has a period of 1 s, and contains between 2000 and 15000 cycles. The cyclic load amplitude is constant, with a single amplitude in the range 9 MN to 15 MN. The actual value depends on the hysteretic soil damping.

It has been indicated that review of the ice strength parameters may reduce the loads to 75% of those given above.

The ice load direction was specified as 65° to the bridge axis. The analyses described in this report were made with the load in the direction of the bridge axis.

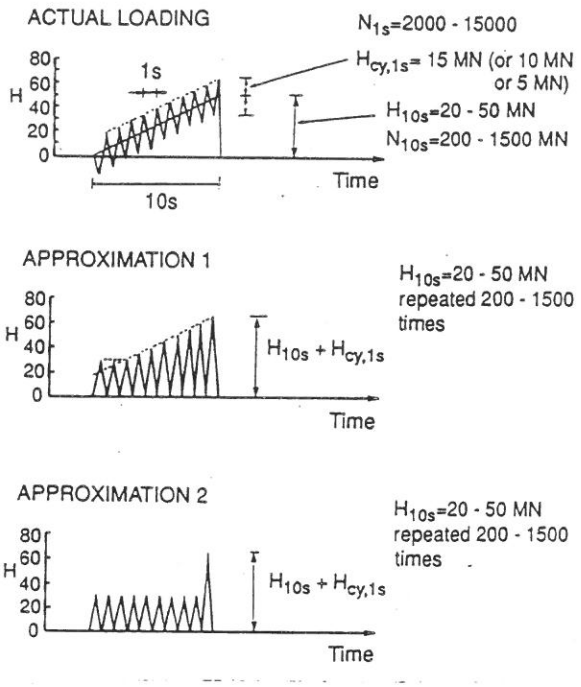

Fig. 3. Load histories used as approximations to the actual ice load history

EQUIVALENT NUMBER OF CYCLES

The cyclic load history was simplified to reduce the complexity of the analyses. Two approximations were used (Fig. 3). Approximations 1 and 2 will give cyclic degradation on the high and low side, respectively.

The cyclic load histories were transformed to an equivalent number of cycles of constant amplitude in the analyses. The equivalent number of cycles was determined by the strain-accumulation procedure (Andersen et al., 1978). The procedure utilized cyclic shear strain contour diagrams established from the cyclic laboratory tests. The contour diagram for Storebælt clay till with OCR=3 is shown in Fig. 4. In the approximate load histories, the cyclic and the average loads are the same. The contour diagram was therefore established for the condition of $\tau_{cy}=\tau_a$

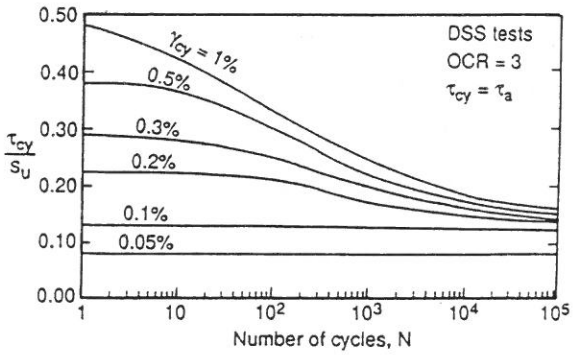

Fig. 4. Cyclic shear strain diagram for clay till with OCR=3

from the data in Fig of Kleven and Andersen, 1991.

The equivalent number of cycles of maximum loads, i.e. H = 50 MN + $H_{cy,1s}$, that gives the same cyclic effect as the irregular cyclic load histories, are summarized in Table 1. The equivalent number of cycles

was determined for various assumptions of high frequency cyclic load, $H_{cy,1s}$, and number of low frequency cycles, $N_{10\ s}$.

The real number of equivalent cycles is between the upper and lower values in Table 1, i.e., between 30 and about 500.

Table 1. Equivalent No. of cycles of maximum load.

N_{10s}	$H_{cy,1s}$		
	0	5	15
200	30	35[2]-50[1]	40-100
500	80	90-200	105-290
1500	300	315-590	375-750

1) For approximation 1 in Fig. 3

2) For approximation 2 in Fig. 3

STRESSES IN THE GROUND

The effective vertical stresses in the ground, σ'_{vc}, are due to the overburden of the soil and the weight of the pier. The effective vertical stresses beneath and outside the piers are summarized in Tables 2 and 3. The effective vertical stress from the weight of the pier was calculated by assuming a 1:3 stress distribution in the soil beneath the pier (Fig. 1a). The effective vertical overburden stress was calculated by using a submerged unit soil weight of 12 kN/m^3. It was assumed that the soil is fully consolidated under the weight of the pier. The effective stresses are relatively constant with depth beneath the pier, because the reduction in vertical stress from the weight of the pier with depth is about the same as the increased vertical stress from the overburden. It was thus not necessary to divide the soil beneath the pier into many layers.

Table 2. Vertical effective stresses and undrained static shear strengths for Site A.

	z	σ'_{vc}= p'_o+ (W/A)	p'_c	OCR	s_u^C	s_u^{DSS}	s_u^{DSS}
	(m)	(kPa)	(kPa)		(kPa)	(kPa)	(kPa)
Beneath pier	1½-13	365	1095	3	385	260	200
Outside pier	0-3	18	1095	60	225	110	80
	3-6	54	1095	20	280	150	120
	6-13	114	1095	10	310	190	160

Table 3. Vertical effective stresses and undrained static shear strengths for Site B.

	z	σ'_{vc}= p'_o+ (W/A)	p'_c	OCR	s_u^C	s_u^{DSS}	s_u^{DSS}
	(m)	(kPa)	(kPa)		(kPa)	(kPa)	(kPa)
Beneath pier	1½-11½	290	570	2	220	160	110
	11½-22½	365	1095	3	385	255	200
Outside pier	0-3	18	570	32	145	70	55
	3-6	54	570	11	155	95	80
	6-11½	105	570	5	160	105	90
	11½-22½	204	1095	5	305	205	175

The overconsolidation ratio (OCR), defined as the ratio between the preconsolidation stress (p'_c) and the present effective vertical stress (σ'_{vc}), are also given in Tables 2 and 3. Beneath the piers, the OCR is 3 in the "stiff" clay till and 2 in the "soft" clay

till. Outside the piers, the OCR varies more and reaches high values close to the soil surface.

The shear stress varies from element to element in the soil. Simplified shear stress conditions are illustrated in Fig. 5. The shear stresses are composed of average, τ_a, and cyclic, τ_{cy}, components. The stress paths also vary, with some elements having stress paths similar to DSS tests, whereas other elements have stress paths similar to triaxial compression or extension tests.

The average shear stress, τ_a, is composed of 1) an initial shear stress, τ_o, due to the weight of the soil and the pier, and 2) an additional average shear stress, $\Delta\tau_a$, which is due to the average ice load. It was assumed that the soil is consolidated under the initial shear stress, τ_o, but that the additional shear stress, $\Delta\tau_a$, acts under undrained conditions.

The cyclic shear stress, τ_{cy}, is caused by the cyclic ice load component, and it was assumed to act under undrained conditions.

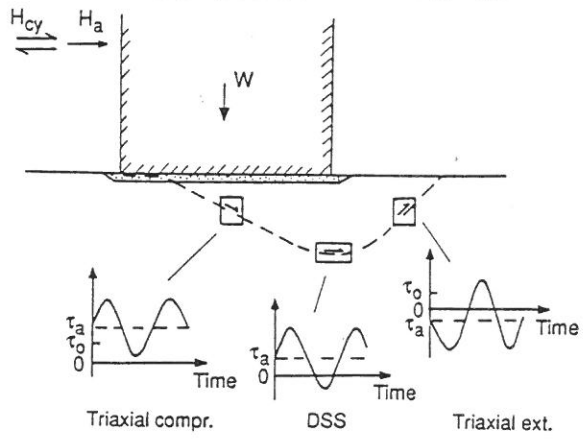

Fig. 5. Simplified shear stress conditions beneath a pier.

SOIL PARAMETERS

The soil properties were determined from the results of the laboratory tests on the clay till. Static and cyclic triaxial and DSS laboratory tests were run on clay till with overconsolidation ratios of 1 and 3. These tests cover the stress conditions beneath the piers, where the overconsolidation ratio is 3 and 2 for the "stiff" and the "soft" clay tills, respectively. Outside the piers, the overconsolidation ratio can be much higher, and the laboratory test results on the clay till had to be extrapolated. The extrapolation was guided by the results of tests on Drammen clay (Andersen et al., 1988a).

Static Shear Strengths

The undrained static shear strengths are functions of the vertical effective stress and the OCR, as shown in Fig. of Kleven and Andersen, 1991. The laboratory tests also indicate that the static shear strength is anisotropic, with different strengths in triaxial compression, DSS, and triaxial extension. The following symbols are used in this paper:

s_u^C - triaxial compression strength
s_u^{DSS} - direct simple shear strength
s_u^E - triaxial extension strength

The static shear strengths in the soil beneath and outside the piers were determined based on the vertical stresses and the OCR in Tables 2 and 3, and the relationships in Fig. of Kleven and Andersen, 1991. The result-

ing static shear strengths are given in Tables 2 and 3. The static triaxial compression strength in the upper layers outside the pier is 225 and 145 kPa for Sites A and B, respectively. The shear strengths are considerably higher beneath the piers, due to the higher effective stresses from the weight of the piers.

Cyclic Shear Strengths

The cyclic shear strength of a soil is defined as the sum of average and cyclic shear stresses that cause failure after a given number of cycles (Andersen et al., 1988b); i.e.:

$$\tau_{f,cy} = (\tau_a + \tau_{cy})_f$$

The cyclic shear strength was established for clay till with OCR of 1 and 3 and disturbed clay till from the diagrams in Figs and in Kleven and Andersen, 1991. The resulting cyclic shear strengths are presented in Figs 6 and 7 for load histories with 1, 10, 50, 100 and 1000 cycles. The strengths for OCR=2 were established by interpolation between strengths for OCR = 1 and OCR = 3. There is relatively little difference between normalized cyclic shear strengths for clay till with OCR=1 and OCR=3. It was therefore assumed that the normalized cyclic shear strengths of the clay till are relatively little influenced by OCR, and the normalized cyclic shear strengths for OCR=3 were used for high OCR-values.

Failure under cyclic loading may occur as large cyclic strains, large average (perma-

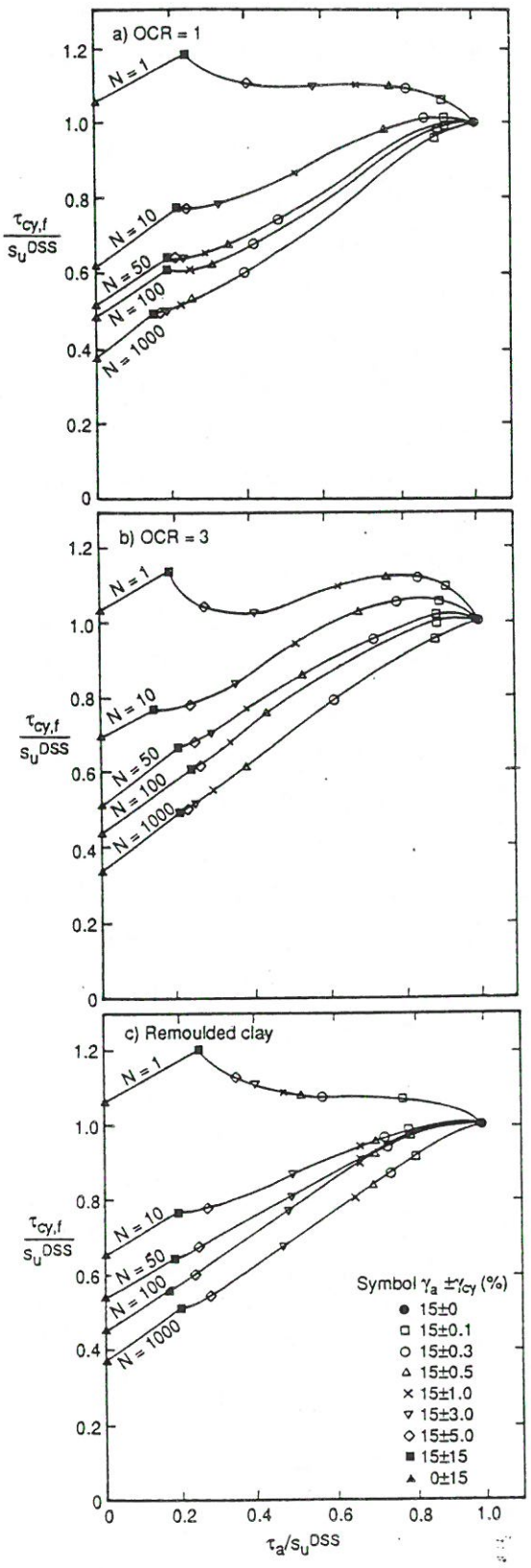

Fig. 6. Cyclic DSS shear strengths of clay till

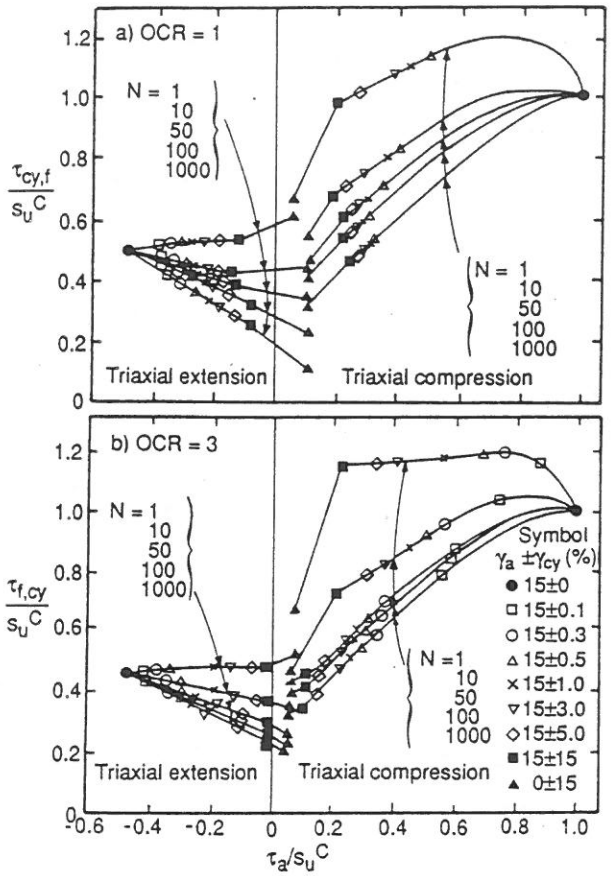

Fig. 7. Cyclic triaxial shear strengths of clay till

nent) strains, or a combination of the two. The failure mode, i.e. the combination of average and cyclic shear strains at failure, depends on the average shear stress. The failure mode is also determined from the cyclic laboratory tests and is indicated along the cyclic shear strength curves in Figs 6 and 7.

The cyclic shear strengths were based on cyclic laboratory tests with a 10 s period. A few cyclic DSS tests indicated that the cyclic shear strength of the clay till will be higher if the period is 1 s (Kleven and Andersen, 1991).

Stress-Strain Properties for Cyclic Loading

To calculate the permanent and the cyclic displacements of the piers under cyclic loading, it is necessary to know the relationships between:

- cyclic shear stresses and cyclic shear strains, and
- average shear stresses and average shear strains

after the equivalent number of cycles.

To calculate the backbone curve used to determine the soil stiffnesses in the dynamic analyses, it is necessary to know the relationship between cyclic shear stresses and cyclic shear strains.

In general, cyclic and average shear strains depend on both cyclic and average shear stresses. This can be seen from Fig. 9, which shows average and cyclic shear strains measured in the laboratory tests on clay till with OCR=3 after 100 cycles.

For the ice loading analysed in this report, it was possible to work with simplified stress-strain relationships. This is illustrated in Fig. 8. The cyclic and average ice load components are equal in the approximate ice load histories. It was thus believed reasonable to assume that the cyclic and average shear stresses due to the ice loading are equal in the soil elements in the ground, and that a soil element will follow the 45° line in Fig. 8. With this assumption, one could establish the relationships between cyclic shear stresses and cyclic shear strains, and average shear stresses and average shear strains, as illustrated in Fig. 8. The asymptotes of the

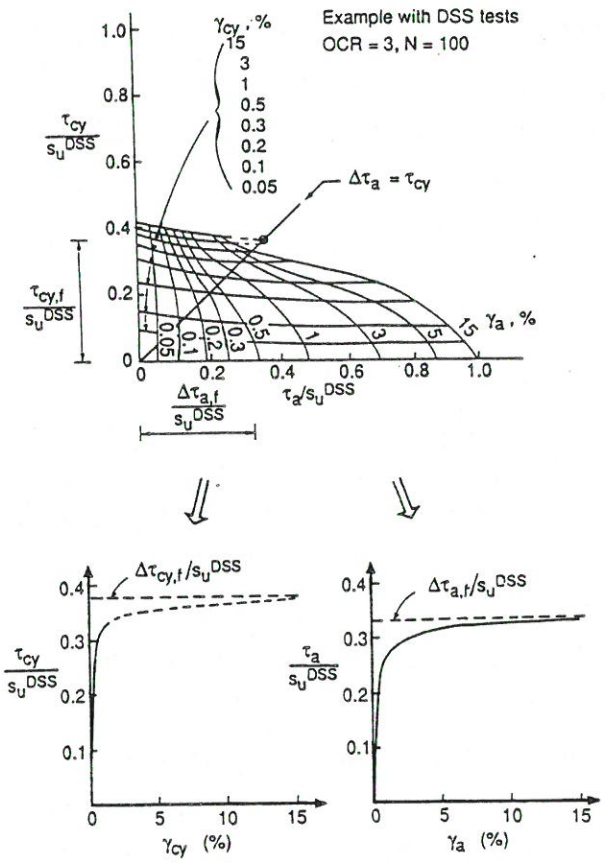

Fig. 8. Illustration of how soil parameters in finite element analyses are determined from laboratory tests

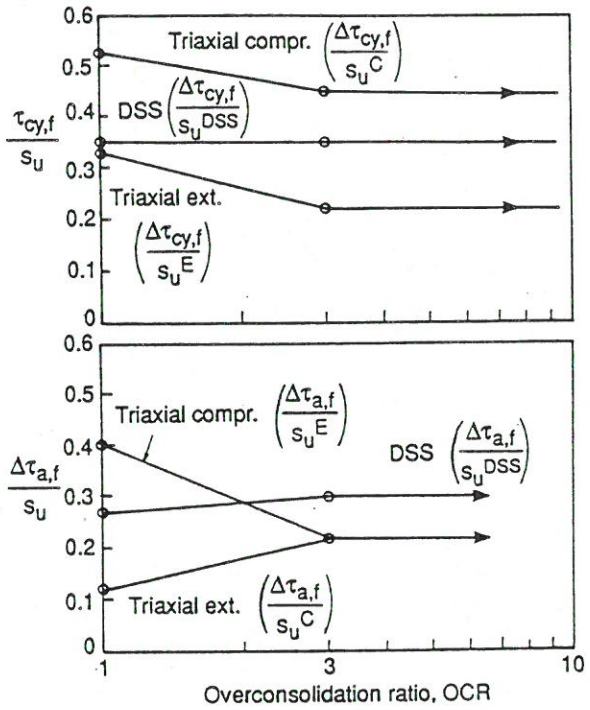

Fig. 9. Values of $\tau_{cy,f}$ and $\Delta\tau_{af}$ as functions of type of test and OCR

stress-strain curves were denoted $\tau_{cy,f}$ and $\Delta\tau_{a,f}$.

The relationships between shear stresses and shear strains are different for triaxial compression, DSS, and triaxial extension, and they also depend on the OCR. The relationships for triaxial tests were determined in the same way as illustrated for DSS tests in Fig. 8. For triaxial tests, the 45° line was drawn from the point on the horizontal axis where $\tau_a = \tau_o$.

The values of $\tau_{cy,f}$ and $\Delta\tau_{a,f}$ are given as functions of OCR in Fig. 9.

The relationships between shear stresses and shear strains were normalized with respect to $\tau_{cy,f}$ and $\Delta\tau_{a,f}$ and plotted in Fig. 10a and b. The curves are the mean of the curves for triaxial compression, DSS, and triaxial extension. The curves for OCR > 3 are based on extrapolation guided by results of Drammen clay.

The initial shear modulus was utilized to increase the accuracy of the stress-strain curves at low shear stresses. The initial shear modulus is plotted as function of OCR in Fig. of Kleven and Andersen, 1991.

In the finite element analyses, the same general soil model was used for analysis under average and cyclic loads. The shear stress at failure, τ_f, was expressed as a func

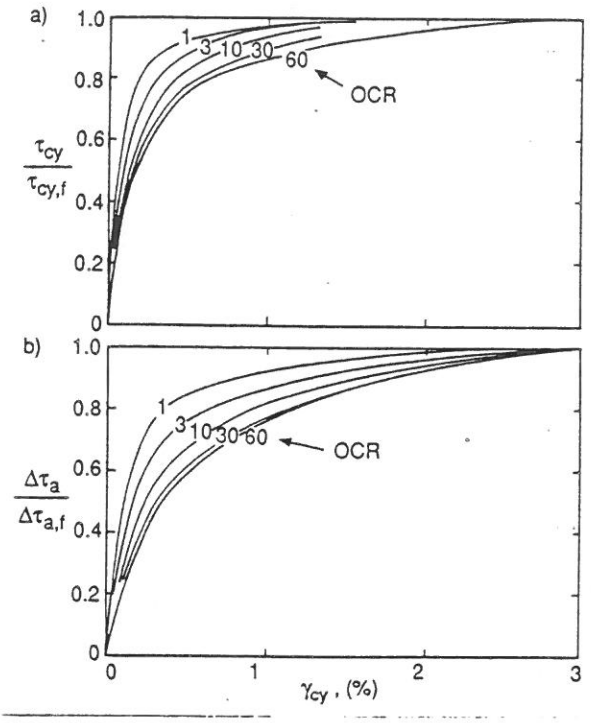

Fig. 10. Normalized stress-strain relationships for clay till after 100 cycles

tion of the angle α between the maximum compressive principal stress and the vertical axis, i.e.:

$$\tau_f(\alpha) = S_0 + S_1 \cos(2\alpha) + S_2 \cos(4\alpha)$$

The constants S_i were determined such that the failure stresses $\tau_{cy,f}$ or $\Delta\tau_{a,f}$ in Fig. 9 were obtained.

The stress-strain curves in Fig. 10 were expressed in terms of the tangential shear modulus by the expression:

$$\log\left(G_t/\tau_f(\alpha)\right) = \log\left(G_o/\tau_f(45°)\right) - C_1\zeta - C_2\zeta^2 - C_3\zeta^3$$

where

$$\zeta = \frac{\tau_{max}}{\tau_f(\alpha)}$$

The deformation properties were determined from cyclic laboratory tests with 10 s load period. A few cyclic DSS tests indicated that the shear strains will be smaller if the period is 1 s (Kleven and Andersen, 1991). The effect seems greatest for average shear strains and smaller for cyclic shear strain, but it was difficult to quantify the effect based on the few tests available.

Hysteretic Soil Damping

The Seed-Idriss (1970) damping curve for clay was used as an approximation for clay till with 10 s load period after 100 cycles (Kleven and Andersen, 1991).

A few tests with 1 s period seemed to indicate that the Seed-Idriss (1970) curve may possibly give damping on the high side for the high frequency ice load component with a period of 1 s.

The laboratory test results also indicated that for a given shear strain, the damping may decrease with increasing number of cycles.

Gravel

Failure is not likely to occur in the 1.5 m gravel layer. The gravel was in the analyses therefore represented by a constant shear modulus unless vertical tension occured.

The shear modulus was estimated from data on sand and gravel in the literature (Seed and Idriss, 1970 and Seed et al., 1986). The shear modulus relating cyclic stresses and

strains was estimated to be 68 MPa. The shear modulus relating average shear stresses and strains was estimated to be 38 MPa. This last value is a virgin loading value divided by a factor of 1.5 to account for cyclic effects. The shear modulus values given above should be used together with a Poisson's ratio of 0.0.

BEARING CAPACITY

The bearing capacity under cyclic ice loading was calculated with limiting equilibrium methods following the procedure described by Andersen et al. 1988b. Both horizontal sliding along the gravel/clay interface at 1.5 m depth and deep-seated failure surfaces extending into the clay till were investigated.

The normalized cyclic shear strengths were determined from Figs 6 and 7. The absolute cyclic shear strength values were found by multiplying the normalized cyclic shear strengths by the static shear strengh values in Tables 2 and 3. The normalized cyclic shear strengths depend on OCR. The OCR-values beneath and outside the piers are included in Tables 2 and 3. Cyclic shear strengths for OCR=2 were established by interpolation between the curves for OCR=2 and 3 in Figs 6 and 7. The curves for OCR=3 were also used for OCR>3.

The cyclic bearing capacity analyses were also performed for the case of a thin disturbed clay till layer at the top of the clay till. The static DSS shear strength in the disturbed clay till was assumed to be $s_u^{DSS} = 0.33 \cdot \sigma'_{vc}$ (Kleven and Andersen, 1991). The normalized cyclic shear strength diagram for the thin disturbed clay till layer is shown in Fig. 6c.

The gravel layer was assumed unable to support tensile stresses, and an effective width was used. The effective width was calculated by subracting twice the eccentricity from the original pier width. The eccentricity is equal to the ratio of the overturning ice load moment and the pier weight.

Deep-seated failure surfaces were analyzed by the computer programme CAP (Lauritzsen and Schjetne, 1976). Three-dimensional effects were accounted for by using an empirical side friction of $0.5 \cdot s_u^{DSS}$.

The calculation procedure is based on the assumption that:

- the combination of average and cyclic shear strains is the same along the potential failure surface (strain compatibility), and on
- the condition that the average shear stresses along the potential failure surface must be in equlibrium with the soil weight, pier weight and average ice load.

The calculations were performed for various combinations of γ_a and γ_{cy}, and the strain combination that gave the lowest bearing capacity was determined. The cyclic shear strengths for the selected strain combinations were determined from Figs 6 and 7.

The results of the cyclic bearing capacity analyses are given in Table 4. Horizontal sliding in a thin disturbed layer at the top of

but the influence of τ_a is larger than for the DSS tests. For accurate estimates of the cyclic shear modulus, $G_{cy} = \tau_{cy}/\gamma_{cy}$, the results show that it is necessary to consider the effect of the average shear stress. As discussed in Andersen et al., 1991 in the ice loading analyses of the Storebælt bridge piers, the average and the cyclic shear stresses in the foundation soil elements could be assumed to be of equal magnitude. The diagrams in Figs 10 and 11 made it possible to establish relevant relationships between cyclic shear stress and cyclic shear strain, and average shear stress and average shear strain, for this stress condition.

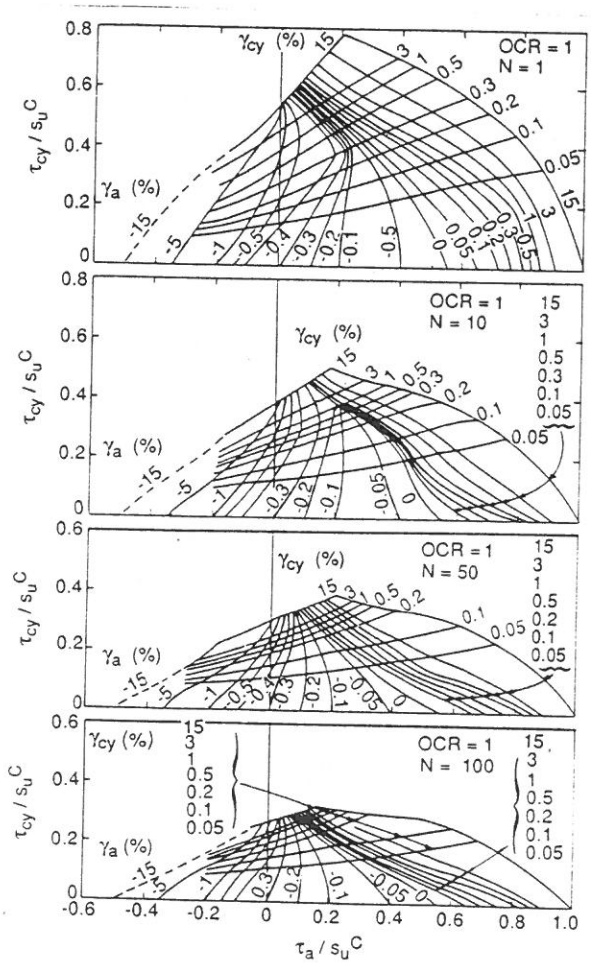

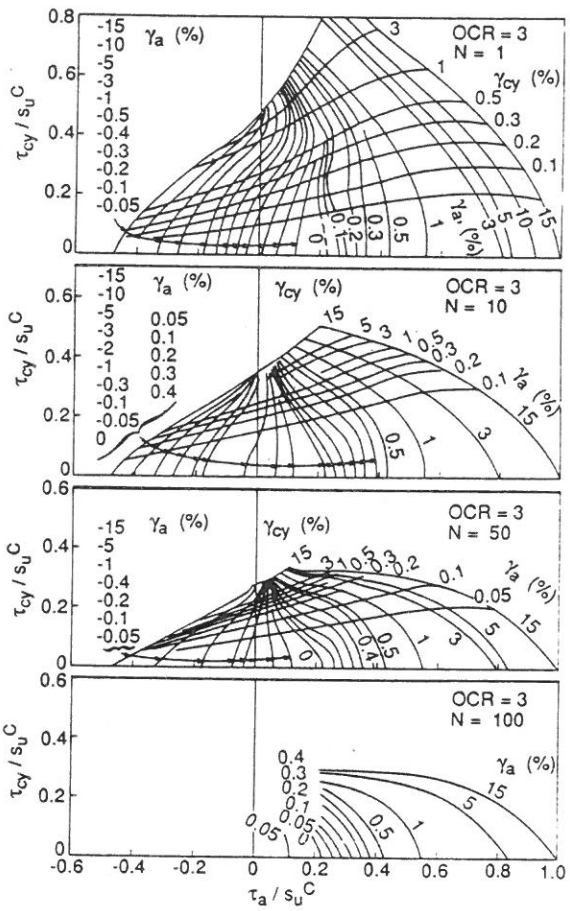

Fig. 11. Average and cyclic shear strains in triaxial tests on Storebælt clay till:
(a) OCR=1
(b) OCR=3

The three cyclic DSS tests run with a load period of 1 s showed that a 1 s load period gives a smaller rate of increase of average and cyclic shear strains with number of cycles compared to the 10 s period.

Initial Shear Modulus

As outlined in Andersen et al., 1991 the cyclic and permanent displacement components

are the results of shear strains integrated over the entire soil foundation. In the far field part of the soil volume, the shear stresses and the shear strains will be small, and it is necessary that the shear modulus is reasonably accurate also in the small strain range.

A comprehensive laboratory test program was carried out to investigate the small strain behaviour of the Storebælt clay till. The program consisted of resonant column tests and G_{max} measurements by piezoceramic bender elements. The number of tests performed is shown in Table 2. Description of the resonant column test can be found for example in Richart et al. (1970), while the piezoceramic bender element (PCBE) technique to measure the shear wave velocity is described in Dyvik and Madshus (1985).

The PCBE test has the advantage of being non-destructive,and the bender elements can be used in different testing apparatues (eg. triaxial, oedometer and direct simple shear). The small strain behaviour can thus be measured on the same test specimen and under the same stress conditions as the large strain behaviour.

The best estimate of the initial shear modulus of the Storebællt clay till is presented in Fig. 12. The initial shear modulus was used in the foundation analyses described by Andersen et al. 1991.

The initial shear modulus was also used to guide the shear strain contours in Figs 10 and 11 in the low strain range.

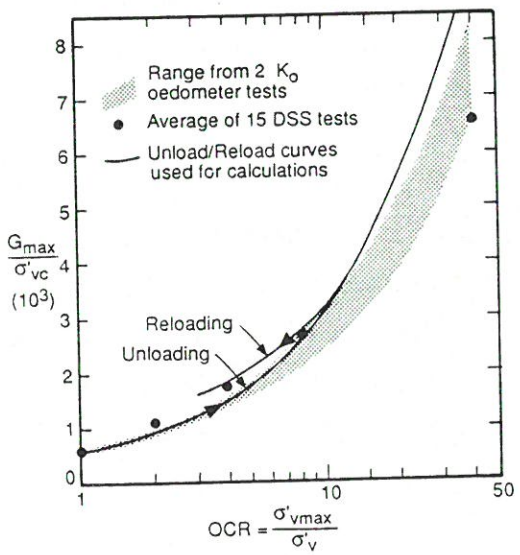

Fig. 12. Initial shear modulus measurements on Storebælt clay till.

DAMPING

The hysteretic damping from cyclic triaxial and direct simple shear tests was evaluated together with the viscous damping obtained in the resonant column tests. The triaxial test results were calculated on the basis of the data without any smoothing or filtering. Some of the results from the DSS tests were smoothed before calculation of damping, but checks carried out showed small effect of this smoothing on the calculated damping.

An example of the results is presented in Fig. 13. The example shows results from cyclic DSS tests and resonant column tests for clay till with OCR=3. Also shown on the diagram is the Seed-Idriss (1970) recommended damping curve for clay.

In general, it was found that the damping was reduced with number of cycles and especially during the first 10 cycles. For the

Table 4. Calculated cyclic bearing capacities for deep-seated failure surfaces and horizontal sliding at 1.5 m. Values for horizontal sliding in ( ).

No. of cycles	Horizontal failure load (MN)	
	Site A	Site B
50	48 (42)	48 (47)
100	48 (39)	47 (44.5)
1000	45 (36)	41 (37.5)

the clay till is more critical than deep-seated failure surfaces in "intact" clay till. The critical failure mode is large average shear strains ($\gamma_a = 15\%$) and smaller cyclic shear strains ($\gamma_{cy} < 15\%$). At failure, the permanent (average) displacement components of the pier will thus be greater than the cyclic displacement components.

DISPLACEMENTS AND BACKBONE CURVES

Computer Program

The computer program INFIDEL (Hansteen, 1988) was used in the analyses.

INFIDEL is a non-linear, 3D finite element program. It is primarily intended for soil-structure interaction analyses during design of offshore structures.

The soil volume is separated into a near-field and a far-field by a cylindircal boundary.

The far-field elements are layer elements which extend from the cylindrical boundary to infinity in the horizontal direction. The material in these elements is assumed to behave linearly because of low stress levels.

The near-field soil elements are ring elements. Their upper and lower faces are horizontal, while their inner and outer faces are vertical elliptic or circular cylinders. The elements are interconnected along the four corner node circles (ellipses).

The program also offers structural elements that model flexibilities in skirts and other parts of offshore platforms. These elements were not used in the present calculations.

The soil elements (near-field and far-field) are based on a mixed variational principle with independent assumptions on hydrostatic stress as well as displacements. The global system of equations expresses explicitly the volumetric compressibility constraints in the soil as well as the equilibrium conditions. The non-linear shear deformability of the soil is implicit in the equilibrium equations.

Simple isoparametric interpolation is used for the displacements in the vertical and radial directions. The pressure is assumed constant within the near-field elements. In the ring direction, an expansion in Fourier series is used.

In a non-circular computational model, and also in a circular model with non-linearities and horizontal and moment loads, the coefficient matrix of the system of equations will exhibit coupling between the Fourier terms considered. Therefore, the program solves simultaneously for all the Fourier terms, and only a limited number of terms can be con-

sidered (3 terms when vertical load and horizontal/moment load are applied separately, 2 terms for each when they are applied simultaneously). In the present analyses, two Fourier terms were used for each of the components.

The program also computes the hysteretic damping ratio by means of numerical integration of the hysteresis area over the soil volume. In each integration point, the maximum shear strain is determined from the principal strains. The local damping ratio is found as a function of the maximum shear strain. The hysteresis area is found from the shear strains and the corresponding deviatoric stresses.

Computation Model

The horizontal cross section of the bridge piers are rectangular. In the INFIDEL models, they were represented by ellipses with the same area, and the same ratio between the half axes as the ratio between the sides of the rectangular cross section.

The soil profile was modeled down to a depth 20 m below seabed for the pier on stiff clay till, and 27.5 m below seabed for the pier on soft clay till. In both cases the profile was modeled with 14 layers of soil elements. The numbers of near-field "doughnut" elements were 420 for the stiff case, and 476 for the soft case.

Computed Displacements and Load-Displacement Curves

Two sets of displacement components are given for each pier. One set represents the cyclic response, which has an increasing amplitude (for the same load level) as the number of load cycles increases. The other set represents the permanent response, i.e. gradual, non-recoverable displacements. Also the permanent displacements increase (for the same load level) as the number of load cycles increases.

Separate analyses were performed to obtain cyclic and permanent displacements. The displacement calculations were performed for an equivalent number of load cycles of 100. The soil parameters needed in the analyses are presented in Figs 8, 9 and 10.

Loads were applied incrementally to the structure. The cyclic and the average load increments were equal. The ice loads were applied at a level corresponding to sea surface, along the weakest axis of the pier (i.e., along the bridge axis). The displacements of most interest are displacements at bridge deck level, 20.0 m above sea surface. The displacements are due to:

- a horizontal displacement at seabed level, and
- a rotation about a horizontal axis.

The second of these components is dominating, both for the cyclic and for the permanent displacements.

The bearing capacity calculations are con-

sidered to yield better predictions for the ultimate loads than the finite element analyses do. Figure 11 shows a load-displacement curve where the results from both types of calculation was integrated. The curve was obtained by simple curve fitting.

The calculated displacements in Fig. 11 indicate that the permanent (average) displacement component greater than the cyclic displacement component. This agrees with the bearing capacity analyses, which indicated that the permenent displacements would be greater than the cyclic displacements.

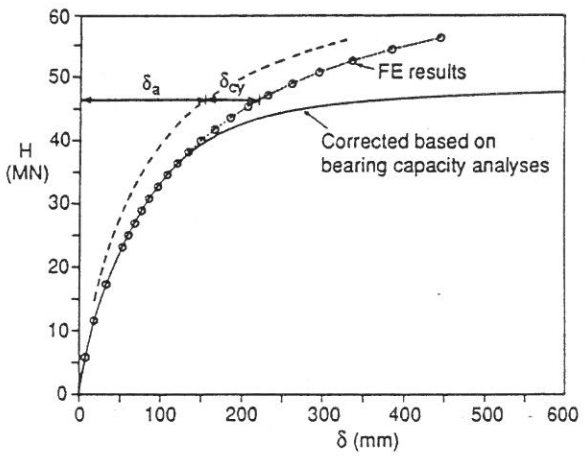

Fig. 11. Displacements at bridge deck vs ice load. Site A.

Backbone Curves

The backbone curves were established from the results of the cyclic displacement calculations. The backbone curve is intended for nonlinear, dynamic analysis of the pier response under irregular dynamic loads. These analyses should use the backbone curve in a kinematic plasticity model of the "soil spring".

Under the cyclic ice loading, the base of the pier both translates horizontally and rotates about a horizontal axis. The soil spring was specified as a rotational spring about the rotation center. The origin of the curve is located at M - ½ M_{max}, where M_{max} is the maximum moment due to average and cyclic loads.

The backbone curve was found by means of curve fitting, where the curve (for the pier on stiff clay till), was required to satisfy the following conditions:

- The curve should pass through the point corresponding to computation results for 20 MN cyclic load (single amplitude).
- The hysteretic damping ratio for loops corresponding to 5.8 MN (single) load amplitudes should be 4.4%, as found from the INFIDEL computations.
- The hysteretic damping ratio for loops corresponding to 17.3 MN (single) load amplitudes should be 7.8%, as found from the INFIDEL computations.
- The initial stiffness of the curve should be ≈60% of the stiffness found by finite element calculations with the initial shear modulus, G_{max}, of the soil.

The load level of 20 MN in the first of these conditions is somewhat arbitrary. If a load level of 11.6 MN had been chosen instead, the secant stiffness at this level would have been ≈20% higher than what is implied by the backbone curve presented. If 25 MN had

been used as the "characteristic" load, the secant stiffness at this level would have been ≈12% lower than implied by the backbone curve presented.

The reason for these apparent discrepancies is that in the soil models developed by NGI for cyclically loaded clays, the previous load history is built into the model in such a way that when the response to a load f_* (characteristic) load is calculated, the previous load history is also scaled to f_* (design load history). In the incremental calculation procedure f is increased gradually from 0 upwards. Thus, only in the final result is the full design load history accounted for. The backbone curve, on the other hand, should represent in an adequate manner the response of the soil to small and large load cycles, with the full effect of the previous load history accounted for all the time. Therefore, the load-displacement curve obtained from the incremental calculations cannot be used as a backbone curve. For values of $f < 1$, the backbone curve is expected to fall below the curve from the calculations, and at $f = 1$ (i.e., at the characteristic load) the two curves intersect.

The last condition with reduction in the initial stiffness was imposed to account for reduction in modulus due to pore pressure generation due to cyclic loading. The reduction is somewhat on the high side because of the uncertainties associated with the G_{max} values found in the laboratory. A too high initial stiffness, with correspondingly too high curvature in the backbone curve at low load levels, would be non-conservative in the non-linear dynamic analyses.

The curves were derived in the form of numerical tables and computer plots. Figure 12 shows an example plot.

The curve is given for moments corresponding to cyclic load amplitudes up to 27 MN. However, if the total load (cyclic plus average) exceeds the ultimate load, the backbone curve is no longer applicable. The pier will then fail with large permanent displacements.

The cyclic ice loading will generate pore pressures in the clay till. These pore pressures will not have time to dissipate during the duration of the design ice load history. The

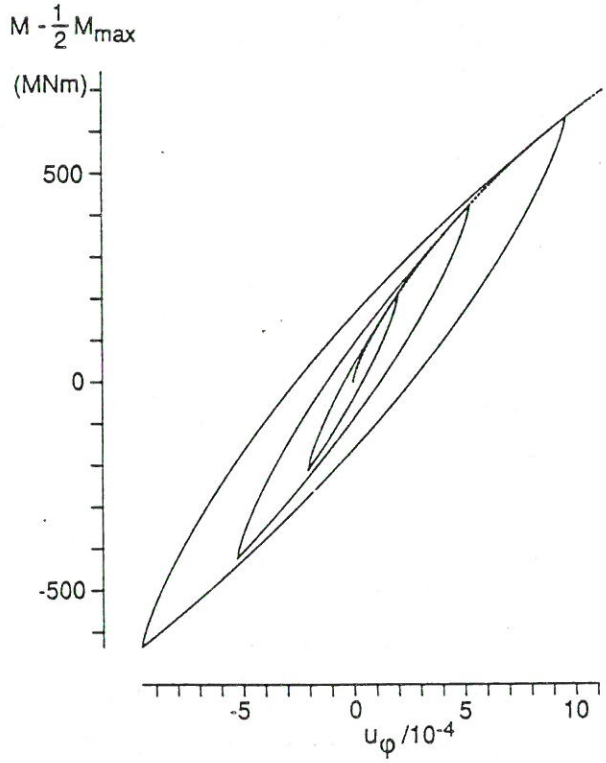

Fig. 12. Backbone curve and example hysteresis loops. Site A

displacements that occur during the design ice load history will therefore occur under undrained conditions and be due to shear strains in the clay till. The calculated displacements in Fig. 11 are based on this assumption.

The pore pressures generated by the cyclic ice loading will dissipate with time, however. This will give settlements and permanent displacements in addition to the permanent displacements in Fig. 11.

The pore pressure generated by cyclic loading is a function of τ_a and τ_{cy}, as shown in Figs and of Kleven and Andersen (1991). The pore pressure also depends on the stress path and is different for triaxial and DSS tests.

The values of τ_a and τ_{cy} and the stress path beneath the piers can be determined from the finite element analyses used to calculate the displacements in Fig. 11. Then the pore pressure can be determined from the pore pressure diagrams like Figs and of Kleven and Andersen (1991).

When the pore pressure dissipates, the effective stresses increase, and the vertical displacement, δ_v, can be calculated by:

$$\delta_v = \int u(z) \cdot dz/M_r$$

where z is the depth beneath the pier and M_r is the reloading modulus of the clay till. M_r was determined from the reloding branch of the K_o-oedometer tests (Fig of Kleven and Andersen, 1991).

The displacemens due to dissipation of cyclically induced pore pressure were small and could therefore be calculated in a simple, conservative way. These calculations gave vertical settlements of less than 25 and 37 mm for Site A and Site B, respectively. If another conservative assumption is made, that these vertical settlements should occur only beneath one side of the pier, the tilt would give a horizontal displacement at bridge deck level of 60 mm and 67 mm for Site A and Site B, respectively.

REFERENCES

Andersen, K.H., O.E. Hansteen, K. Høeg and J.H. Prévost (1978). Soil deformations due to cyclic loads on offshore structures. Numerical methods in offshore engineering. Ed. by *O.C. Zienkiewics, R.W. Lewis and K.G. Stagg*. Chichester, Wiley, pp. 413-452. Also publ. in: *Norwegian Geotechnical Institute*. Publication, 120.

Andersen, K.H., A. Kleven and D. Heien (1988a). Cyclic soil data for design of gravity structures. *ASCE Journal of Geotechnical Engineering*, Vol. 114, No. 5, May, 1988, pp. 517-539. Also publ. in: *Norwegian Geotechnical Institute*. Publication, 175.

Andersen, K.H., R. Lauritzsen, R. Dyvik and P.M. Aas (1988b). Cyclic bearing capacity analysis of gravity platforms; calculation procedure; verification by model tests, and application for the Gullfaks C platform. Proc. International Conf. the Behaviour of Offshore Struc-

tures, *BOSS'88*, Vol. 1, pp. 311-324.

Gravesen, H. (1991). Brief description of ice load - structure - soil system. Dynamic Properties of Soils for Ice Load. A case history of bridge pier design for Western Bridge, Storebælt. *DGF Bulletin* No. 8.

Hansteen, O.E. (1988). Description of INFIDEL - a non-linear, 3-d finite element program. *NGI Report* 514090-1, 13 September 1988.

Kleven, A. and K.H. Andersen (1991). Cyclic test of Storebælt till. Dynamic Properties of Soils for Ice Load. A case history of bridge pier design for Western Bridge, Storebælt. *DGF Bulletin* No. 8.

Kristensen, P.S. (1991a). Geology for Western Bridge. Dynamic Properties of Soils for Ice Load. A case history of bridge pier design for Western Bridge, Storebælt. *DGF Bulletin* No. 8.

Kristensen, P.S. (1991b). Bearing capacity of ice exposed pier. Effect of torsion. Comparison between conventional and advanced design. Dynamic Properties of Soils for Ice Load. A case history of bridge pier design for Western Bridge, Storebælt. *DGF Bulletin* No. 8.

Lauritzsen, R. and K. Schjetne (1976). Stability calculations for offshore gravity structures. *Offshore Technology Conference*, 8. Houston 1976. Proceedings, Vol. 1, pp. 75-82.

Seed, H.B. and I.M. Idriss (1970). Soil moduli and damping factors for dynamic response analysis. *University of California*, Berkeley, College of Engineering. Earthquake Engineering Research Center. Report, EERC 70-10, 18p.

Seed, H.B., R.T. Wong, I.M. Idriss and K. Tokimatsu (1986). Moduli and damping factors for dynamic analyses of cohesionless soils. *ASCE Journal of Geotechnical Engineering*, Vol. 112, No. 11, November 1986, pp. 1016-1032.

5. ACCIDENTAL LIMIT STATE ICE LOADS ON BRIDGE PIERS

ACCIDENTAL LIMIT STATE ICE LOADS ON BRIDGE PIERS

by

F.T. CHRISTENSEN, Danish Hydrualic Institute, DK-2970 Hørsholm

H. GRAVESEN, Carl Bro Group Ltd., DK-2600 Glostrup

J.R. THOMSEN, LICengineering Ltd., DK-2900 Hellerup

F. ENNEMARK and S. SPANGENBERG, The Great Belt Link Ltd., DK-1601 Copenhagen V

(Denmark)

ABSTRACT

The design of the West Bridge across the western channel of the Great Belt in Denmark was governed by sea ice loads, wave loads and ship collision loads. Ice loading was designed for an accidental limit state involving probabilities of exceedance of less than 10^{-4} per year. The resulting sea ice loads are dynamically fluctuating loads. Physical model tests with both ice and soil, and computational modelling had to be applied to ensure that oscillations of the bridge-subsoil system were within acceptable limits. Non-linearity of the foundation stiffness was instrumental in damping of resonant oscillations. This article describes the design philosophies and their implications for the applied methods for determination of sea ice loads.

SOMMAIRE

La conception du pont traversant le chenal ouest du Grand-Belt fut déterminée par les charges dues à la glace, aux vagues et aux collisions des navires. La charge due à la glace fut évaluée pour une condition-limite accidentelle d'une probabilité d'excédance inférieure à 10^{-4} par an. Les charges obtenues dues à la glace sont des charges d'oscillations dynamiques. Des essais sur modèle réduit avec la glace et le sol, et des essais sur modèle mathématique ont dû être effectués pour vérifier si les oscillations du système pont/sous-sol étaient acceptables. La rigidité non-linéaire de la fondation a contribué à l'amortissement des oscillations résonnantes. Cet article décrit la philosophie du projet et ses implications pour les méthodes appliquées pour la détermination des charges dues à la glace.

KEYWORDS

Design philosophy, ice loads, dynamic response.

MOTS-CLEFS

Philosophie du projet, charges dues à la glace, réponse dynamique.

1.0 INTRODUCTION

The fixed link across the Great Belt in Denmark consists of four main elements, viz.: a combined railway and road bridge across the western channel between Fyn and the tiny island of « Sprogø », at the centre of the Great Belt; an extensive dredging and land reclamation project increasing Sprogø to three times its original size; a railway tunnel beneath the eastern channel between Sprogø and Sjaelland; and, finally, a suspension bridge for road traffic across the eastern channel, which is also the main shipping channel.

This article concerns the West Bridge, which is a 6.6-km-long low clearance (18 metres) concrete structure. The piers must be designed to withstand environmental loads caused by wind, current, waves, ice pressure, settlement action, scouring and temperature changes, as well as loads from human activities such as braking of traffic, ship collisions, fires and explosions.

Most of the environmental loads are designed for an ultimate limit state with design probabilities of exceedance of 10^{-2} per year, corresponding to an average recurrence time of 100 years. The ice pressure, however, was designed for an accidental limit state with a design probability of exceedance of less than 10^{-4} per year, corresponding to an average recurrence time of more than 10,000 years. It is fairly unusual to determine ice loads with such extremely small exceedance probabilities, but, in reality, accidental limit state design offers a more consistent way of selecting appropriate safety factors.

Only loads from level ice are considered in this article. For the West Bridge, ice ridges and rafted ice have been found to cause ice load increases similar to those from dynamic amplification of level ice loads on the final layout.

This article concerns the overall design philosophy and implementation of the final pier design. Future papers are intended to describe in detail the soil tests and the physical model tests in ice, using the final pier layout in compliant suspension.

2.0 DESIGN PHILOSOPHY

High levels of safety are integral to the design and operation of the Great Belt Link, cf. Vincentsen and Spangenberg (1990). Risk acceptance criteria address two kinds of risks :

- Service disruptions
- User accidents

Separate sets of criteria have been established for each kind of risk. The main ' criteria are those pertaining to service disruptions, and they have been stipulated by the Danish Parliament. User accident criteria relating to standard highway and railway risk levels have been defined by the Great Belt Link Organization. Only disruption criteria are described here.

2.1 DISRUPTION RISKS FOR THE ENTIRE LINK

The approved risk acceptance criteria for disruption address disruptions of traffic lasting more than one month. Three criteria shall be met :

- A criterion for simultaneous disruptions of both road and rail traffic, referred to as « common mode » disruption.
- A criterion for road traffic disruption which includes the events affecting road failures only **and** the common mode failures.
- A criterion for rail traffic disruption which includes the events affecting rail failures only **and** the common mode failures.

The three criteria are independent of each other, and the risk levels associated with each are shown in Table 2.1. The individual modes in Table 2.1 include the common mode failure in each case. If the probability of disruption of both road and rail traffic for more than one month, i.e. common mode, is equal to the approved risk acceptance criterion, 0.02 per 100 years, then the maximum allowed probability of disruption for more than one month of the road **only** is 0.08 per 100 years (0.1 - 0.02). The same applies for disruption of the rail only.

Consequence	Length of Disruption	Criterion Probability/-100 Years
APPROVED CRITERIA Service Disruption	> 1 Month	
Common Mode		0.02
Road		0.1
Rail		0.1
GUIDANCE Temporary Outage	2 - 30 days	
Common Mode		0.2
Road		1*
Rail		1*

*Table 2.1 Approved criteria for service disruption and guidance for temporary outage of the entire link. * Expected number of occurrences in 100 years, as opposed to a probability.*

2.2 PRELIMINARY RISKS ALLOCATED TO THE WEST BRIDGE

The risks pertaining to the entire link have to be distributed between the various elements. Disruption risks allocated to the West Bridge are shown in Table 2.2. Only common mode failure is considered, since the road and railway are part of the same bridge in the Western Channel. Of the 2.0 x 10^{-4} per year risk for common mode failure for the entire link, 1.8 x 10^{-4} per year is allocated to the West Bridge. Common mode failure is considered very unlikely in the Eastern Channel, where road and rail are separated.

Consequence	Length of Disruption	Criterion Probability/-100 Years
APPROVED CRITERIA Service Disruption	> 1 Month	
Common Mode		0.018
- due to ship impact		0.01
Road		0.04*
Rail		0.04*
GUIDANCE Temporary Outage	2 - 30 days	
Common Mode		0.18
Road		0.4*
Rail		0.4*

*Table 2.2 Approved criteria for service disruption and guidance for temporary outage of the West Bridge. * The individual failure modes include the common mode failure in each case.*

Ice loads that threat the piers are relevant to the common mode failure with an exceedance probability of 1.8 x 10^{-4} per year. This risk has to be shared between ship collisions, dynamic ice loading, and other accidental actions. This resulted in the following preliminary risk budget for the West Bridge (tender design) :

- Ship collisions :	1.0 x 10^{-4} per year
- Dynamic ice loads :	0.2 x 10^{-4} per year
- Scour beneath piers :	0.1 x 10^{-4} per year
- Other acc. actions and contingency :	0.5 x 10^{-4} per year
Total disruption risk :	1.8 x 10^{-4} per year

During the process of detailed design, changes in the risk budget have been made in order to optimize the design. The above budget is therefore not the final risk budget for the West Bridge.

3.0 SEA ICE LOADS

3.1 HISTORICAL DEVELOPMENT

In the fall of 1987, available data regarding ice conditions in the Great Belt were gathered in order to gain an

overview of the situation with respect to design of the bridge piers. The report included a preliminary extreme value analysis of the product of thickness and strength in order to account for their interdependence, and theoretical predictions of ice loads on various proposed layouts.

In January 1988, a report was issued on ice loading of multi-legged bridge piers, and a field measurement programme for ice strength was proposed. Field measurements were favoured by the Great Belt Link Ltd., but ice conditions during 1988-90 have not made the programme possible. Early 1988, the relative importance of ultimate limit state (ULS) ice loads and accidental limit state (ALS) ice loads was analyzed. The rationale behind considering ice loads in the ALS is explained in Section 3.2.

From the many designs proposed in the outline design phase, three were selected for the tender design phase, cf. Christensen et al. (1989a). Tenderers were allowed to propose designs of their own within certain acceptance criteria. The deadline for submission of tenders was on 30 November 1988.

In April 1988, a physical model test programme was carried out at the Hamburgische Schiffbau Versuchsanstalt (HSVA) in Hamburg, then West Germany, cf. Schwarz (1985, 1987). Models of two of the tender design piers were suspended rigidly, and tested as described by Christensen et al. (1989a) in urea model ice, cf. Timco (1980). An empirical scaling method proposed by HSVA was used to determine full-scale design ice loads. In the preliminary project report by Christensen and Ottesen Hansen (1988a), qualifications were made regarding the effects of dynamic excitation of the full-scale structure. These effects were studied in the fall of 1988, and presented in the second project report by Christensen and Ottesen Hansen (1988b), and in the subsequent paper by Christensen et al. (1989b). For head-on ice floe collisions it was found, on the basis of simple damping estimates, that dynamic excitation raised the equivalent static load a factor of 1.8 over the peak load on a perfectly rigid structure. The model test programme had reduced the static ice load to nearly half of the ice load based on the code of practice, but amplification of the dynamic part of the ice load led to an equivalent design ice load nearly equal to the static load from the code of practice. Consequently, the original tender design basis was maintained, and it was planned to carry out a verification study once the final pier layout had been selected. Although the test programme at HSVA did thus not result in ice load reductions, it helped obtain a far more soundly based design basis, and it opened our eyes to the importance of the dynamic structural response for the West Bridge.

For construction of the West Bridge a contract was signed on June 29, 1989, with a consortium called European Storebaelt Group (ESG), who had proposed an alternative pier layout. The selected pier layout has a waterline cross-section quite different from those tested at HSVA during the tender design phase. Two rectangular pier shafts of 12.55 m by 5 m and 7.2 m by 5 m, respectively, support the road and railway girders, cf. Figure 3.1. This pier design will for large ice attack angles appear as a wide structure with aspect ratios (pier width to ice thickness) up to about 30, cf. Figure 3.2. The evaluation of dynamics in the HSVA tests was based on a pier with two cylindrical legs and a single-leg aspect ratio near 6. Based on the tender design studies, the actual design ice load for the selected pier was 44 MN and the torsional moment 220 MNm.

In the late summer of 1989, a verification study was initiated in order to document that the actual design (equivalent) ice load of 44 MN complied with the risk acceptance criteria. Two effects separate the selected layout from the tested tender design layout. The dynamic load factor of 1.8 mentioned above was determined for head-on ice action (zero attack angle) on the tender design pier. The tests indicated that this load factor was conservative for large attack angles. Furthermore, the modified waterline cross-section might affect ice failure modes. The large aspect ratio will promote buckling, cf. Blanchet et al. (1989), thus shifting energy to lower frequencies of the power spectrum. The lower buckling frequencies are likely to be closer to the natural frequency of the pier than the typical crushing frequencies. This could lead to increased dynamic load factors. These two effects were assumed to balance each other.

In September 1989, a number of ice laboratories were asked to give their estimates for a model test programme in which the final pier layout was to be tested in both rigid

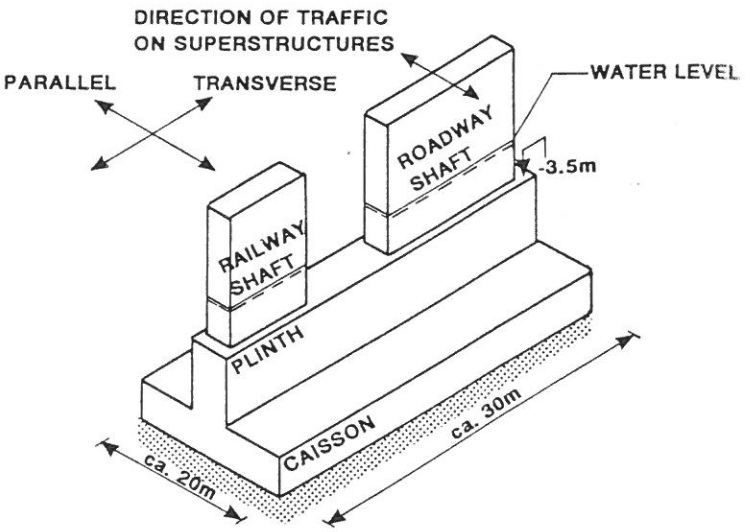

Fig. 3.1 - Sketch of final pier layout.

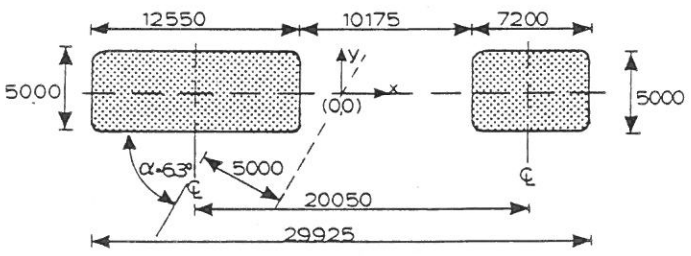

Fig. 3.2 - Cross-section of pier shafts at still water level.

and compliant suspension. The contract was awarded to the Hydraulics Laboratory of the National Research Council of Canada, referred to as NRC in the remainder of this article, cf. Pratte and Timco (1981). The verification study was carried out in the winter 1989-90 and reported by Christensen et al. (1990). It appeared that the actual design ice load was about 6 % too small to comply with the criteria. The details of the analysis will be described below.

3.2 CODE OF PRACTICE, DS410

The Danish Code of Practice, published by the Danish Engineering Association (1982), prescribes ice loads in a relatively simple way. In short, horizontal loads from pack ice of thickness h and uniaxial compressive strength σ_u are found from :

$$F = k\sigma_u dh \quad (3\text{-}1)$$

where k is an aspect ratio factor and d the projected structure width. The aspect ratio factor is given as :

$$k = 1 + 3/(1 + d/h) \text{ for } d/h \leq 9 \quad (3\text{-}2)$$

$$k = 1.75 - 0.05\ d/h \text{ for } 9 \leq d/h \leq 15 \quad (3\text{-}3)$$

$$k = 1.00 \text{ for } 15 \leq d/h \quad (3\text{-}4)$$

and the recommended values of strength and thickness are 1.25 MPa and 0.6 metres, corresponding to an exceedance probability of 2×10^{-2} per year. The resulting load is considered a live load. In the Danish system of safety factors (called partial coefficients), this means that loads and material properties will be adjusted by appropriate safety factors. These factors are, however, not tuned to ice loads, as the Great Belt Project is the first to take such a detailed account of ice loading in Danish waters.

The philosophical basis for the Danish Code of Practice prescribing loads on structures has been adopted from the Nordic Committee for Building Codes (1987), from which the following is quoted :

« Accidental loads can be divided into two groups :

- *accidental loads from human activities.*
- *exceptional environmental loads which are not included in live loads.*

Examples of exceptional environmental loads are :

- *earthquakes*
- *snow- and soil slides*
- *loads from snow, ice, wind, and waves.*

For some accidental loads there can be corresponding live loads with the same origin. As an example, an environmental load with a return period of 50 years is a live load, whereas the same load type can be treated as an accidental load if it has a far longer return period.

In practice it will be necessary to neglect the most improbable loads. The probability for the accidental loads, which can be neglected in the analysis, should not be greater than 10^{-4} for any given structure ».

This means that in theory any given structure with certain environmental loads may be calculated both for live loads subject to safety factors and for accidental loads, and the greater one of these loads will govern the design of the structure. A similar approach was used for the Sprogø coastal protection structures, which are also part of the Great Belt Link, cf. Juul Jensen et al. (1991).

In theory the two approaches should give the same result, because the selected partial coefficient should typically reduce the associated risk level to less than 10^{-4} per year. As demonstrated by Christensen et al. (1989a), the cumulative probability distribution for ice loads is much steeper in Danish waters than corresponding distributions for, e.g., wave loading, which has formed the basis for safety factors recommended by the Code of Practice. The use of these factors for ice loads is consequently without meaning. The bridge must comply with risk acceptance criteria in both servicibility, and ultimate and accidental limit states.

It was concluded in February 1988 that, for practical application, the ice load could be calculated as an accidental load. Equation (3-1) could then be used with the value of σ_u and h resulting from the extreme value analysis. Loads calculated in this way were relatively large, and it was decided to carry out model tests in order to investigate possible reductions of the ice forces. The experiments are described in Section 5.

3.3 EXTREME VALUE ANALYSIS OF ICE PROPERTIES

The revised extreme value analysis was carried out late 1989, and the result has been published by Christensen and Skourup (1991). The applied method consists of defining the product of compressive ice strength, σ_u, and ice thickness, h, as :

$$\sigma_u h = \sigma_o f(S,T) h(T(t),t) \quad (3\text{-}5)$$

where σ_o is a reference strength independent of salinity and temperature described as a stochastic parameter, f(S,T) is a function of salinity (S) and temperature (T) which describes the influence of the parameters on compressive strength, and the thickness h is a function of the temperature history and of time. Using test data, distributions for the reference strengths were determined. Using temperature records, distributions for the remainder of the product, f(S,T) h(T(t),t), were determined. These were combined through integration into an extreme value distribution for the product $\sigma_u h$, since σ_o and the remainder of the product can safely be assumed to be statistically independent.

In this way, a direct account of the amount of correlation between thickness and strength was circumvented. The resulting product was divided into a thickness and a strength, observing that realistic values were used. The results are shown in Table 3.1 for various exceedance probabilities. A total of 114 years of temperature data were used for this analysis, while only 19 winters were included in the preliminary version described by Christensen et al. (1989a). For further details of the revised analysis, the reader is referred to Christensen and Skourup (1991).

RETURN PERIOD (Years)	(10)	50	100	1000	10000	25000	50000
$\sigma_u h$ (MN/m)	(0.81)	1.26	1.48	2.05	2.58	2.82	2.96
K (^oC-days)	(243)	410	482	721	960	1055	1127
h (m)	(0.42)	0.57	0.63	0.78	0.91	0.96	0.99
σ_u (MPa)	(1.93)	2.21	2.35	2.63	2.84	2.94	2.99
σ_u with snow						2.67	2.82

Table 3.1 Extreme values of the product of uniaxial compressive ice strength and ice thickness. The product is split into a strength and a thickness by calculating a theoretical thickness based on the freezing degree-day index, K. The values for a 10-year recurrence period are not reliable with the method used.

It appears implicity from Table 3.1 that the probabilistic analysis assigns all the probability to ice formation. In the preliminary analysis from late 1987, it was justified by the argument that for the ice to reach the calculated thickness, it would have to exist for months, and would thus be bound to move at some time. By the time dynamic effects had been found important (December 1988) and a final layout had been selected (June 1989), it was too late to reformulate the probabilistic analysis to take ice velocities into account. This is partly because the number of load cycles is of importance to the soil so that an all-winter scenario must be defined, and partly due to the fact that no ice velocity observations at all are available in Danish waters.

The results of the extreme value analysis have made it clear that the Danish Code of Practice needs to be revised. The compressive ice strength to be used in equation (3-1) has been raised to 1.6 MPa for a 2 x 10^{-2} per year probability of exceedance in conjunction with a recent update of the code. Further changes with respect to ice loads will be considered for the next revision.

4.0 DYNAMIC BEHAVIOUR OF BRIDGE

4.1 PRINCIPAL DYNAMIC SYSTEM

The bridge is divided into 6 sections, each consisting of 10 or 11 spans, cf. Figure 4.1. Between each section there is an expansion joint. The central pier in each section is fixed to the bridge. The rest of the piers can move parallel to the bridge when the relatively small friction in the bearings is exceeded.

In the transverse direction the bearings are fixed between parallel steel rods. Both the bearings for the rail girder and the road girder, respectively, are fixed except for a small temperature tolerance. This strengthens the integrity of the structure by taking advantage of the strength of both of the bearings instead of only one.

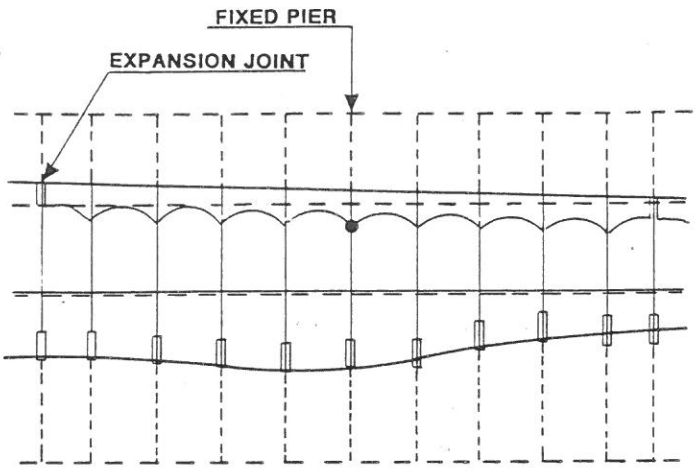

Fig. 4.1 - Bridge section used for calculation.

It is of major importance for the behaviour of the dynamic system that the quite large mass of the superstructures thereby follows the pier shaft when piers oscillate in the transverse direction, while they follow the bridge piers in the parallel motion and during rotation only until the bearing friction is exceeded.

4.2 MAIN ELASTIC ELEMENT

The piers are relatively stiff components, from which follows that the « elastic » element in the system for all important frequencies is the supporting soil.

Based on preliminary estimates of the foundation response matrix, the typical full-scale values of frequencies and stiffnesses for a unit load acting in still water level, as shown in Table 4.1, were determined.

Direction	Transverse X	Parallel Y	Rotation R
Eigenfrequency (Hz)	0.78	0.84	2.07
Generalized Stiffness			
- in GN/m	1.17	0.467	-
- in GNm/rad	-	-	299
Bearing Friction	-	0.02	-

Table 4.1 Typical full-scale values of eigenfrequencies and stiffnesses. The transverse direction stiffness was adjusted in the model tests corresponding to a full-scale value of 0.403 GNm instead of 1.17 GNm, cf. text.

4.3 NON-LINEARITIES

The three main non-linearities are the frictional bearings of the bridge girders, the non-linear buffers between the rail sections (for each 10 or 11 spans), and the non-linear soil with large hysteresis and a frequency shift due to the change of stiffness.

The friction coefficient for the bearings of the bridge girders has been estimated, and a typical value of 0.02 resulted. Minimum and maximum values were 0.005 and 0.05. The characteristic of the buffers between railbridge sections is shown in Figure 4.2.

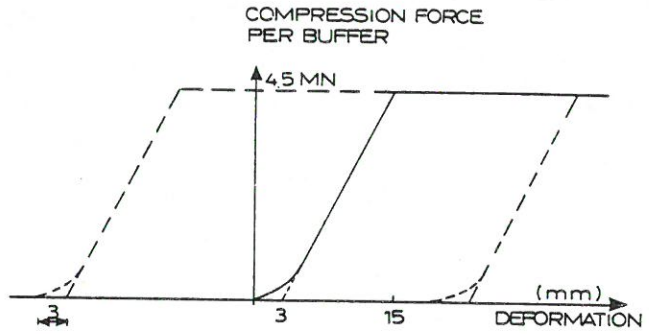

Fig. 4.2 - Characteristics of buffer. Note that there are 2 buffers per expansion joint in the railway girder.

4.4 SIMPLE ESTIMATE OF DAMPING

It is important to be able to estimate at an early stage the relative damping of the structural oscillations in order to allow prediction of the severity of the expected resonance. Simple energy methods were used. The oscillating pier is shown schematically in Figure 4.3. The external ice load acting at the water level is :

$$F = F_o \cos(\omega t) \tag{4-1}$$

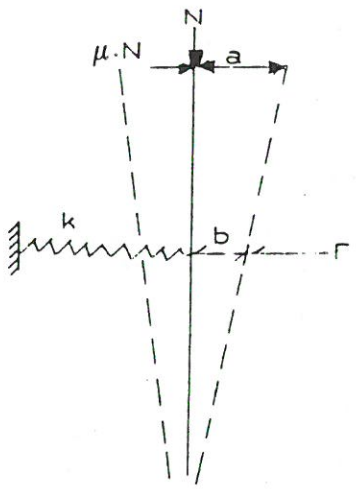

Fig. 4.3 - Driving and damping forces in bearings.

The stiffness related to the same level is denoted k, the gravity load from the superstructure is N, and the friction force in the bearings amounts to μN, where μ is assumed to be constant. The deflection of the pier top is denoted a, and the deflection at water level is denoted b. The total elastic energy, E_t, and the absorption, ΔE, by the friction force becomes :

$$E_t = \tfrac{1}{2}\, b\, F_o \tag{4-2}$$

$$b = \frac{F_o}{k} \tag{4-3}$$

$$\Delta E = 4\, a\mu N \tag{4-4}$$

With δ_f denoting the logarithmic decrement from frictional forces, the damping can be determined from :

$$2\delta_f = \frac{\Delta E}{E_t} = \frac{4a\mu N}{\tfrac{1}{2}bF_o} = 8\mu \frac{N}{F_o}\frac{a}{b} \tag{4-5}$$

$$\zeta_f = \frac{\delta_f}{2\pi} = \frac{2}{\pi}\mu \frac{N}{F_o}\frac{a}{b} \quad \text{(critical damping } \zeta_f = 1.0) \tag{4-6}$$

For heavy superstructures, even a small friction factor can give rise to significant damping. This is especially true for small amplitudes, e.g. in the ultimate and servicibility limit states, while for large force amplitudes the soil damping becomes relatively more important.

From computational modelling with elastic soil, the motion at the point of loading ($b = x_2 + x_3$) as well as the motions of the foundation plate (x_1, ϕ_x) for unit loads can be determined. By use of the energy principle sketched in Figure 4.4, the relative weighting of the internal damping ratio in soil and structure, respectively, can be determined. The internal structural elastic energy, E_i, and the soil elastic energy, E_s, are given by :

$$E_i = \tfrac{1}{2}\, F_o\, x_3 \tag{4-7}$$

$$E_s = \tfrac{1}{2}\, F_o\, x_2 \tag{4-8}$$

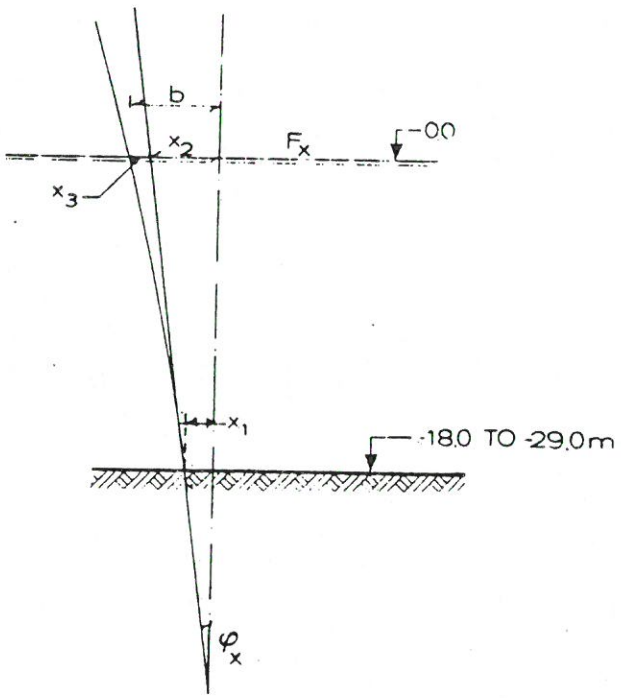

Fig. 4.4 - Parallel deformations of pier.

with the definitions in Figure 4.4. For parallel motion the preliminary estimate resulted in :

$$\zeta_{x1}\,(\text{total}) = \zeta_{xf} + 0.14\,\zeta_{xi} + 0.86\,\zeta_{xs} \tag{4-9}$$

where ζ_{xf} is the frictional damping, ζ_{xi} the internal structural damping, and ζ_{xs} the internal hysteretic soil damping. This result, together with the damping values in Table 4.2, demonstrate that the internal damping is dominated by internal hysteretic soil damping for large amplitudes (such as ALS), while at small amplitudes frictional damping will dominate. The preliminary estimates of total damping are

shown in Table 4.2. The final values turned out somewhat differently, because the dynamic response was significantly smaller than first assumed, due to soil backbone curvature and hysteresis, cf. Section 6.

MODE	FREQUENCY (Hz)	FRICTION ζ_f	BUFFER ζ_b	STRUCTURE ζ_1	SOIL ζ_s	WEIGHTED AVERAGE ζ
Trans-versal	0.78	-	-	0.02	0.13-0.28	0.09-0.20
Parallel a) 1 pier	0.84	0.03-0.06	-	0.02	0.09-0.24	0.11-0.27
b) whole bridge section	(0.50)	-	0.04	0.02	0.09-0.24	0.12-0.25
Torsion	2.07	0.04-0.07	--	0.02	0.07-0.22	0.10-0.26

Table 4.2 Preliminary damping estimates applicable for accidental limit state. Friction and buffer damping are given relative to the total energy, while soil and structural damping are given relative to the sub-system energy. Frictional damping values are conservative estimates, i.e. small.

5.0 ICE LOAD MODELLING

5.1 ICE MODEL TEST PROGRAMME

The physical model test programme was carried out at NRC during the winter of 1989-90, cf. Timco et al. (1990) and Christensen et al. (1990). A total of 62 tests were completed at scale 1 : 30 in EG/AD/S ice, cf. Timco (1986). Three main categories of tests were carried out. The first 15 tests modelled the tender design pier (two circular cylindrical shafts) in a rigid suspension. These tests were essentially a copy of similar tests carried out at a larger scale two years previously at the Hamburgische Schiffbau Versuchsanstalt and published by Christensen et al. (1989a, 1989b). The copy tests were included to investigate scale effects, and an evaluation based on the comparison will be published soon, Christensen and Klinting (199x). The conclusion from that comparison is that Froude scaling should be applied for the West Bridge. The following 12 tests modelled the final pier, cf. Figure 3.2, in rigid suspension for ice attack angles of 0°, 65°, 90° and 115°, and velocities of 0.1, 0.2 and 1.0 m/sec full-scale. The zero degree ice attack angle is perpendicular to the direction of road traffic on the bridge. The next 12 tests repeated the former 12 only in a compliant suspension with 3 degrees of freedom, viz. : horizontal translations and rotation around a vertical axis. The last 23 tests were sensitivity tests in which variations of speed, ice strength, natural frequency, number of degrees of freedom, damping and coefficient of friction were investigated.

Because of the sensitivity of the full-scale piers to dynamic amplification, it was imperative to model the dynamic behaviour as accurately as possible in the model tests. Dynamic ice-structure interaction has been the subject of many research programmes in recent years, cf. Sodhi (1988), but most computational and physical models are still one-dimensional, cf. Sodhi (1989). With literally no relevant experience available, assumptions must be made carefully. Three important assumptions are :

- that the dynamic load fluctuations caused by the EG/AD/S model ice is representative of similar fluctuations in full scale,
- that the basic eigenmode of the full-scale pier, which is a rocking motion over the foundation (rigid structure and compliant foundation), can be modelled as a translation at water level, and
- that the coupling between modes in the various degrees of freedom is limited.

The latter assumption was necessary because the full-scale pier, owing to its geometry and foundation conditions, has quite different stiffnesses in the horizontal directions, while the natural frequencies are almost similar. With the available testing technology developed by NRC, the natural frequency is that of a simple linear oscillator $f = 2\pi(k/M)^{0.5}$ where k is the stiffness and M the mass. Thus, the ratios of horizontal stiffnesses and horizontal frequencies are tied together, except if the oscillating mass could be made dependent on direction. This would, however, require time for development of a satisfactory test rig and probably increase the damping unacceptably. It was decided to scale the frequencies correctly, thereby maintaining their ratio of 0.93 (transverse to parallel), and accept an adjusted stiffness instead. In the authors' view, the ratio of frequencies is more important than the ratio of stiffnesses for coupling effects. The transverse direction stiffness was reduced by a factor of roughly three below the value required by Froude's law in order to accommodate the frequencies, cf. Table 4.1. The resulting increased deflections were assumed not to affect loading and response in the parallel direction significantly. Finally, it should be realized that the physical model is a linear oscillating system with a relatively small damping, while the full-scale pier is non-linear in the accidental limit state, due to curvature of the soil backbone curve.

The pier model was instrumented with dynamometers in each shaft to measure ice loads, and a dynamometer was also used to measure « foundation loads » between carriage and compliance simulator. The set-up for compliant tests was similar in principle to that described by Timco et al. (1989) and by Frederking and Timco (1987). When using dynamometers based on strain gauge technology, it is important to realize that the measured loads are really calibrated deflections. In terms of Newton's second law with time invariant coefficients :

$$\frac{1}{\omega_n^2}(k\ddot{x}) + \frac{2\zeta}{\omega_n}(k\dot{x}) + kx = F(t) \qquad (5\text{-}1)$$

this means that measured loads are kx, not the external ice loads, F(t). In Eq. (5-1) ω_n is the natural cyclic frequency, ζ is the generalized damping, and k is the stiffness. A filtering technique was used to convert kx measurements to

F(t) as described by Christensen and Klinting (199x) for the analysis of scale effects. Response simulations were made with raw data (kx) after a simple low-pass filtering. The removal of damping and d'Alembert forces through filtering is quite complicated for the compliant test set-up, because it consists of three impedances coupled in series.

In most tests with quartering and beam-on attack angles (65°, 90° and 115°), the ice would crush at the high velocity, while buckling would dominate at the two lower velocities. The measured average loads (kx) generally increase with velocity, but the peak loads have a maximum at intermediate velocities, where the ice failure process causes resonant vibrations of the bridge pier. During a buckling event, some localized spalling of the ice at the contact face takes place. The actual failure might be a combination of spalling, brittle fracturing, microcracking and more, but it is referred to as spalling here. Typical full-scale frequencies for this spalling are near 1 Hz, whereas the crushing frequencies are in the range 5-10 Hz, and the buckling frequencies in the range below 0.2 Hz. It is therefore the spalling which induces resonant vibrations, not the buckling.

The recorded loads compared favourably with theoretical crushing and buckling loads. The key, however, is the response of the pier. At intermediate velocities, violent resonant vibrations with amplitudes in the order of 1 cm were observed, corresponding to the full-scale pier rocking with an amplitude of ± 30 cm at the water level. If this resonance occurs for the full-scale structure, extremely high amplification will result.

5.2 COMPUTATIONAL MODELLING OF ICE LOADS AND RESPONSE

A computational (finite element) model of the pier was used to simulate the tests. The recorded force time series were run through the computational model, using a linear foundation description corresponding to the model test set-up. The computational model was capable of reproducing the resonant response of the physical model, and so the numerical model was accepted as adequate. Because of the lack of a feedback effect to create a frequency lock-in with the computational model, typical time series were stretched and compressed to determine the maximum resonance instead. Within limits, a similar effect would result from changing the ice velocity.

During resonance, the general force level of the low-frequency part of the signal, i.e. the buckling part, doubled relative to the rigid suspension tests. The same doubling also took place when increasing the ice-structure friction factor substantially. This change seemed to be caused by the ice being forced to buckle in the second mode rather than the first, viz.: the contact face was fixed at the water level rather than sliding vertically on the structure. For high friction it appears natural, but it is somewhat surprising that the resonant spalling vibrations apparently promote the second buckling mode. In any case it is clear that dynamic structural response affects the failure mode of the ice.

It was not possible, at least within the time frame, to model the modulation of natural frequencies during extreme response and frequency lock-in. This modulation is caused by a transfer of energy to the ice, resulting in vibrations of the ice and thus wave generation. Apart from modulation of the natural frequency, the pier responses were identical.

The foundation description was then modified to include the non-linearity of the soil backbone curve. The resonant model tests were repeated in rigid suspension, and the external loads from those tests were used for response simulation with the non-linear model at the intermediate velocities, which had caused resonance in the linear physical model. The non-linearity dampened the system sufficiently to limit resonance. This was possible partly because the calculations were carried out in the accidental limit state, leading to the use of a large portion of the soil backbone curve.

Using the non-linear response model, a maximum impact velocity of 0.81 m/sec determined from environmental conditions in the area, and a maximum ice floe size of 2000 x 2000 x 1 metres, the extreme interaction event was determined to consist of approximately 12 successive buckling events. The first buckling causes a relatively low load because the pier is not yet fully embedded in the ice, and because it takes several load cycles to build up dynamic amplification. Taking all these effects into account, an equivalent static buckling load of 43 MN superimposed by a spalling load of ± 8 MN was determined for design in the accidental limit state.

In the servicibility limit state, only the lower part of the soil backbone curve is used, and additional damping from non-linearity cannot be expected in this range. On the other hand, the importance of other damping elements increases. Detailed calculations showed that the modified ice parameters and velocities corresponding to the servicibility limit state precluded the occurrence of resonant buckling.

6.0 FOUNDATION MODELLING

6.1 TYPICAL SOIL CONDITIONS

The soil conditions vary quite substantially over the length of the bridge. Two typical cases include a stiff and a soft clay till. A few of the piers are furthermore placed on limestone.

The ice load is most critical for the piers in deeper water, 23-29 metres. This case, where the soil conditions correspond to stiff clay till, is shown in Figure 6.1 as a typical simplified soil profile. The most important part of the profile are the upper layers where overturning and sliding may occur.

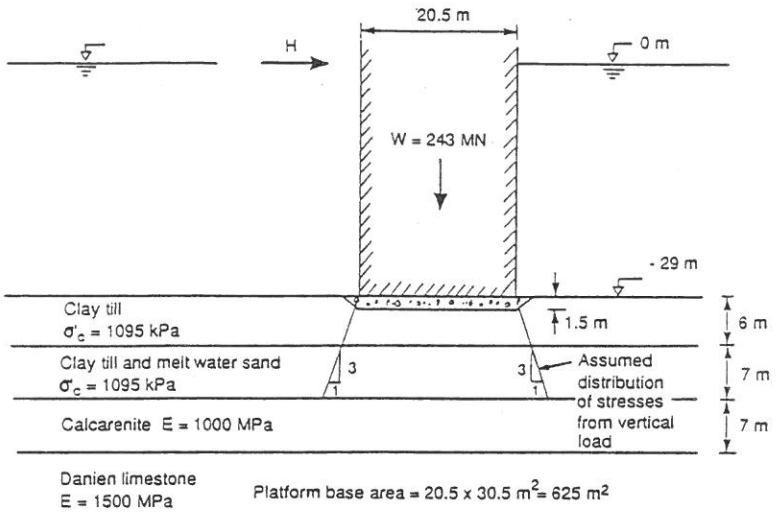

Fig. 6.1 - Geometry and soil profile for stiff clay till site.

6.2 PRELIMINARY ESTIMATE OF ICE LOAD

One main problem for this type of investigations is that they basically require all the results to be known a priori, in order to allow correct ice model tests, cyclic soil tests and foundation modelling. So it is necessary to initiate the investigations using realistic assumptions. By certain re-analysis and adjustments, the design may finally be completed through a series of iterations. As shown in Figure 6.1, the expected results, i.e. the required caisson base plate area, has been estimated a priori. This is also the case for the expected ice-induced foundation forces, the initial estimate of which is shown in Figure 6.2.

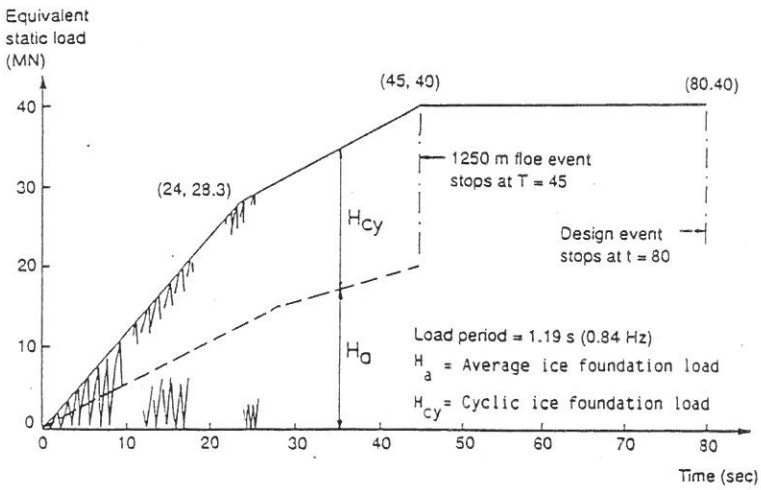

Fig. 6.2 - Initial estimate of design ice foundation load from a 1250-meter-diameter ice floe and from a 2500-meter-diameter ice floe.

The expected ice load has a cyclic load component with an amplitude equal to the average load component. Note that Figure 6.2 is **not** an estimate of the direct ice load, but an estimate of the equivalent force at the foundation base plate level.

6.3 SOIL TEST PROGRAMME

In order to benefit from experiences obtained from their previous cyclic soil analyses for offshore platforms, the advanced soil tests were carried out at the Norwegian Geotechnical Institute by Andersen and Hansteen (1990). The static tests consist of :

- Triaxial compression tests
- Triaxial extension test (one only)
- Direct simple shear tests.

A complete programme of cyclic direct simple shear tests and cyclic triaxial tests was performed on intact samples of both the soft and the stiff clay types. The tests were performed with varying average shear stress and with a constant, but different cyclic amplitude in order to establish a global relationship between the following parameters :

- Average shear stress
- Cyclic amplitude of the cyclic stress
- Number of cycles
- Pore pressure build-up
- Average strain
- Cyclic strain
- Cyclic stress-strain relationship

A complete programme of cyclic simple shear tests was also performed on disturbed glacial clay till, in order to evaluate the consequences at the transition zone between intact soil and stone bed.

6.4 SOIL TEST RESULTS

The main results of the tests were as follows :

STATIC TESTS

- The direct simple shear tests showed an undrained shear strength of approx. 70 % of the shear strength determined by triaxial compression tests.
- One triaxial extension test showed an undrained shear strength of approx. 50 % of the value obtained by triaxial compression test.

CYCLIC TESTS

- Large strains (failure) are observed for shear stresses lower than the static undrained shear strength. The higher the number of cycles, the lower the stresses that may result in large strains.
- This effect is more pronounced for tests with a cycle time of 10 seconds than for tests with a cycle time of 1 second.
- The static undrained shear strength is smaller just after cyclic loading has taken place, before drainage takes place.
- Hysteretic, internal damping, has been found to agree reasonably with recommendations by Seed and Idriss (1970).

The direct results of the tests interpolated to give overall design values may be illustrated as shown in Figure 6.3. Alternatively, the results may be interpreted as relative shear strain in the points considered below the foundation plate. For a certain load condition, both the cyclic and average shear strain may be found as shown in Fig. 6.4. The results from more load cases may afterwards be combined as illustrated in Figure 6.5. By means of a finite

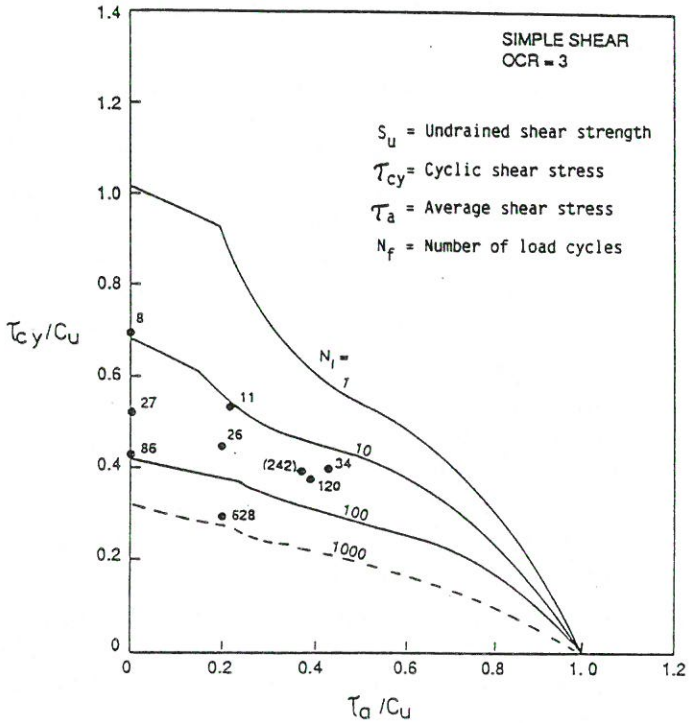

Fig. 6.3 - Number of load cycles to failure in direct simple shear tests as a function of normalized cyclic and average shear stresses.

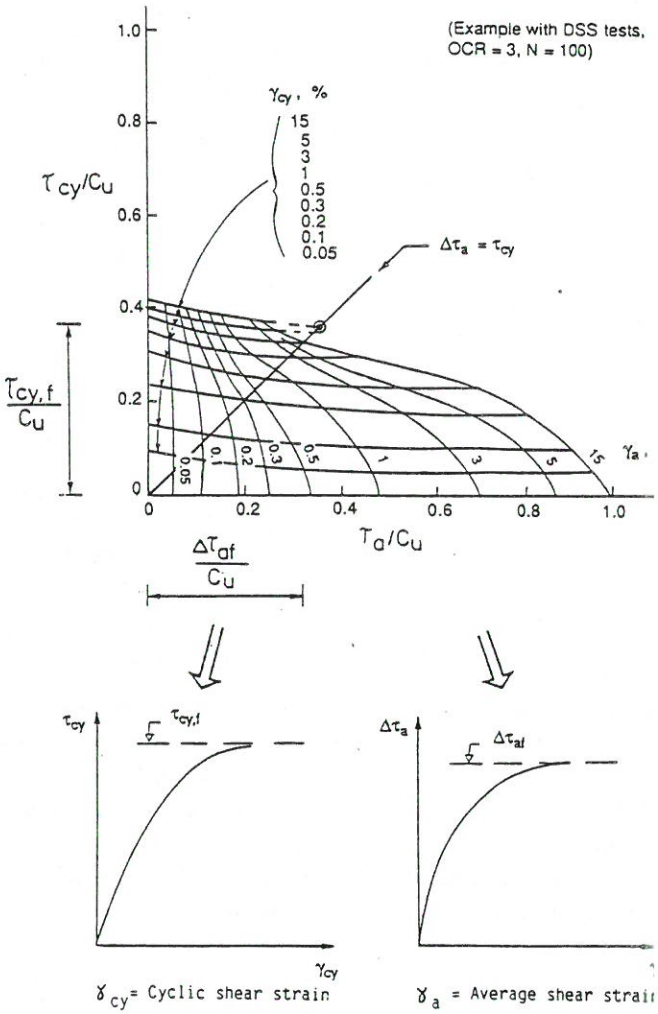

Fig. 6.4 - Illustration of how parameters to be used i computational analyses are determined from labor tory tests.

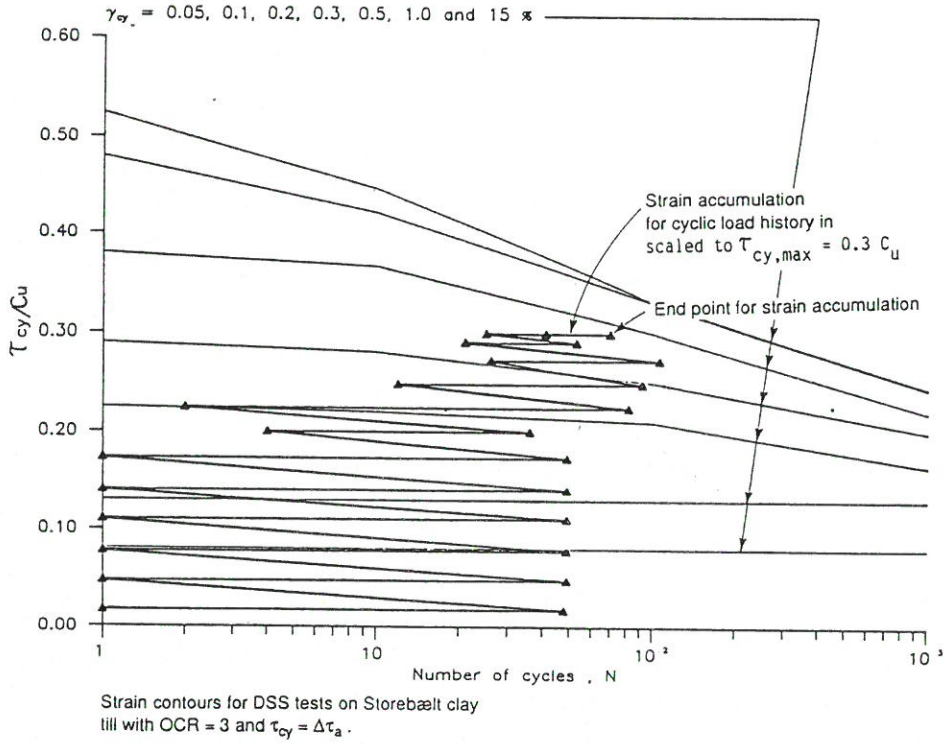

Fig. 6.5 - Result of strain accumulation for the preliminary ice load history.

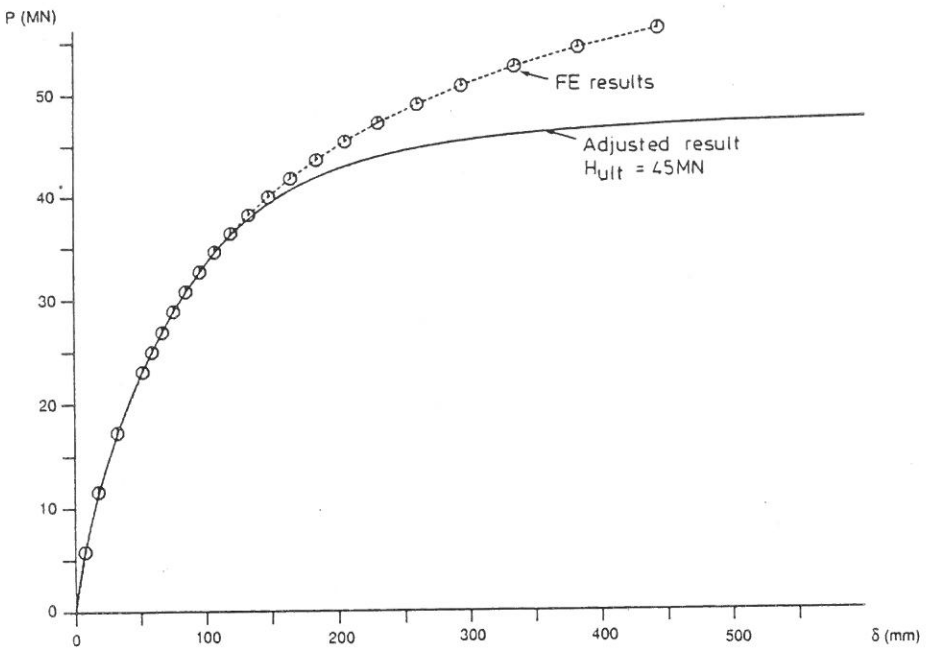

Fig. 6.6 - Total displacements at bridge deck versus ice load for a pier on stiff clay till.

element model, the average cyclic and total foundation displacements may be determined. This is shown in Figure 6.6. Another result of the analysis is the stiffness and the damping from which a resulting backbone curve may be determined, cf. Figure 6.7.

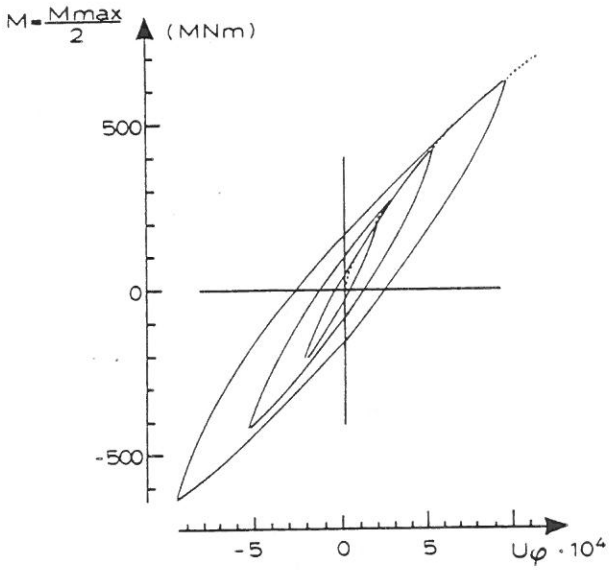

Fig. 6.7 - Backbone curve and examples of hysteresis loops for a pier on stiff clay till. The solid curve represents the adjusted result due to a revised estimate of the foundation failure load.

7.0 IMPLEMENTED DESIGN

7.1 DAMAGE CRITERIA

The damage criteria are defined to be a « Maximum total motion of the top of the pier shafts relative to the superstructure less than 0.5 m in the parallel direction ». Such a deformation a) just exceeds the maximum deformation which the selected bearings allow for without damage, while b) the additional destabilizing moment induced by the large dead weight force from the superstructure is still acceptable.

7.2 SELECTED DESIGN ICE LOAD

The non-linear structural model was used to calculate the effect of the scaled ice force on the full-scale bridge with its different damping and with its different structural behaviour from that of the experimental set-up. The non-linear behaviour of soils was fully incorporated.

From the calculations it could be determined whether the bridge would be in resonance or not. With a linear bridge model, a heavy resonance could develop, as shown in Figure 7.1. It turned out that the curvature of the soil load-deflection curve, combined with its hysteresis and the hysteresis of the bearings, made the structural system sufficiently non-linear in the Accidental Limit State (ALS) so that no resonance could be created.

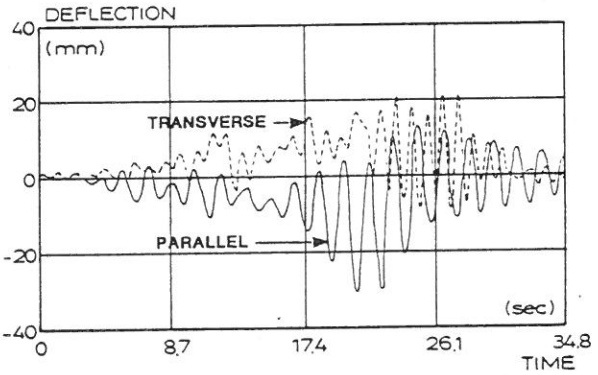

Fig. 7.1 - Deflection of road girder in global coordinates during resonance with the linear model. Time was stretched by a factor of 1.1 in this plot to obtain maximum dynamic response.

With no lock-in present for buckling frequencies, there would be only limited amplification of the ice buckling loads. Therefore, in ALS the buckling loads could be fixed to the range 31-64 MN. The selected total ice force time series are shown in Figure 7.2.

The forces parallel to the bridge on both the railway and roadway shafts are shown in Figure 7.3, while the torsional moment is shown in Figure 7.4. By stretching the time series, maximum resonance could be obtained. With the dynamic amplification in the ALS, it was found that an equivalent static load of 8 MN should be used as the force amplitude for the spalling loads, corresponding to half the width of the indicated band in Figure 7.2.

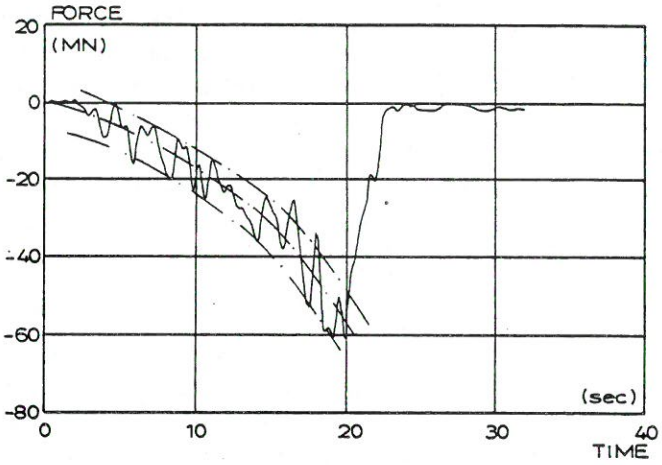

Fig. 7.2 - Selected design ice force time series to be scaled appropriately to both the desired force level and frequency. The indicated band envelopes load fluctuations caused by spalling.

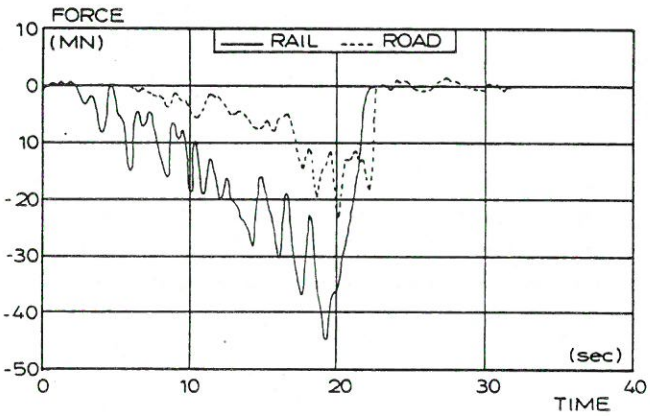

Fig. 7.3 - Forces parallel to the bridge at still water level.

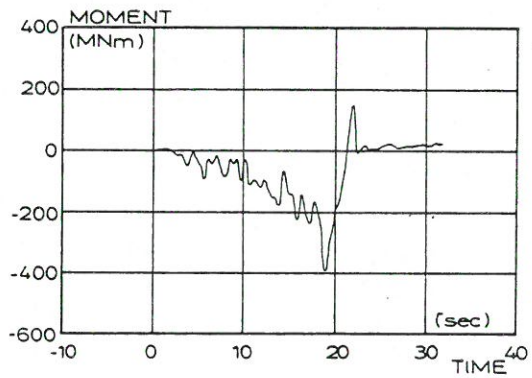

Fig. 7.4 - Total torsional moments on a complete pier at still water level.

7.3 LIMITATIONS TO POSSIBLE LOAD SCENARIOS

With a load level of 31-64 MN, it was checked whether or not such forces can in fact be generated in the Great Belt with its particular dimensions and environmental conditions, even in the ALS. It was found that the forces were so high that they would arrest the movement of the large ice floes, see Figures 7.5 and 7.6.

In case of large drifting ice floes, a few buckling events can be expected before the bridge pier arrests the ice. This means that a sustained situation as tested in the laborato cannot exist in practice in the Great Belt. Therefore, tl expected buckling load will be smaller than the maximu load determined in the ice model tests.

Applying the short-term statistics for peak buckling forc for ice sheet impacts gave a peak buckling load of 43 MN.

The sequence leading from model test results to selecte forces for an exceedance probability of 0.2 x 10^{-4} per year illustrated in Table 7.1.

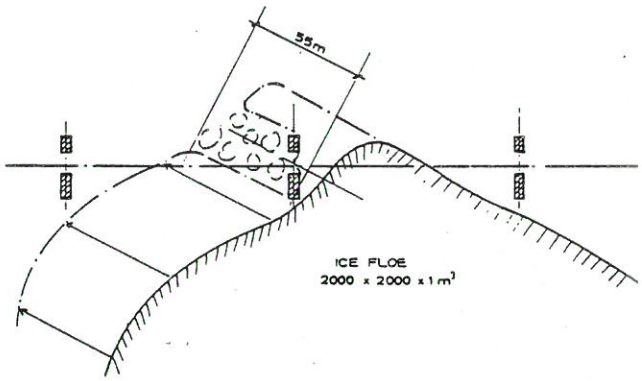

Fig. 7.5 - Impact of a 2000 x 2000 x 1 m ice floe under 115° incidence angle.

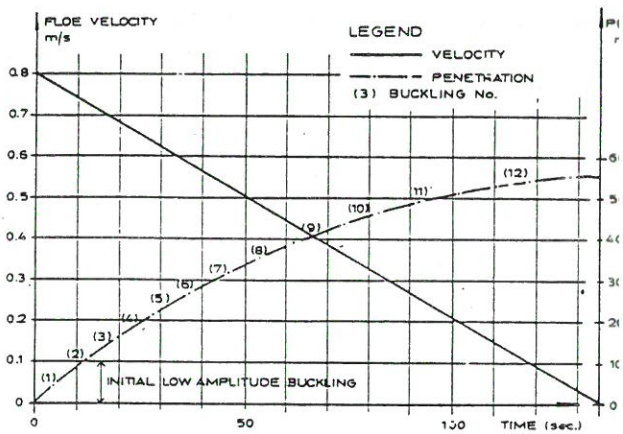

Fig. 7.6 - Velocity variation during penetration of ice floe.

SOURCE	BUCKLING MODE	FORCE (MN)	COMMENT
ICE MODEL TESTS			
1. Rigid model	1 mode	31-64	Average = 43 MN
2. Compliant Model ζ = 0.03 and 0.05			
2.1 High surface friction	2 mode	70-110	
2.2 Normal surface friction			
2.2.1 No lock-in between spalling and buckling	1 mode	31-64	Average = 43 MN
2.2.2 Lock-in between Spalling and buckling	2 mode	70-150	Linear resonance
NUMERICAL MODEL			
3. Linear model Resonance spalling Eventually lock-in	1 or 2 mode	31-64 70-150	
4. Non-linear model Weak resonance with Dynamic load factor for spalling of 1.5	1 mode	(31-64) ± 8	
5. Limited load scenario	1 mode	43 ± 8	Final design

Table 7.1 Selected design ice forces with a 2 x 10^{-5} per yea exceedance probability.

7.4 FINAL RESULTS OF NON-LINEAR RESPONSE MODELLING

The final analysis with the structural model included non-linear foundation modules, friction in bearings, and a non-linear buffer. Some of the results are illustrated below.

Figure 7.7 shows the moment/angular deflection plot for overturning parallel to the bridge, illustrating how the backbone curve defined in Figure 6.7 acts in practice.

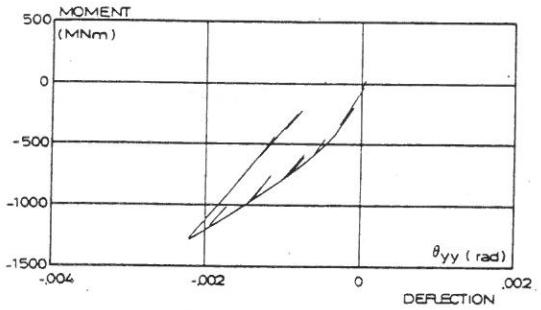

Fig. 7.7 - Forces and deformations at foundation.

The major non-linear element is a stiffness shift and much less hysteretic effect than assumed preliminarily in Section 4.4.

The moments at the base plate level are shown in Figure 7.8. The time series show only limited tendency towards resonance, although the loading time series have been tuned to show maximum resonance between the spalling force and the pier eigenfrequencies.

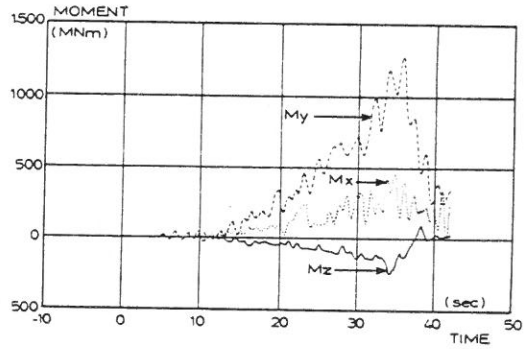

Fig. 7.8 - Sectional forces at foundation level.

The results of the ice model tests (Figure 7.2) necessitated a re-analysis of the number of equivalent load cycles, because the vibration component was significantly reduced relative to the preliminary estimate. The simplified ice load history is shown in Figure 7.9.

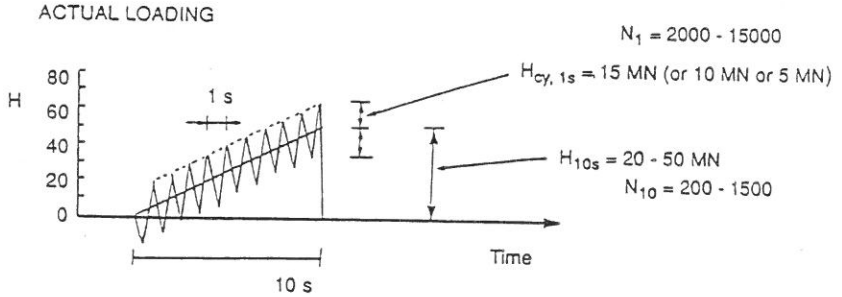

Fig. 7.9 - Load history used as approximation to the revised actual ice load history.

The equivalent number of load cycles could be estimated as shown in Figure 7.10, cf. Andersen and Hansteen (1990). The actual load case may be estimated to be equal to an equivalent number of load cycles N = 20. Finally, the bearing capacity of a centrally loaded pier versus number of load cycles could be determined as shown in Figure 7.11.

No. of equivalent cycles, N_{eqv}, with H = 50 MN + $H_{cy,\,1s}$

N_{10s} \ $H_{cy,\,1s}$	0	5	15
200	30	35 [2] - 50 [1]	40 - 100
500	80	90 - 200	105 - 290
1500	300	315-590	375 - 750

1) APPROXIMATION 1 2) APPROXIMATION 2

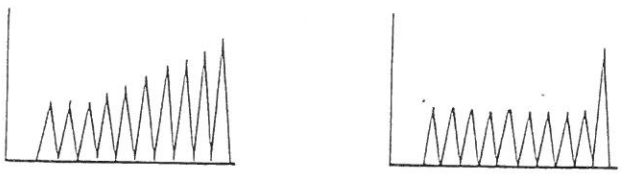

N_{eqv} at failure
N_{eqv} smaller below failure

Fig. 7.10 - Equivalent number of load cycles for the revised ice load history.

The results in Figure 7.11 include :
- Anisotropy of glacial till
- Strength increase due to dead load
- Existence of gravel pad
- Soil degradation due to cyclic loading

The original design basis was much more simple, as it was based on the following assumptions :
- Isotropic soil
- No strength increase due to dead load
- No gravel pad

The effect of the quantified changes, including torsion relative to the original design basis, have been determined through an equivalent factor α acting on only one parameter - the shear strength - and describing the difference between the original design basis and final ice load design. This required among others determination of actual undrained shear strength relative to the original undrained shear strength at foundation level, determined during the site investigations by vane shear tests, CPT-point resistance, and/or the assumption that vane shear tests reflect the results of the triaxial compression tests. This quite complicated analysis has led to the main results shown in Table 7.2, cf. Kristensen and Gravesen (1990).

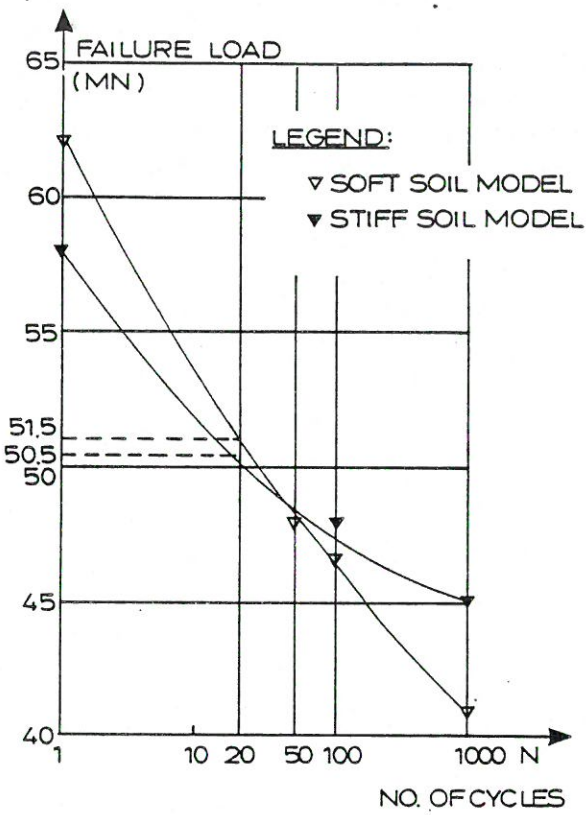

Fig. 7.11 - Horizontal failure load at still water level.

	STIFF SOIL MODEL	SOFT SOIL MODEL
Foundation slab (m²)	20.5 x 30.5	22 x 34
C_u, Static (kN/m²)	225	150
C_u, Dynamic (kN/m²)	209	140
Reduction Factor α (-)	0.93	0.93
Vertical load (MN)	243	215

Table 7.2 Deep seated failure. Results of comparison of a static design, based on original undrained shear strength with a dynamic design accounting among others for actual undrained shear strength.

Another result shows that for the case of sliding failure, the dynamically reduced sliding resistance, k, should be determined from :

$$k = \tau_u/\sigma'_v = 0.38 \qquad (7\text{-}1)$$

where τ_u is the sliding shear stress and σ'_v the effective vertical stress.

8.0 RESULTS

8.1 ICE LOADS AND RISK LEVELS

Ice model tests, soil tests, and structural response modelling all assume the result of each other to be available a priori. Some analyses, particularly certain soil tests, were interpreted iteratively. Preliminary interpretations were used in response simulations which in turn resulted in revised interpretations of the soil tests. In the end all these analyses were combined, and the final result showed that the load corresponding to a 0.2 x 10^{-4} per year exceedance probability exceed the actual design loads by 6 %. The increased risk is acceptable within the total risk budget.

The dynamic amplification was found to be smaller than estimated in the tender design studies mentioned in Section 3.2. The revised extreme value analysis of ice properties resulted in higher ice strengths than originally estimated.

The exceedance of 6 % mentioned above reflects a comparison of two very different design bases. The determined extreme ice load of 43 ± 8 MN cannot be compared directly with the 44 MN mentioned as the actual design load because they relate to different design approaches. The contractor is bound to follow a fairly simple design approach as part of the contract. The verification study presented here, however, was free to incorporate advanced analyses to any extent. The two analyses were compared by means of the necessary undrained shear strength of the soil at foundation level to ensure stability. It was this comparison that showed a 6 % lower load resistance capacity of the actual design as compared to that resulting from the advanced analyses in the verification study.

8.2 ESTIMATES AND ASSUMPTIONS

The ice load design is a mixture of statistically determined parameters and selected deterministic scenarios.

The estimated risk is associated with one of the most exposed piers, e.g. a deep water pier in the eastern part of the bridge, where local current conditions cause large incidence angles. The fact that more than one pier is exposed to the same risk does not result in significantly increased risk of disruption of the bridge, because the risk of damage is associated with the same extreme winter event. The possible disruption caused by various piers is thereby nearly 100 % correlated to the same event.

For certain parameters conservative estimates have been used, e.g. the extreme ice strength and thickness, the effect of a snow cover, the selected ice load scenario of floe size and associated incidence angle, and the scaling of laboratory results using Froude's law without scale effects.

With respect to scaling, there is an ongoing discussion between ice specialists, as some advocate a scaling leading to lower forces than predicted by Froude scaling. But the published arguments for a different scaling relate to rounded structures with aspect ratios typically in the range 1-10. With a flat-faced bridge pier and aspect ratios near 25-30, there is no sufficient material available to justify a milder scaling.

At some points, relatively optimistic estimates and physical interpretations of ice model test results have been

applied, e.g., the average model test buckling force was used, resonance was assumed unlikely for buckling forces, and a reduction was allowed of the dynamic response due to a non-linear moment/deflection curve in the soil, and other damping effects.

The combination of all the mentioned estimates and the resulting loads represent the best possible overall estimate with the selected risk level.

8.3 EXPERIENCE OBTAINED

The following conclusions and recommendations for future projects are given :

- Ice loads have a high dynamic component very likely to lock in the resonance frequencies of the bridge structure.
- The bearing capacity of the soil is dependent on the number and type of load cycles, so advanced soil tests are a must with large ice forces.
- Damping in soil and change of stiffness cause very important reductions of the dynamic response.
- If acceptable, bridge piers should be rounded, so that unnecessary large ice forces are avoided.
- If acceptable, the piers should be given an inclined surface at the water level.
- Alternative connections should be included in the structural system for large relative deformations between piers and superstructure, so that local damage on a single pier can be avoided during accidental loading.
- The key word for structures designed in accidental limit state is ductility. All appropriate means to increase ductility should be used.
- Comprehensive formulations of design ice conditions should be made as early as possible in the project. For dynamically sensitive structures, the ice velocity should be included in the probabilistic model.

Few structures have to date been designed for ice loads on the basis of scaled test results for absolute force levels. Model tests have primarily been used as a tool for evaluating qualitatively the behaviour of various structural designs. Since full-scale loads and amplification factors determined in this project seem reasonable in relation to experience and theories, the result was found reliable. It appears that physical model tests can be used for design, provided that appropriate data processing takes place to account for structural vibrations of the model, and provided that the model ice represents the dynamics of the failure process in the full-scale ice well. This latter point might require improved model ice types and certainly needs continued investigation.

Physical model tests in ice showed that some dynamic amplification and frequency lock-in are likely to occur. Ice loading typically contains energy at higher frequencies than for example storm-wave loading, and the available experience with dynamic soil properties is quite limited for marine structures in the high-frequency range. The bearing capacity is furthermore very dependent on the number of load cycles, so detailed dynamic soil tests are necessary for accurate design. Hysteresis and backbone curvature for the soil contribute significantly to system damping in accidental limit state design. Consequently, structural ductility should also be encouraged in the design.

9.0 CONCLUSION

Dynamic ice loads for the Great Belt Western Bridge have been investigated in order to verify that the specified design complies with risk acceptance criteria. For some of the piers, the dynamic ice loading is governing for the design.

The presented investigation has combined advanced analyses of extreme ice properties, of ice-structure interaction in both physical and numerical models, of marine dynamic soil mechanics, of structural response, and of risk strategies to check the final design of the Great Belt West Bridge for extreme ice loads. The advanced level of the analyses was necessary because of some relatively unique features of the bridge. The length of the bridge and the geography of the area leave the relatively light-weight piers exposed to ice forces from unusually large attack angles.

The design was carried out in the accidental limit state, while certain critical points were checked in ultimate and servicibility limit states as well. For the West Bridge, the real advantage of designing in the accidental limit state is that the engineer is forced to think in terms of consequences as well as design forces, and thus favour ductility as well as large load resistance capacity.

The final result of the analyses is that, with the actual design ice load of 44 MN, the risk for a disruption exceeding one month due to extreme ice loads is slightly larger than originally estimated, but still within acceptable limits.

10.0 ACKNOWLEDGEMENT

The analyses described were carried out on behalf of the Great Belt Link Ltd., who also funded the preparation of this article. The permission and funding to publish the results are gratefully acknowledged.

The authors wish to acknowledge the substantial contributions to the project made by N.-E. Ottesen Hansen of LICengineering, P. Klinting of the Danish Hydraulic Institute, and P. Sandgård Kristensen of COWIconsult. Special reviewers of the project on behalf of the Great Belt Link Ltd. have been Dr. H.R. Kivisild of HRK Consulting Inc., and Mr. P. Tryde of Tryde Consult.

The first and third authors represent the joint venture of the Danish Hydraulic Institute and LICengineering Ltd., acting as special consultants to the Great Belt Link Ltd. in all matters related to water and ice. The second author represents the joint venture CCL consisting of COWIconsult Ltd., Carl Bro Group Ltd. and Leonhardt Andrä und Partner, acting as general consultants to the Great Belt Link Ltd.

REFERENCES

- Andersen, K.H. and O.E. Hansteen (1990): « Storebaelt Western Bridge - Bearing Capacity, Displacements and Backbone Curves under Ice Loading », Report by the Norwegian Geotechnical Institute for the Great Belt Link Ltd.
- Blanchet, D., A. Churcher, J. Fitzpatrick and P. Badra-Blanchet (1989): « An analysis of observed failure mechanisms for laboratory, first-year and multi-year ice », Special Report 89-5, pp. 77-124, Cold Regions Research and Engineering Laboratory, Hanover, New Hampshire, U.S.A.
- Christensen, F.T. and P. Klinting (199x): « Ice loads on a vertical bridge pier at two different model scales », in preparation.
- Christensen, F.T. and N.-E. Ottesen Hansen (1988a): « Storebaelt Ice Model Tests. Vertical Piers for the Western Bridge », Project Report by the Danish Hydraulic Institute and LICengineering to the Great Belt Link Ltd., Issue No. 1, 15 July 1988.
- Christensen, F.T. and N.-E. Ottesen Hansen (1988b): « Storebaelt Design Ice Forces, Vertical Piers for the Western Bridge », Project Report by the Danish Hydraulic Institute and LICengineering to the Great Belt Link Ltd., Issue No. 2, 15 December 1988.
- Christensen, F.T. and J. Skourup (1991): « Extreme ice properties », ASCE J. Cold Regions Engineering, accepted and tentatively scheduled for June 1991.
- Christensen, F.T., N.-E. Ottesen Hansen, K.-U. Evers, S. Spangenberg and L.J. Vincentsen (1989a): « Design of the Great Belt Western Bridge for Ice Forces », 8th int. conf. on Offshore Mechanics and Arctic Engineering (OMAE-89), Vol. 4, pp. 365-376, the Hague, the Netherlands.
- Christensen, F.T., N.-E. Ottesen Hansen, S. Spangenberg and L.J. Vincentsen (1989b): « Dynamic Ice Loads on the Great Belt Western Bridge », Proc. 10th int. conf. on Port and Ocean engineering under Arctic Conditions (POAC-89), Vol. 1, pp. 453-466, Luleaa, Sweden.
- Christensen, F.T., P. Klinting, B. Pedersen, J. Skourup, J.R. Thomsen and N.-E. Ottesen Hansen (1990): « Dynamic Ice Loads on the Great Belt Western Bridge », Project report by the Danish Hydraulic Institute and LICengineering to the Great Belt Link Ltd., Issue No. 2 of 10 May 1990 and Addendum of 29 June 1990.
- Danish Engineering Association (1982): « Danish Code of Practice for Safety Regulations for Structures », 3rd issue June 1982, DS409 and DS410, Copenhagen, Denmark.
- Frederking, R.M.W. and G.W. Timco (1987): « Ice loads on a rigid structure with a compliant foundation », Proc. 9th int. conf. on Port and Ocean engineering under Arctic Conditions (POAC-87), Vol. 3, pp. 409-418, Fairbanks, Alaska, U.S.A.
- Juul Jensen, O., J. Juhl, N.-E. Ottesen Hansen, P. Lundhus and S. Spangenberg (1991): « Perimeter Protection of the Artificial Island of Sprogø », Permanent Int. Assoc. of Navigation Congresses (PIANC), Bulletin 72, (Present issue).
- Kristensen, P.S. and H. Gravesen (1990): « Dynamic properties soil for ice load », Project Report by COWIconsult, Carl Bro a Leonhardt Andrä und Partners joint venture to the Great Belt Li Ltd., Revision 0 dated 16 July 1990.
- Nordic Committee for Building Codes (1987): « Guidelines for det mination of load and safety for structural systems », in Swedi NKB-paper No. 55, June 1987.
- Pratte, B.D., and Timco, G.W. (1981): « A New Model Basin for Testing of Ice-Structure Interaction », Proc. 6th int. conf. on Port a Ocean engineering under Arctic Conditions (POAC-81), Vol. pp. 857-866, Quebec City, Canada.
- Schwarz, J. (1985): « Physical modelling techniques for offsh structures in ice », Proc. 8th int. conf. on Port and Ocean engine ing under Arctic Conditions (POAC-85), Vol. 3, pp. 1113-1131, Nar arssuaq, Greenland.
- Schwarz, J. (1987): « Advances in ice mechanics in West Germany ASME Applied Mechanics Reviews, 40(9):1208-1213.
- Seed, H.B. and I.M. Idriss (1970): « Soil moduli and damping fact for dynamic response analysis », Report EERC 70-10, Earthqua Engineering Research Center, Univ. of California, Berkeley, Calif nia, U.S.A.
- Sodhi, D.S. (1988): « Ice-induced vibrations of structures », state-of-the-art report on ice forces, Proc. 9th Int. Assoc. Hydr. R (IAHR) Ice Symposium, Vol. 2, pp. 625-657, Sapporo, Japan. (A available in Special Report 89-5, Cold Regions Research a Engineering Laboratory, Hanover, New Hampshire, U.S.A.).
- Sodhi, D.S. (1989): « Ice-structure interaction during indentati tests », Proc. Symposium on Ice-structure interaction, co-sponsored the Int. Union of Theoretical and Applied Mechanics and the I Assoc. Hydr. Res. (IUTAM/IAHR), St. John's, Newfoundland, Canad To be published by Springer-Verlag.
- Timco, G.W. (1980): « The mechanical properties of saline-doped a carbamide (urea)-doped model ice », Cold Regions Science and Techn logy, 3(1):45-56.
- Timco, G.W. (1986): « EG/AD/S: A New Type of Model Ice Refrigerated Towing Tanks », Cold Regions Science and Technolo 12:175-195.
- Timco, G.W., R.M.W. Frederking and S.K. Singh (1989): « T transfer function approach for a structure subjected to ice crushing Proc. 10th int. conf. on Port and Ocean engineering under Arc Conditions (POAC-89), Vol. 1, pp. 420-430, Luleaa, Sweden.
- Timco, G.W., E.R. Funke and O.G. Nwogu (1990): « Model tests dynamic ice loads on the West Bridge piers of the Great Belt Lin Denmark », Controlled Technical Report CTR-HY-037, by the Hydra lics Laboratory, Division of Mechanical Engineering, Nation Research Council, Ottawa, Canada, for the Danish Hydraulic Ins tute and LICengineering.
- Vincentsen, L.J. and S. Spangenberg (1990): « Safety manageme system for the Great Belt Link », Proc. 2nd symposium on Str Crossings, Trondheim, Norway. Published by A.A. Balkema, R terdam, the Netherlands.